

**EXPERIMENTAL DETERMINATION OF TRANSFER FUNCTIONS FOR A CAR
BODY-IN-WHITE**

**A THESIS SUBMITTED TO
THE GRADUATE SCHOOL OF NATURAL AND APPLIED SCIENCES
OF
THE MIDDLE EAST TECHNICAL UNIVERSITY**

BY

SABRI SENTÜRK

**IN PARTIAL FULLFILLMENT OF THE REQUIREMENTS FOR THE DEGREE OF
MASTER OF SCIENCE
IN
THE DEPARTMENT OF MECHANICAL ENGINEERING**

APRIL 2004

Approval of the Graduate School of Natural and Applied Sciences

Prof. Dr. Canan Özgen
Director

I certify that this thesis satisfies all the requirements as a thesis for the degree of Master of Science.

Prof. Dr. Kemal Ider
Head of Department

This is to certify that we have read this thesis and that in our opinion it is fully adequate, in scope and quality, as a thesis for the degree of Master of Science.

Prof. Dr. Y. Samim Ünlüsoy
Supervisor

Examining Committee Members

Prof. Dr. H. Nevzat Özgüven (Chairman)

Prof. Dr. Y. Samim Ünlüsoy (Supervisor)

Prof. Dr. Mehmet Çalışkan

Prof. Dr. Metin Akkök

Prof. Dr. H. Bülent Ertan

ABSTRACT

EXPERIMENTAL DETERMINATION OF TRANSFER FUNCTIONS FOR A CAR BODY-IN-WHITE

Sentürk, Sabri

M.S., Department of Mechanical Engineering

Supervisor: Prof. Dr. Y. Samim Ünlüsoy

April 2004, 134 pages

Vibration generated from various sources (engine, road surface, tires, exhaust, etc.) should be considered in the design of a car body. These vibrations travel through transfer systems (drivetrain, suspension, body, etc.) to the steering wheel, seats and other areas where it is detected by the passengers of the vehicle. Transmission routes must be studied and efforts made to keep transfer systems from amplifying vibration and to absorb it instead. Since the superior vibration transfer system is the car body, finite element analysis and experimental vibration analysis are performed on car body-in-white. Body vibration analysis entails understanding and improving the body's dynamic characteristics that act as vibration transfer channels.

In the previous study, a finite element model has been created for a car body-in-white available in Automotive Laboratory (Mechanical Engineering

Department, Middle East Technical University, Ankara) and its natural frequencies and mode shapes have been determined using finite element analysis software. In this study, vibration tests have been performed on actual car body-in-white. Frequency response functions between 34 response locations and force application point have been measured. Using these frequency response functions, natural frequencies and mode shapes of the body-in-white have been determined. Finite element analysis and experimental results have been compared to evaluate the finite element model reliability.

Keywords: Vibration Testing, Frequency Response Function, Body-in-White, Sine Sweep, Shaker, Natural Frequency, Mode Shape

ÖZ

BİR OTOMOBİL GÖVDESİNİN TRANSFER FONKSİYONLARININ DENEYSEL OLARAK ELDE EDİLMESİ

Sentürk, Sabri

Yüksek Lisans, Makina Mühendisliği Bölümü

Tez Yöneticisi: Prof. Dr. Y. Samim Ünlüsoy

Nisan 2004, 134 sayfa

Araba gövdesinin tasariminda çeşitli kaynaklardan (motor, yol yüzeyi, lastikler, egzoz vb.) gelen titresimler dikkate alınmalıdır. Bu titresimler, transfer sistemleri (aktarma organlari, süspansiyon, gövde vb.) üzerinden yolcular tarafından hissedilecekleri yerler olan direksiyon, koltuklar ve diger alanlara iletilirler. Transfer sistemlerinin titresimi artirmak yerine emici özellikte olmaları için çaba harcanmalı ve iletim rotasi çalışılmalıdır. Baskın olan titresim transfer sistemi gövde olduğu için, gövde üzerinde sonlu elemanlar ve deneysel titresim analizleri yapılır. Gövde titresim analizi, gövdenin titresim transfer sistemi kanali olarak görev yapmasını sağlayan dinamik karakteristiklerinin anlaşılmasını ve geliştirilmesini gerektirir.

Bundan önceki çalışmada, Otomotiv Laboratuvarı'nda (Makine Mühendisliği Bölümü, Orta Dogu Teknik Üniversitesi, Ankara) bulunan bir araba

gövdesinin sonlu elemanlar modeli hazırlandı ve sonlu elemanlar analiz programı kullanılarak doğal frekans ve mod şekilleri bulundu. Bu tez çalışmasında, araba gövdesi üstünde titreşim testleri gerçekleştirildi. Gövde üstünde 34 tepki noktası ile kuvvet uygulama noktası arasında frekans tepkisi fonksiyonları ölçüldü. Bu frekans tepkisi fonksiyonları kullanılarak gövdenin doğal frekansları ve mod şekilleri bulundu. Sonlu elemanlar analiz sonuçlarıyla deneysel sonuçlar karşılaştırılarak sonlu elemanlar modelinin güvenilirliği değerlendirildi .

Anahtar Kelimeler: Titreşim Testi, Frekans Tepkisi Fonksiyonu, Otomobil Gövdesi, Sinüs Tarama, Titreşim Motoru, Doğal Frekans, Mod Şekli

To my love, Duygu

ACKNOWLEDGEMENTS

I am deeply grateful to my supervisor, Professor Y. Samim Ünlüsoy, for his guidance and constant encouragement throughout the duration of this thesis.

I would like to thank technical staff of the Department of Mechanical Engineering, but especially technician of the Automotive Laboratory, Mr. Özdemir Emen.

My thanks are also due to Mr. Gökhan Osman Özgen, for his helpful advice and discussions.

I would like to express my sincere gratitude to my mother-in-law, my father-in-law and Asli for their support and making me feel at home.

Special thanks are due to my mother, my father and my brother for all their love, patience and support during the course of this work.

Finally, I wish to express my gratitude and love to Duygu who made my life easier and more meaningful in the last one year.

TABLE OF CONTENTS

| | |
|---|------|
| ABSTRACT | iii |
| ÖZ | v |
| ACKNOWLEDGEMENTS | viii |
| TABLE OF CONTENTS | ix |
| LIST OF TABLES | xiii |
| LIST OF FIGURES | xiv |
| LIST OF SYMBOLS AND ABBREVIATIONS | xx |
| CHAPTER | |
| 1. INTRODUCTION | 1 |
| 1.1 Structural Vibration | 1 |
| 1.2 Vibration Analysis | 4 |
| 1.3 Vibration Studies on Car Bodies | 6 |
| 1.4 Structure of Thesis | 12 |
| 2. VIBRATION TESTING | 14 |
| 2.1 Frequency Response Function | 14 |
| 2.2 Frequency Response Measurements | 22 |
| 2.2.1 Supporting the Structure | 23 |
| 2.2.2 Exciting the Structure | 26 |

| | |
|--|----|
| 2.2.2.1 Shaker Testing | 28 |
| 2.2.3 Data Acquisition | 29 |
| 2.2.4 Data Implementation | 32 |
| 2.2.5 An application of quadrature peak picking method | 35 |
| | |
| 3. TEST SETUP | 38 |
| 3.1 Supporting the Structure | 39 |
| 3.2 Exciting the Structure | 42 |
| 3.3 Data Acquisition and Signal Conditioning | 45 |
| 3.4 Instruments | 48 |
| 3.4.1 Shaker | 48 |
| 3.4.2 Signal Analyzer | 49 |
| 3.4.3 Impedance Head | 50 |
| 3.4.4 Accelerometer | 50 |
| 3.4.5 Charge Amplifier | 51 |
| 3.4.6 Microphone and preamplifier | 51 |
| 3.4.7 General View of Setup and Instruments | 52 |
| | |
| 4. EXPERIMENTAL PROCEDURE AND TEST RESULTS | 53 |
| 4.1 Experimental Procedure | 53 |
| 4.2 Test Results | 58 |
| 4.2.1 Frequency Response Function | 58 |
| 4.2.2 Natural Frequencies of Body-in-White | 76 |
| 4.2.3 Mode Shapes of Body-in-White | 78 |

| | |
|---|-----|
| 4.2.4 Identification of modes | 92 |
| 4.2.5 Sound Pressure Level | 93 |
| | |
| 5. COMPARISON OF TEST AND FINITE ELEMENT ANALYSIS | |
| RESULTS | 96 |
| 5.1 Finite Element Model | 96 |
| 5.2 Finite Element Analysis | 97 |
| 5.3 FEA and Test Results | 99 |
| 5.3.1 Natural Frequencies | 99 |
| 5.3.2 Mode Shapes | 100 |
| 5.3.3 Frequency Response Functions | 109 |
| | |
| 6. DISCUSSION AND CONCLUSION | 116 |
| 6.1 Test Setup | 116 |
| 6.2 Experimental Procedure and Test Results | 117 |
| 6.3 FEA and Experimental Results | 119 |
| 6.4 Conclusion | 120 |
| 6.5 Recommendation for Future Studies | 120 |
| | |
| APPENDIX | |
| 1. CONTITECH FS 70-7 Air Spring Technical Details | 121 |
| 2. LDS V450 Shaker Technical Details | 122 |

| | |
|--|-----|
| 3. AGILENT 35665A 2-Channel Dynamic Signal Analyzer Technical Specifications | 123 |
| 4. BRUEL&KJAER Impedance Head Type 8001 Technical Specifications | 124 |
| 5. BRUEL&KJAER Accelerometer Type 4384 Technical Specifications | 125 |
| 6. BRUEL&KJAER Charge Amplifier Type 2635 Technical Specifications | 126 |
| 7. BRUEL&KJAER Microphone Type 4165 Technical Specifications | 127 |
| 8. BRUEL&KJAER Microphone Preamplifier Type 2660 Technical Specifications | 128 |
| 9. BRUEL&KJAER Calibration Exciter Type 4294 Technical Specifications | 129 |
| 10. CASTLE Microphone Calibrator Type GA 601 Technical Specifications | 130 |
| 11. BRUEL&KJAER Accelerometer Type 4375 Technical Specifications | 131 |
| REFERENCES | 132 |

LIST OF TABLES

Table

| | |
|---|-----|
| 2.1 Forms of transfer function | 17 |
| 4.1 Natural frequencies of body-in-white | 78 |
| 4.2 Identification of modes | 92 |
| 4.3 Peak frequencies from SPL measurement | 93 |
| 4.4 Peak frequencies from vibration and sound measurements | 94 |
| 5.1 Natural frequencies and modes from FEA | 98 |
| 5.2 Natural frequencies | 99 |
| 5.3 Mode shapes and corresponding natural frequencies from FEA and experiments | 100 |

LIST OF FIGURES

Figures

| | | |
|------|--|----|
| 1.1 | Vibration test and analysis for a plane | 4 |
| 1.2 | Daewoo body-in-white | 7 |
| 1.3 | Honda NSX aluminum monocoque body | 7 |
| 1.4 | Honda Insight aluminum hybrid body | 8 |
| 1.5 | Detailed body model substructures for Nissan Quest | 9 |
| 1.6 | Detailed body model for Nissan Quest | 9 |
| 1.7 | Primary automotive components contributing to interior noise in the passenger compartment | 10 |
| 1.8 | Mode numbers for primary automotive components | 11 |
| 1.9 | Fiat small size saloon car body-in-white | 12 |
| 2.1 | SDOF system | 15 |
| 2.2 | FRF magnitude plot for SDOF | 19 |
| 2.3 | FRF real part plot for SDOF system | 19 |
| 2.4 | FRF imaginary part plot for SDOF system | 20 |
| 2.5 | FRF plot for 3 DOF system | 21 |
| 2.6 | SDOF contributions in MDOF system response | 21 |
| 2.7 | Test setup configuration for frequency response measurements | 22 |
| 2.8 | Suspension of spacecraft part with cables | 23 |
| 2.9 | Suspension of diskette drive | 24 |
| 2.10 | Suspension of car body using elastic ropes | 24 |
| 2.11 | Locomotive cab supported with air springs | 25 |
| 2.12 | Satellite dish with constrained support | 25 |

| | |
|--|----|
| 2.13 Impact hammer excitation of Taurus launch vehicle [14] | 27 |
| 2.14 Shaker excitation of Taurus launch vehicle | 27 |
| 2.15 Step relaxation excitation of Taurus launch vehicle | 28 |
| 2.16 Shaker attachment to structure [15] | 28 |
| 2.17 Suspended shakers [16] | 29 |
| 2.18 Impedance head connected to bridge base model [17] | 30 |
| 2.19 Accelerometer mounting methods [19] | 31 |
| 2.20 Accelerometer mounting using bees-wax | 31 |
| 2.21 Freely suspended structure, shaker testing | 32 |
| 2.22 FRF, magnitude and phase | 33 |
| 2.23 FRF, real and imaginary parts | 33 |
| 2.24 Quadrature peak picking method | 34 |
| 2.25 Circle fit method | 35 |
| 2.26 Freely supported plate | 35 |
| 2.27 Plate FRF | 36 |
| 2.28 Measurement locations on plate | 36 |
| 2.29 Mode 1 | 37 |
| 2.30 Mode 2 | 37 |
| 3.1 Planned test setup configuration | 38 |
| 3.2 ContiTech air spring type FS 70-7 | 39 |
| 3.3 Front air spring support parts together | 40 |
| 3.4 Front support assembled | 40 |
| 3.5 Rear air spring support parts together | 41 |
| 3.6 Rear support assembled | 41 |
| 3.7 Body-in-white with air spring supports | 42 |
| 3.8 Shaker suspended | 43 |
| 3.9 Elastic ropes and mechanical jack | 43 |
| 3.10 Alignment adjustments for shaker | 44 |
| 3.11 Stinger and its connections | 44 |
| 3.12 Excitation instruments and source signal transmission | 45 |
| 3.13 Impedance head attached to front top adaptor part | 46 |

| | |
|--|----|
| 3.14 Impedance head in place | 46 |
| 3.15 Stinger and cable connections to impedance head | 46 |
| 3.16 Accelerometer mounted on body using bees-wax | 47 |
| 3.17 Charge amplifiers connected to two input channels of analyzer | 47 |
| 3.18 LDS V450 electrodynamic shaker | 48 |
| 3.19 LDS V450 electrodynamic shaker fan unit | 48 |
| 3.20 LDS PA 500 power amplifier | 49 |
| 3.21 Agilent 35665A 2-channel dynamic signal analyzer | 49 |
| 3.22 B&K impedance head type 8001 | 50 |
| 3.23 B&K accelerometer type 4384 | 50 |
| 3.24 B&K charge amplifier type 2635 | 51 |
| 3.25 Microphone and preamplifier used for SPL measurements | 51 |
| 3.26 General view of setup and instruments | 52 |
| 4.1 FRF measurements for two different air spring pressures | 54 |
| 4.2 Rigid body frequency change by changing air spring pressure | 55 |
| 4.3 Input force spectrum used in the tests | 56 |
| 4.4 Point mobility @ shaker excitation location | 57 |
| 4.5 Measurement and force application locations on body-in-white | 58 |
| 4.6 FRF between force at point o and response location 1 | 59 |
| 4.7 FRF between force at point o and response location 2 | 59 |
| 4.8 FRF between force at point o and response location 3 | 60 |
| 4.9 FRF between force at point o and response location 4 | 60 |
| 4.10 FRF between force at point o and response location 5 | 61 |
| 4.11 FRF between force at point o and response location 6 | 61 |
| 4.12 FRF between force at point o and response location 7 | 62 |
| 4.13 FRF between force at point o and response location 8 | 62 |
| 4.14 FRF between force at point o and response location 9 | 63 |
| 4.15 FRF between force at point o and response location 10 | 63 |
| 4.16 FRF between force at point o and response location 11 | 64 |
| 4.17 FRF between force at point o and response location 12 | 64 |

| | |
|---|----|
| 4.18 FRF between force at point o and response location 13 | 65 |
| 4.19 FRF between force at point o and response location 14 | 65 |
| 4.20 FRF between force at point o and response location 15 | 66 |
| 4.21 FRF between force at point o and response location 16 | 66 |
| 4.22 FRF between force at point o and response location 17 | 67 |
| 4.23 FRF between force at point o and response location 18 | 67 |
| 4.24 FRF between force at point o and response location 19 | 68 |
| 4.25 FRF between force at point o and response location 20 | 68 |
| 4.26 FRF between force at point o and response location 21 | 69 |
| 4.27 FRF between force at point o and response location 22 | 69 |
| 4.28 FRF between force at point o and response location 23 | 70 |
| 4.29 FRF between force at point o and response location 24 | 70 |
| 4.30 FRF between force at point o and response location 25 | 71 |
| 4.31 FRF between force at point o and response location 26 | 71 |
| 4.32 FRF between force at point o and response location 27 | 72 |
| 4.33 FRF between force at point o and response location 28 | 72 |
| 4.34 FRF between force at point o and response location 29 | 73 |
| 4.35 FRF between force at point o and response location 30 | 73 |
| 4.36 FRF between force at point o and response location 31 | 74 |
| 4.37 FRF between force at point o and response location 32 | 74 |
| 4.38 FRF between force at point o and response location 33 | 75 |
| 4.39 FRF between force at point o and response location 34 | 75 |
| 4.40 Natural frequencies from FRF plot @ location 13, 10-60 Hz | 76 |
| 4.41 Natural frequencies from FRF plot @ location 31, 60-100 Hz | 76 |
| 4.42 Coherence for FRF measurement @ location 13 | 77 |
| 4.43 Imaginary part of FRF @ 27.7 Hz, location 1 | 79 |
| 4.44 Displacement @ location 1, 27.7 Hz | 80 |
| 4.45 Circle fit region @ location 1, 41.1 Hz | 80 |
| 4.46 Mode shape factor estimation by circle fit @ location 1, 41.1 Hz | 81 |
| 4.47 Mode shape @ 21.7 Hz | 81 |
| 4.48 Mode shape @ 27.7 Hz | 82 |

| | |
|---|-----|
| 4.49 Mode shape @ 32.4 Hz | 82 |
| 4.50 Mode shape @ 35.9 Hz | 83 |
| 4.51 Mode shape @ 37.1 Hz | 83 |
| 4.52 Mode shape @ 41.1 Hz | 84 |
| 4.53 Mode shape @ 44.7 Hz | 84 |
| 4.54 Mode shape @ 47.3 Hz | 85 |
| 4.55 Mode shape @ 55.0 Hz | 85 |
| 4.56 Mode shape @ 57.0 Hz | 86 |
| 4.57 Mode shape @ 60.3 Hz | 86 |
| 4.58 Mode shape @ 62.7 Hz | 87 |
| 4.59 Mode shape @ 65.8 Hz | 87 |
| 4.60 Mode shape @ 73.2 Hz | 88 |
| 4.61 Mode shape @ 74.9 Hz | 88 |
| 4.62 Mode shape @ 76.3 Hz | 89 |
| 4.63 Mode shape @ 78.2 Hz | 89 |
| 4.64 Mode shape @ 87.2 Hz | 90 |
| 4.65 Mode shape @ 90.3 Hz | 90 |
| 4.66 Mode shape @ 92.5 Hz | 91 |
| 4.67 Mode shape @ 97.0 Hz | 91 |
| 4.68 SPL, 401 points | 93 |
| 4.69 Mode descriptions | 95 |
| 4.70 Sound pressure levels at peaks | 95 |
| 5.1 Surface model of body-in-white | 96 |
| 5.2 FE model of body-in-white | 97 |
| 5.3 1 st torsional mode @ 24.2 Hz, FEA | 101 |
| 5.4 1 st torsional mode @ 21.7 Hz, Test | 101 |
| 5.5 2 nd torsional mode @ 30.1 Hz, FEA | 102 |
| 5.6 2 nd torsional mode @ 27.7 Hz, Test | 102 |
| 5.7 3 rd torsional mode @ 36.0 Hz, FEA | 103 |
| 5.8 3 rd torsional mode @ 35.9 Hz, Test | 103 |
| 5.9 1 st bending mode @ 42.2 Hz, FEA | 104 |

| | |
|--|-----|
| 5.10 1 st bending mode @ 41.1 Hz, Test | 104 |
| 5.11 2 nd bending mode @ 49.2 Hz, FEA | 105 |
| 5.12 2 nd bending mode @ 47.3 Hz, Test | 105 |
| 5.13 Roof models | 106 |
| 5.14 Roof shape @ 21.7 Hz, Test | 106 |
| 5.15 Roof shape @ 27.7 Hz, Test | 107 |
| 5.16 Roof shape @ 35.9 Hz, Test | 107 |
| 5.17 Roof shape @ 41.1 Hz, Test | 108 |
| 5.18 Roof shape @ 47.3 Hz, Test | 108 |
| 5.19 FEA vs. Test FRF plot locations | 109 |
| 5.20 FEA vs. Test FRF plot @ location 1, node 639 | 110 |
| 5.21 FEA vs. Test FRF plot @ location 2, node 13455 | 111 |
| 5.22 FEA vs. Test FRF plot @ location 3, node 16008 | 111 |
| 5.23 FEA vs. Test FRF plot @ location 4, node 33843 | 112 |
| 5.24 FEA vs. Test FRF plot @ location 5, node 112 | 112 |
| 5.25 FEA vs. Test FRF plot @ location 6, node 27859 | 113 |
| 5.26 FEA vs. Test FRF plot @ location 7, node 43046 | 113 |
| 5.27 FEA vs. Test FRF plot @ location 8, node 14135 | 114 |
| 5.28 FEA vs. Test FRF plot @ location 9, node 51841 | 114 |
| 6.1 Accelerometer selection and mounting effects on FRF | 118 |

LIST OF SYMBOLS AND ABBREVIATIONS

| | | |
|------|---|-------------------------------|
| FE | : | Finite Element |
| FEA | : | Finite Element Analysis |
| FEM | : | Finite Element Method |
| EMA | : | Experimental Modal Analysis |
| NVH | : | Noise Vibration and Harshness |
| SDOF | : | Single Degree of Freedom |
| MDOF | : | Multiple Degrees of Freedom |
| FRF | : | Frequency Response Function |
| PC | : | Personal Computer |
| SISO | : | Single Input Single Output |
| CAD | : | Computer Aided Design |
| B&K | : | Brüel&Kjaer |
| BNC | : | Bayonet Neill-Concelman |
| SPL | : | Sound Pressure Level |

CHAPTER 1

INTRODUCTION

1.1 STRUCTURAL VIBRATION

Designing products today offers many challenges: they must be stronger, lighter, safer and quieter. Products have to satisfy a widening range of design criteria, including environmental impacts. To keep development time and cost competitive, companies rely on simulation tools. Finite element analysis (FEA) is a powerful technique to simulate the mechanical behavior of a product. The FEA method has matured to a point where design, meshing, analysis and post-processing are highly integrated and automated. This predictive approach relies on the quality of the model, the software to analyze it and the engineering judgment of the analyst. A finite element model is a great tool to assist in both static and dynamic analyses. But care should be taken not to put too much faith and confidence in a model that has not been verified. It is required to perform experiments on actual system to verify the model. Experimental analysis methods are based on prototype measurements under laboratory conditions or testing real-life situations. They are effective to learn about the product and the environmental conditions. In a competitive world, a trial-and-error design optimization approach involving a series of prototypes is too time-consuming and expensive.

Modeling errors are inevitable to arise when a continuous structure is represented by a discrete FE mesh. In general the accuracy and reliability of the

FE solution is dependent on the shape function of the chosen elements and thus on the elements used in the dynamic analysis. There exist many types of elements in FE packages, e.g. bar, beam, shell, plate, block etc., and each are described by different shape functions. The choice of elements depends to a great extent on the geometry of the structure and to some extent on individual preference, as there is more than one element that can be used to create the FE model. For most complex structures a combination of several types of elements is necessary for an efficient and accurate analysis.

A complex structure is usually assembled from different components through a number of joints. Unfortunately, the modeling of structural joints is still an underdeveloped area in structural dynamics and their idealization normally assumes the elements/nodes between joints to be perfectly connected through fixed-fixed interfaces. Some FE analysts suggest that the nodes between joints may not be directly connected and some forms of joint stiffnesses must be defined. However, this immediately increases the number of degrees of freedom in the model and usually the spring values of a joint are not well-defined in all rotational directions.

As computer performance increases and computer costs decrease, the potential for computer simulation to play an important role in the design of high performance mechanical equipment has increased and spread to many different industries. Yet with all this improvement in computer power and availability, the computer simulations can at times bog down a program with months of number crunching or with doubts due to inconclusive results.

Particularly when a program includes test-analysis correlation, the analysts can be involved in a seemingly endless intensive process of rerunning analyses to try to match test results or to explain differences. Most engineers who are experienced in finite element modeling and dynamic analysis methods will readily define how long it will take to build the models and produce the results but will only venture an estimate with large uncertainty for the time and cost of correlation with test. The very fact that it is still experienced large differences

between test and analysis demonstrates that the test still plays a tremendously important role in the design of mechanical equipment.

The use of light-weight materials, truss frameworks and components milled from solid material makes a modern structure usually very stiff in all directions and provides an ideal solution for the structural optimization problem under a statically-loaded condition. However, this type of light-weight structures will have many flexural modes in the low-frequency range and is more likely to be excited into resonance under normal working conditions which may then cause human discomfort, fatigue cracking and, at worst, result in catastrophic failure. This was experienced in 1942, when wind induced vibration destroyed the new Tacoma Narrows suspension bridge [1]. To this end, the incorporation of vibration analysis in product design has grown considerably in recent years.

Any structure, submitted to an external excitation will deform and vibrate in a characteristic manner that should be known in advance. In fact, vibration is a combination of different modes of vibration defined by the frequency from which the vibration is generated, its shape, the fact that this mode is damped or not, the properties of rigidity, and the inertia characteristic of this mode. All these values are known as the modal parameters of the considered vibration mode and are the result of the original mechanical design. Modes when properly damped are not considered dangerous, as oscillations disappear with time. However, should a structure be excited by a force whose frequency corresponds to one of its modes, the vibrations, instead of being damped down, will increase until the destruction of the structure. It is therefore essential to know the different modes of vibration, especially those which, because of their proximity, influence each other. This step is performed by calculations from theoretical models and by experimentation.

Because of the approximations and suppositions inherent in any numerical calculation, the results obtained will include some errors. Experimentation is therefore the only way to eliminate this dangerous uncertainty, by calculating the real modes from the measured data.

1.2 VIBRATION ANALYSIS

Vibration analysis is based on the measurement of the response of the structure submitted to a defined excitation. The different modes of vibration are obtained from the measured values. A vibration test system will therefore be able to generate, with extreme accuracy, different types of excitation in a controlled way without modifying the structure to be tested. The method of acquisition and measurement of responses will also be optimized. The analysis system, as well as the exciters and transducers, must be precisely calibrated and maintained so that large amounts of data can be processed in an accurate, user-friendly manner. The integration of computerized systems represents a significant advantage but the importance of the user should not be minimized.



Figure 1.1 Vibration test and analysis for a plane

Structural dynamic measurements are often carried out to identify or to verify a mathematical model of a test structure. Vibration modes deduced from analysis of measured data can be compared with corresponding data generated by a finite element model and the results are used to adjust or to correct the theoretical model (Model Updating) by making it suitable for predictive design.

Vibration measurements for modeling purposes are called “Experimental Modal Analysis” (EMA) or “Modal Testing”, which activity is focused on determining a mathematical model of structure’s dynamic behavior from measured applied inputs and resulting outputs.

Undertaking a modal test requires expert knowledge of techniques of instrumentation, signal processing and modal parameter estimation. Essentially, the aspects of the measurement process which demand particular attention are: experimental test rig preparation, correct transduction to measure force input and vibration response, and signal conditioning and processing. Great care must be taken in these aspects during the experiment in order to acquire high-quality data. The first stage of test preparation involves some mechanical topics such as the structure's support and excitation conditions. The second stage consists of transducer selection, which is related to the structure characteristics and to environmental conditions. At the third stage, the vibration response measurement takes place and the experimenter must pay particular attention to acquisition accuracy and data quality. The last stage consists of a detailed analysis of measurement data, including digital signal processing, which should be appropriate to the type of test used.

A basic measurement set-up used for modal tests consists of three major items: (i) an excitation device (attached shaker or hammer), (ii) a transduction system, and (iii) an analyzer which measures the signals in output from the transducers. There are many different possibilities in the area of transduction mechanisms but for the most part, piezoelectric transducers (such as accelerometers) are widely used. As these devices are attached to the tested structure, they often introduce a non-trivial mass loading, especially in light or small structures. In these cases, non-contact transducers are required. Moreover, some applications need vibration measurements to be made at many points in order to have a high spatial resolution, for instance in detecting small-size structural faults. Conventional transducers are often not suitable to perform this type of test.

For most engineering structures the damping values are both small and ill-defined so that the damping matrix cannot be modeled in the same detail as the mass and stiffness matrices of the structure. Finally, the boundary conditions of a test structure and an FE model cannot be matched exactly as it is very difficult

either (i) to achieve free-free or perfect clamped conditions in practice or (ii) to model the elastic boundaries of the measurement stage in detail.

The theoretical and practical considerations of performing a vibration test and data processing have been investigated at length, and a lot of papers have been published in the technical literature over a period of several decades.

In 1947, Kennedy and Panu [2] suggested that certain characteristics of vector response plots - the real and imaginary vector components of vibration response with respect to the applied forces - could be more useful, and discussed their utility in the conduct and interpretation of modal testing. Following the 'characteristic phase lag theory' of damped structures given by Fraeijs de Veubeke (1956) [3], Bishop and Gladwell [4] in 1963 provided the theoretical background to the problem of resonance testing. In addition to Kennedy and Panu's method, Bishop and Gladwell also assessed the accuracy of several modal testing techniques developed by Lewis and Wrisley [5] in 1950, Trasill-Nash [6] in 1958 and Asher [7] in 1958, respectively. In the 1960s and 1970s, there were major advances in vibration measurement equipment and different modal testing techniques which are currently used were established.

More recently, with the availability of computer-controlled measurement equipment and special-purpose analysis software, both the measurement time and human effort have been reduced and the reliability and accuracy of measured response and experimentally-derived data have also been improved significantly. The details of practical implementation of vibration testing have been fully discussed by Ewins [8].

1.3 VIBRATION STUDIES ON CAR BODIES

Today, passenger car bodies are constructed as fully integral bodies (monocoque). Fully integral body is produced by welding the sheet metal (mainly steel is used recently) parts to form a single part body. This single body when the doors and hatches are separated is called body-in-white. A Daewoo car body-in-

white is shown in Figure 1.2. Different types of body construction types are used for trucks and busses.

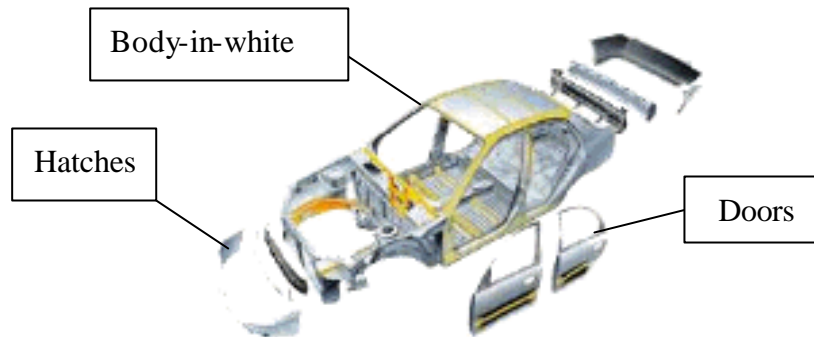


Figure 1.2 Daewoo body-in-white

New designs for car bodies are continuously made by leading companies in automotive industry. The basic goal in these designs is to reduce the weight of the car body to achieve lowest fuel consumption. In order to increase the fuel efficiency, HONDA R&D Department has replaced steel with aluminum for body-in-white [9] and produced Honda NSX in 1990, shown in Figure 1.3.

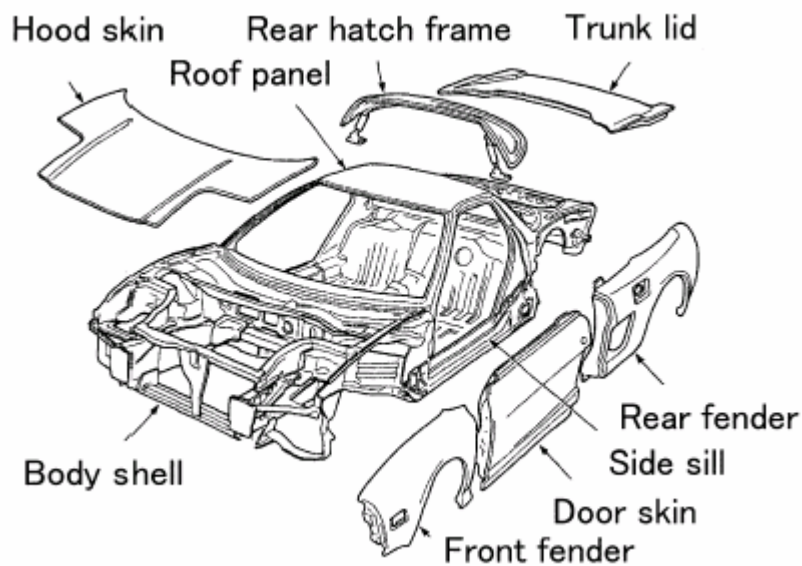


Figure 1.3 Honda NSX aluminum monocoque body

As a result, a body which was 40% lighter than a steel body was obtained. However, aluminum sheets are subject to some major manufacturing restrictions compared with steel sheets. Therefore a new body-in white design, called aluminum hybrid body structure, has been developed combining the monocoque and space frame body structures, shown in Figure 1.4. Compared with the aluminum monocoque body, the aluminum hybrid body has 15% fewer parts and 24% fewer welding points. Since aluminum has a Young's modulus which is one-third of that of steel, using thicker sheets parts in necessary points a lightweight body with high rigidity has become possible.

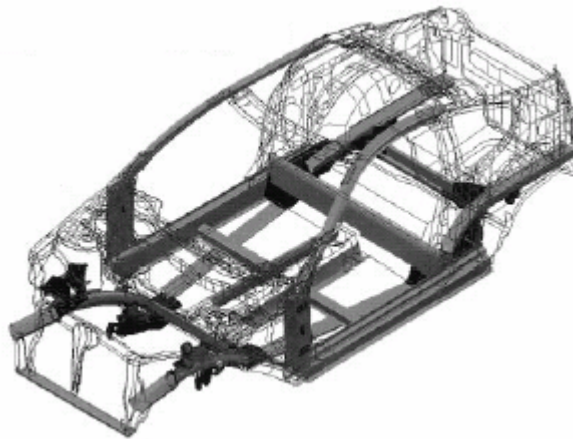


Figure 1.4 Honda Insight aluminum hybrid body

As a result of studies on different type of body structures, it is possible to achieve weight reduction, further improvements in rigidity, high collision safety, cost savings and higher fuel efficiency in automobiles. However, there are some additional considerations on these designs such as the failure and human discomfort due to vibrations in car bodies. All of these studies performed made as a part of noise, vibration and harshness (NVH) analysis of automobiles.

As a part of car body design and development, analytical modeling and simulation activities are utilized extensively to ensure an optimal performance of the vehicle for NVH. Finite element methods are being used routinely to analyze current production automobiles for vibration and dynamic response [10]. A body-in-white FE model is prepared using substructures and then static and dynamic

analyses are performed on the whole body-in-white model using FEA software. Using substructures allows different sections to be modeled concurrently and keeps the time to build the model minimum. Detailed body model substructures for Nissan Quest are shown in Figure 1.5. The final body model consisted of approximately 84,000 DOF, is shown in Figure 1.6 [11].

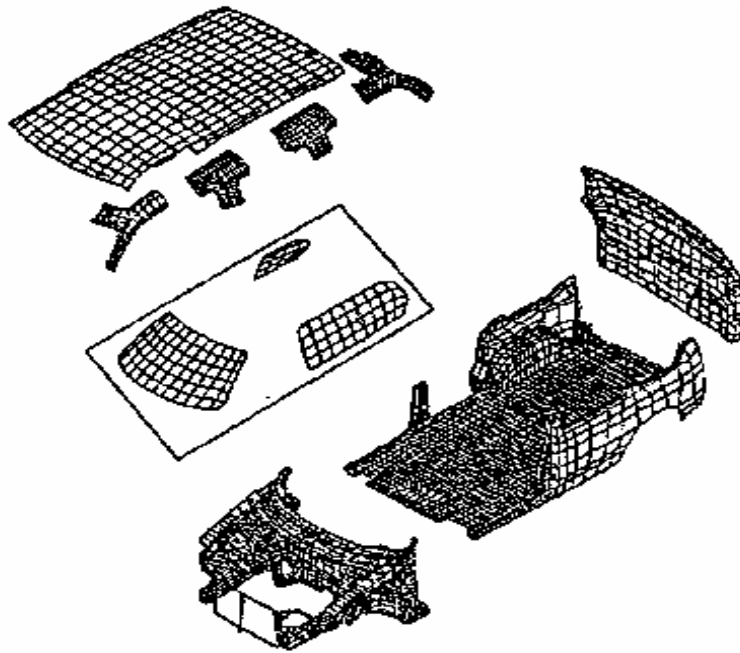


Figure 1.5 Detailed body model substructures for Nissan Quest

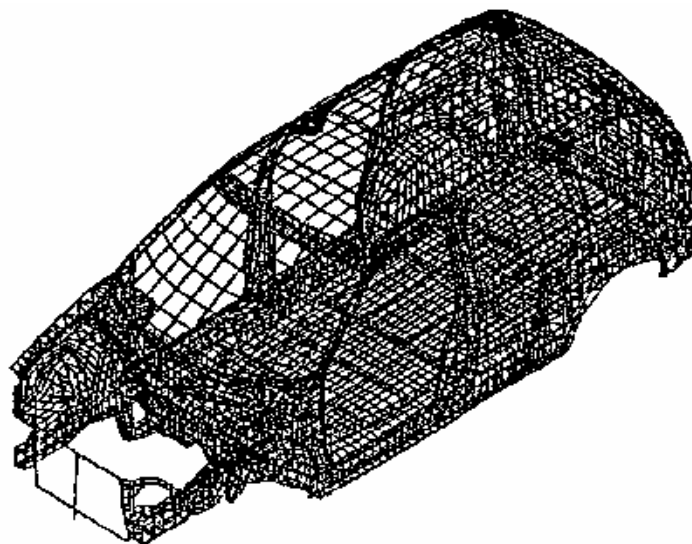


Figure 1.6 Detailed body model for Nissan Quest

Vehicle components such as the engine, transmission, drivetrain, tire and exhaust system transmit noise through the structural connection to the body which dominates the interior cabin noise. The excitations generated within these dynamic components induce structural vibrations. The vibrations are subsequently transmitted across bearings, casing and mounts to the body panels. Interior noise is radiated from these vibrating panels. Primary automotive components and structure-borne paths contributing to the interior noise in the passenger compartment are shown in Figure 1.7.

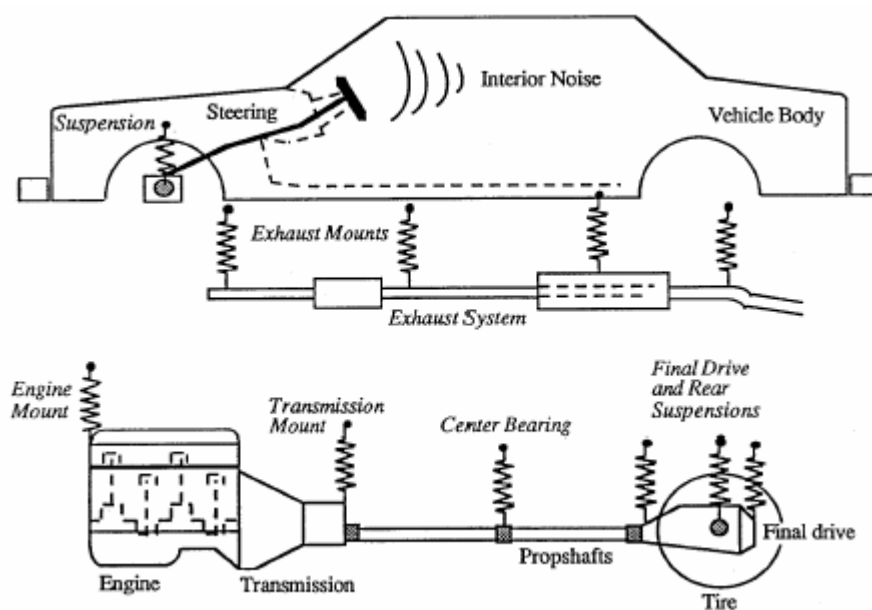


Figure 1.7 Primary automotive components contributing to interior noise in the passenger compartment

It is advantageous to examine the vehicle body structure in isolation prior to a study of the complete vehicle. From a noise generation point of view the vehicle structure is the final radiator in the energy transmission path from the load surface. Therefore, the resonant conditions and mode shapes of the body must be examined for its vibration and noise transmission characteristics.

Typical automotive systems can be divided up into various low, moderate and high modal density components depending on the frequency range of interest.

For most structure-borne noise problems, the examples of low modal density components are engine, transmission and drivetrain, and high modal density component includes the body. Other components such as suspension, steering system and exhaust system have moderate structural modal densities [12]. Figure 1.8 illustrates the typical number of modes below 1000 Hz for primary automotive components.

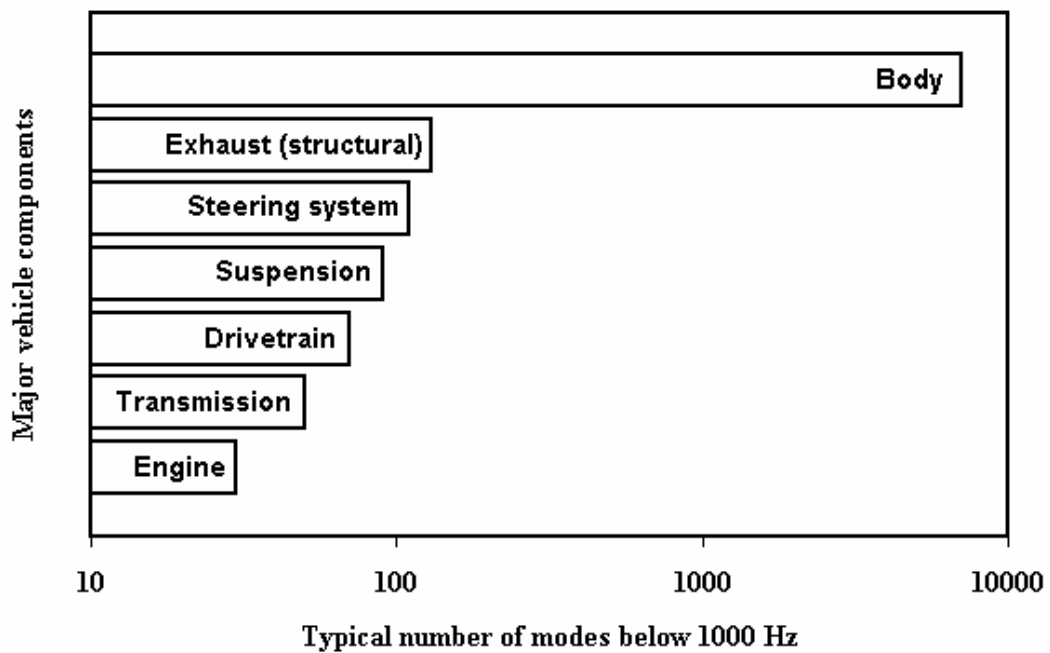


Figure 1.8 Mode numbers for primary automotive components

The finite element method can be used to model low and moderate modal density components reasonably well using very detailed representations. On the other hand, it is desirable to represent high modal density components using experimental frequency response functions. This ensures that the component is represented by actual system response and theoretical modeling errors are eliminated.

Although complete vehicle structural models based on the finite element method have become a practical alternative to testing within the last years, it is still hardly necessary to perform vibration tests on car bodies.

1.4 STRUCTURE OF THESIS

In the previous study, a finite element model of the car body-in-white which is available in Automotive Laboratory, Middle East Technical University, Ankara, has been prepared. The car body-in-white is a fully integral body structure of a Fiat small size saloon car, shown in Figure 1.9. Using Msc.Marc finite element analysis program, static and dynamic analyses have been performed on the body. In dynamic analysis, first 10 modes and the major structural modes have been found for the body-in-white.



Figure 1.9 Fiat small size saloon car body-in-white

The major subjective of this thesis study is to determine the natural frequencies and mode shapes of the body-in-white and to compare the results of finite element analysis and experimental study.

The work reported in this thesis has been divided into four main chapters. Chapter 2 introduces the frequency response function and vibration testing

fundamentals. Chapter 3 presents the experimental setup and instruments used in this study. Chapter 4 is completely devoted to the experimental results. Chapter 5 includes the comparison of finite element analysis and experimental results. Finally, Chapter 6 discusses the results and concludes on the thesis work.

CHAPTER 2

VIBRATION TESTING

One area of structural dynamics testing is vibration testing. Vibration testing and analysis is the process of characterizing the dynamic properties of an elastic structure by identifying its natural frequencies and modes of vibration. Each mode has a specific natural frequency which can be identified from practically any point on the structure. In addition it has a characteristic mode shape which defines the mode over the entire structure. Once these dynamic properties of the structure are defined, the behavior of the structure in its operating environment can be predicted and controlled.

Techniques have been developed which allow the modes of vibration of any structure to be identified from measured transfer function data. Once a set of transfer (frequency response) functions relating points of interest on the structure have been measured and stored, they are used to obtain the natural frequencies and mode shapes of the structure. Responses of many modes can be measured simultaneously and complex mode shapes can be directly identified using these frequency response functions.

2.1 FREQUENCY RESPONSE FUNCTION

It is effective to use single and multiple degrees of freedom lumped models for introducing the concept of transfer function. If the single degree of freedom (SDOF) system shown in Figure 2.1 behaves linearly and the mass is

subjected to any arbitrary force, a corresponding time varying motion will result. This motion can be described by a linear second order ordinary differential equation shown below Figure 2.1.

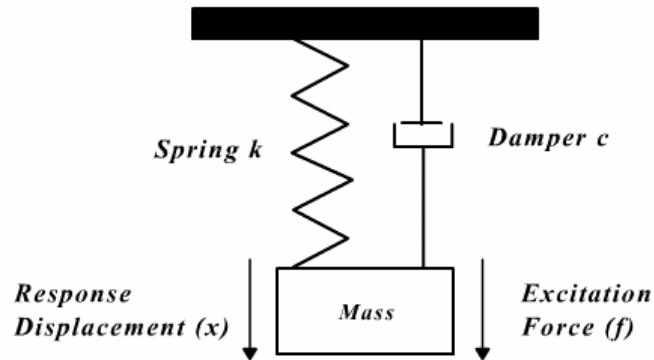


Figure 2.1 SDOF system

$$m \cdot \ddot{x} + c \cdot \dot{x} + k \cdot x = f(t)$$

$f(t)$: applied force

x : resultant displacement

\dot{x} : resultant velocity

\ddot{x} : resultant acceleration

For a multiple degree of freedom (MDOF) system, equations of motion for all the masses in the system are obtained using Newton's second law, and for general n -degree of freedom system, the equation of motion is given in matrix form as:

$$[M]\{\ddot{x}\} + [C]\{\dot{x}\} + [K]\{x\} = \{F\}$$

$[M]$: mass matrix ($n \times n$)

$[C]$: damping matrix ($n \times n$)

$[K]$: stiffness matrix ($n \times n$)

The time domain behavior of a complex dynamic system represented by the equations of motion for n-degree of freedom system is very useful information. However, frequency domain information turns out to be even more valuable in most cases. It is clearer to work on the equation of motion for SDOF when the transfer function is the main concern. Any function of time may be transformed into a function of the complex variable “s” using the formulation:

$$F(s) = \int_0^{\infty} f(t) \cdot e^{-st} \cdot dt$$

Taking the initial velocity and displacement as zero, the Laplace transform of the equation of motion takes the form:

$$[m \cdot s^2 + c \cdot s + k] \cdot X(s) = F(s)$$

Displacement, the resultant variable due to the applied force, in Laplace domain is solved from this equation and the result is found as:

$$X(s) = \frac{F(s)}{m \cdot s^2 + c \cdot s + k}$$

The denominator polynomial is called as the “characteristic equation” and the roots of this equation are called as the “poles” of the system. The roots of the numerator of the system are called the “zeros” of the system. Poles and zeros are critical frequencies of the system. The function X(s) becomes infinite at the poles while the function becomes zero at the zero.

Transfer function of a system is defined as the ratio of the output of the system to the input in the Laplace domain.

$$H(s) = \frac{X(s)}{F(s)}$$

From the equation given above, transfer function for a SDOF system is formulated as:

$$H(s) = \frac{1}{m \cdot s^2 + c \cdot s + k}$$

Transfer functions are called with different names according to the response variable. For example, the transfer function given above is called receptance or compliance transfer function. All types of transfer functions are given in Table 2.1.

Table 2.1 Forms of transfer function

| Definition | Response | Variable |
|-------------------|-----------------|--|
| Accelerance | Acceleration | $\frac{\textit{Acceleration}}{\textit{Force}}$ |
| Mobility | Velocity | $\frac{\textit{Velocity}}{\textit{Force}}$ |
| Receptance | Displacement | $\frac{\textit{Displacement}}{\textit{Force}}$ |

The Fourier transform is obtained by substituting “ $j\omega$ ” for “ s ”. This special case of the transfer function is called the “Frequency Response Function (FRF)”. The frequency response function is simply the transfer function measured along the $j\omega$ axis as formulated:

$$H(\omega) = \frac{1}{-m \cdot \omega^2 + j \cdot c \cdot \omega + k}$$

Using the definitions shown, the classical form of the frequency response function for SDOF system can be written as:

$$H(\omega) = \frac{1}{k \cdot \left[1 + 2 \cdot \zeta \cdot j \cdot \left(\frac{\omega}{\omega_n} \right) - \frac{\omega^2}{\omega_n^2} \right]}$$

$$\omega_n^2 = \frac{k}{m}$$

$$\zeta = \frac{c}{c_{critical}} = \frac{c}{2 \cdot \sqrt{k \cdot m}}$$

For an n degree of freedom (MDOF) system, the equation of motion is given in matrix form:

$$[G(s)] \cdot \{X(s)\} = F(s)$$

$\{F(s)\}$: Laplace transform of the applied force vector

$\{X(s)\}$: Laplace transform of the resulting output vector

$[G(s)]$: $[Ms^2 + Cs + K]$ (system matrix)

Then the transfer matrix $H(s)$ is defined as the inverse of the system matrix. Each element of the transfer matrix $H(s)$ is a transfer function.

$$H(s) = [Ms^2 + Cs + K]^{-1}$$

Most common way of presenting frequency response function (FRF) is to plot magnitude versus frequency. FRF magnitude versus frequency plot for SDOF system mentioned above is shown in Figure 2.2. At resonance, the response magnitude is a maximum and is limited by the amount of damping in the system.

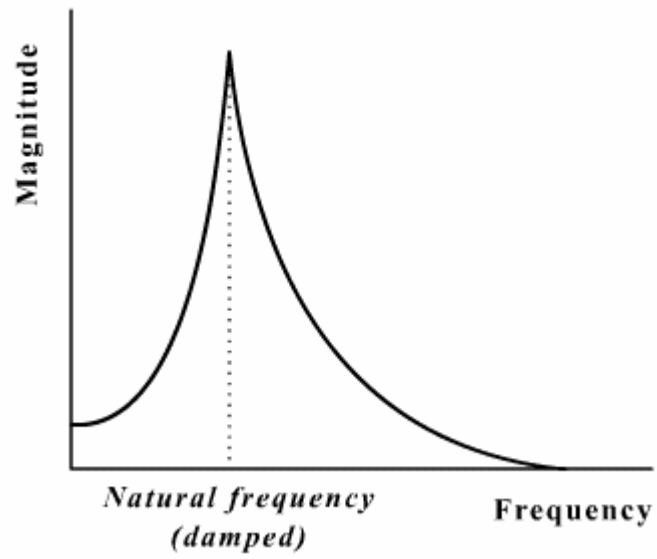


Figure 2.2 FRF magnitude plot for SDOF system

In Figure 2.3 and 2.4, other forms of frequency response presentation are shown. Real part and imaginary part of FRF versus frequency are plotted. For a proportionally damped system, the imaginary part is maximum and the real part zero at resonance.

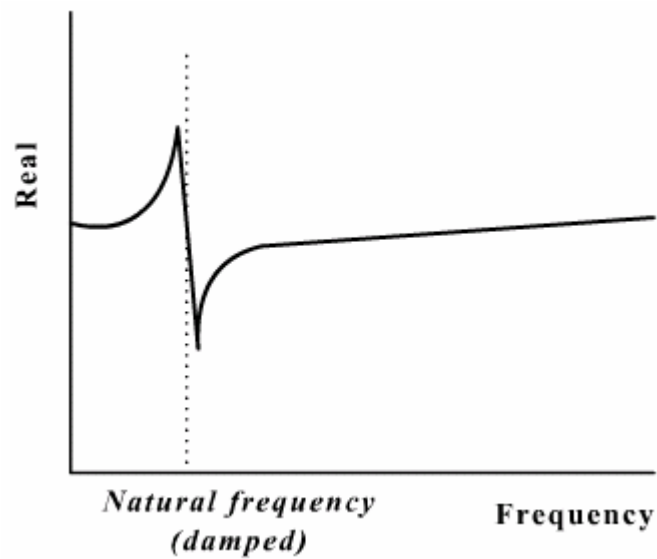


Figure 2.3 FRF real part plot for SDOF system

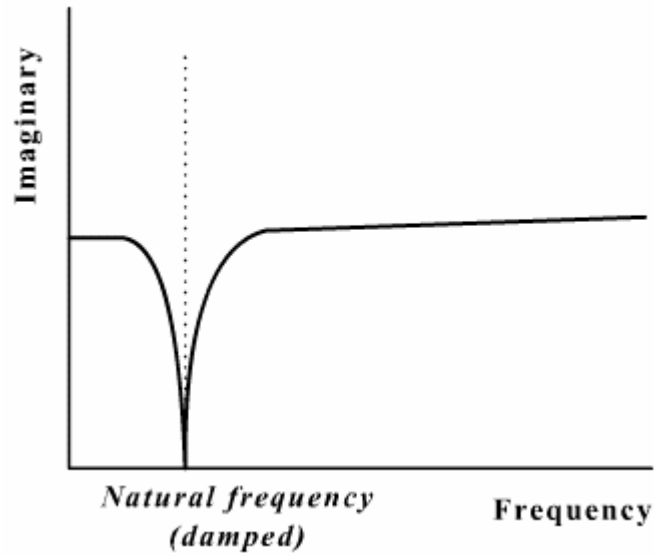


Figure 2.4 FRF imaginary part plot for SDOF system

For the MDOF case, a unique displacement vector called the mode shape exists for each distinct frequency. The “modal coefficients” identifies the amount each mode contributes to total response at a particular point. Assuming linear and stationary system, modal coefficients can be estimated using different SDOF methods explained in following subjects in this chapter. The general form of frequency response function for n degree of freedom system is given as:

$$H(\omega) = \sum_{r=1}^n \frac{A_r}{(\omega_{n_r}^2 - \omega^2) + j \cdot (2 \cdot \zeta \cdot \omega \cdot \omega_{n_r})}$$

ω_n : undamped natural frequency

A_r : modal coefficient

The frequency response of a MDOF system can be presented as the superposition of the SDOF systems. 3 degrees of freedom system response is shown in Figure 2.5. While adding the SDOF responses, the amount each mode contributes to total response at a particular point is also taken into account. The individual contributions of each degree of freedoms are shown in Figure 2.6.

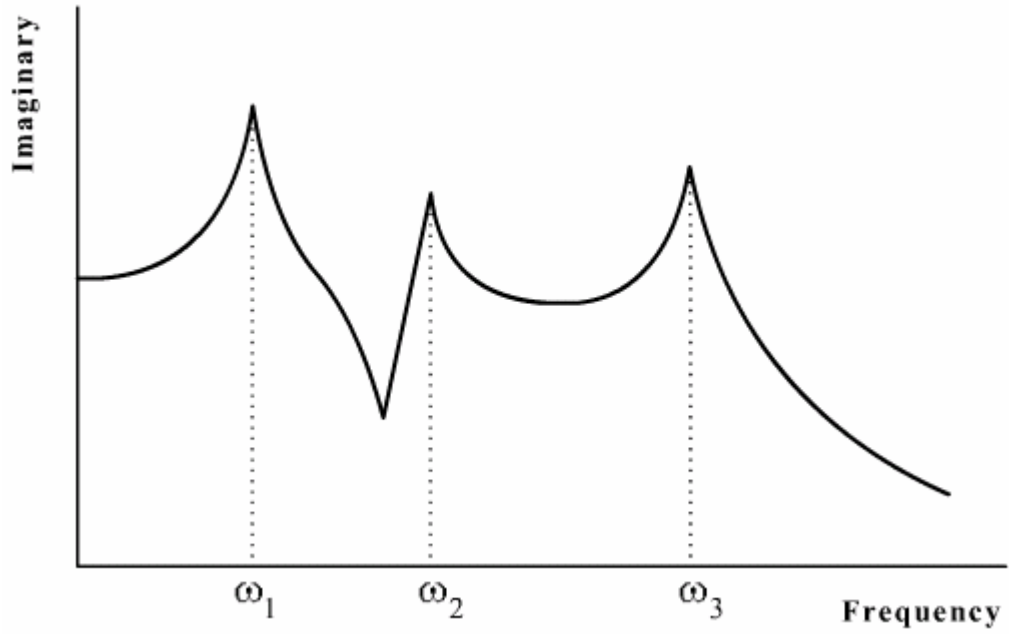


Figure 2.5 FRF plot for 3 DOF system

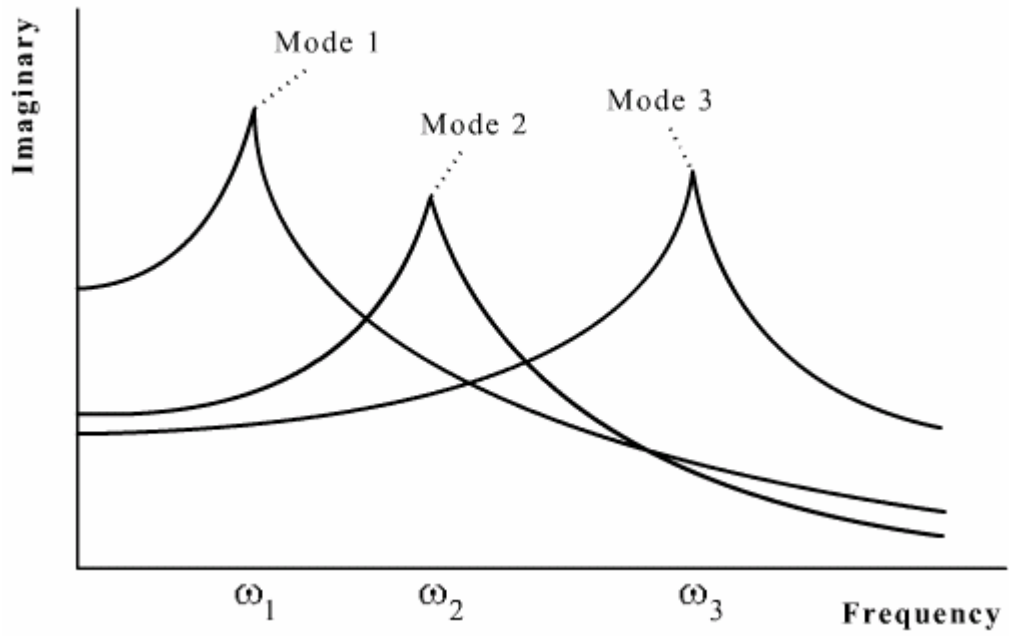


Figure 2.6 SDOF contributions in MDOF system response

2.2 FREQUENCY RESPONSE MEASUREMENTS

The general test configuration for frequency response measurements is shown in Figure 2.7. The major factors to be considered in vibration testing can be listed as:

- Supporting the structure
- Exciting the structure
- Data acquisition and implementation

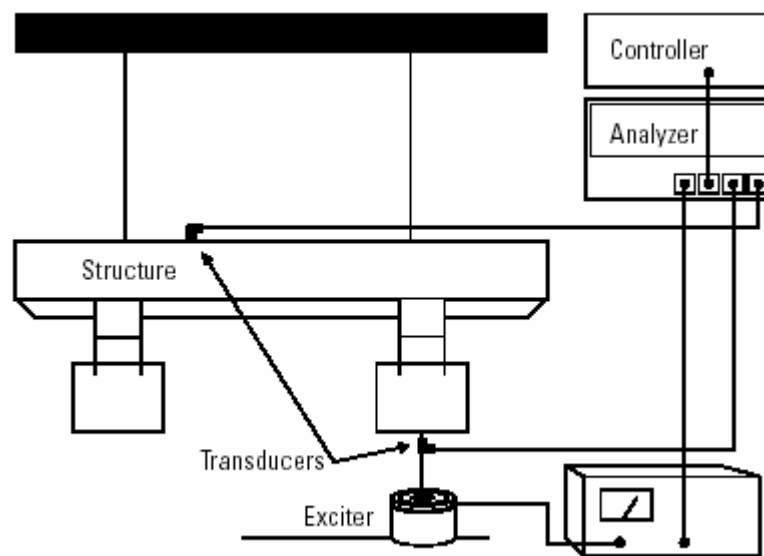


Figure 2.7 Test setup configuration for frequency response measurements

Analyzer provides data acquisition and signal processing operations. It contains several input and measurement channels for force and response measurements. Also it has excitation sources to drive the exciters. Different types of exciters can be used such as hammers and electrodynamic shakers. A signal source, a power amplifier and an attachment device is necessary when a shaker is used as exciter. The signal may be provided by the analyzer. Transducers, with amplifiers for signal conditioning, are used to measure the applied force and the responses from the structure. The controller is the user's analysis device such as a computer to data storage and result implementation.

2.2.1 Supporting the structure

The first step in vibration testing is to prepare the required boundary conditions for the structure. Since the overall structural characteristics are affected by these conditions, this step plays an important role in test setup preparation.

It is possible to have a structure with completely free or completely constrained boundary conditions analytically. But it is not possible to fully achieve these conditions practically. The free condition means that the structure is free in space without any restrictions and connections to ground. Since this condition can not be provided completely, the structure is suspended using very soft elastic ropes or placed on a very soft cushion. Some examples for supporting the test structure with elastic ropes are shown for vibration tests of a spacecraft part, a diskette drive and a car body are shown in Figure 2.8, 2.9 and 2.10.

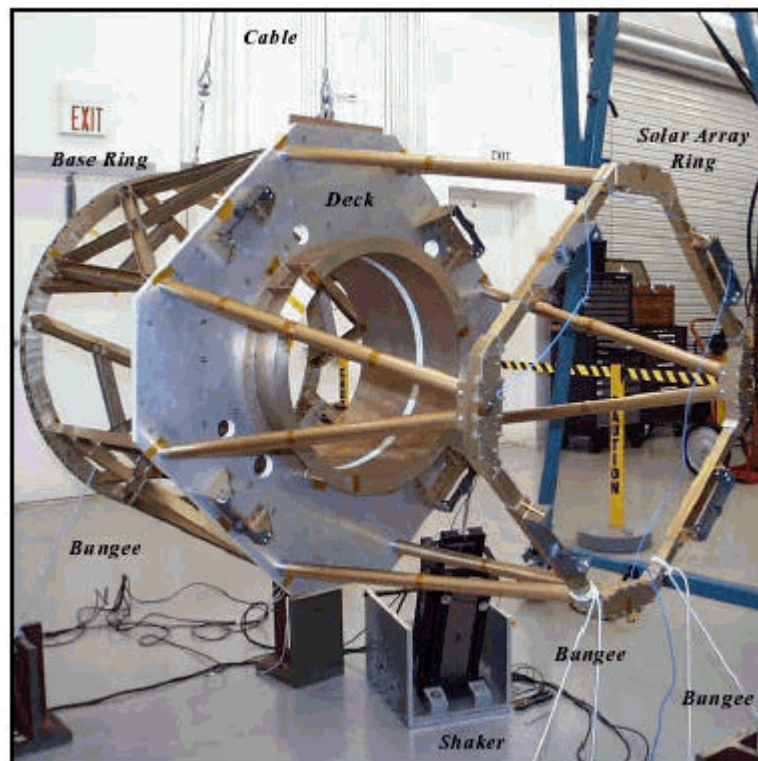


Figure 2.8 Suspension of spacecraft part with cables

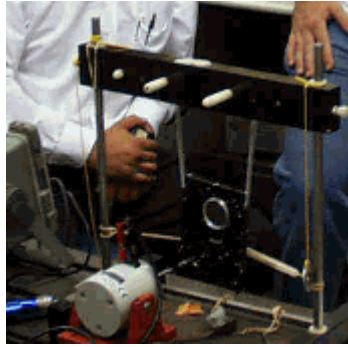


Figure 2.9 Suspension of diskette drive

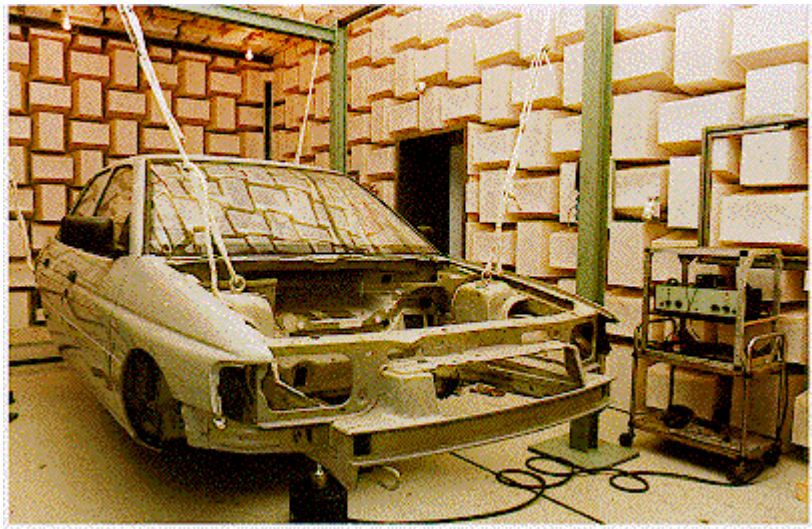


Figure 2.10 Suspension of car body using elastic ropes

By supporting the structure with elastic ropes, the structure is constrained to a degree and the rigid body modes have no longer zero frequency. However, it is possible to have rigid body frequencies much lower than the frequencies of flexible modes. Then they have negligible effects on the structure. As a rule of thumb, the highest rigid body frequency should be 10-20% of the first bending mode frequency.

In addition to placing the structure on a soft cushion, the structure may be placed on soft springs such as air springs. An example to this kind of support is shown in Figure 2.11. A locomotive cab is supported using 4 air springs and one of these supports is shown in the figure [13].



Figure 2.11 Locomotive cab supported with air springs

In constrained boundary conditions, the structure is attached to ground using bolted, riveted or welded connections. But it is difficult to achieve purely grounded conditions. The base will have its own response due to some flexibility. A satellite dish attached to ground is shown in Figure 2.12.

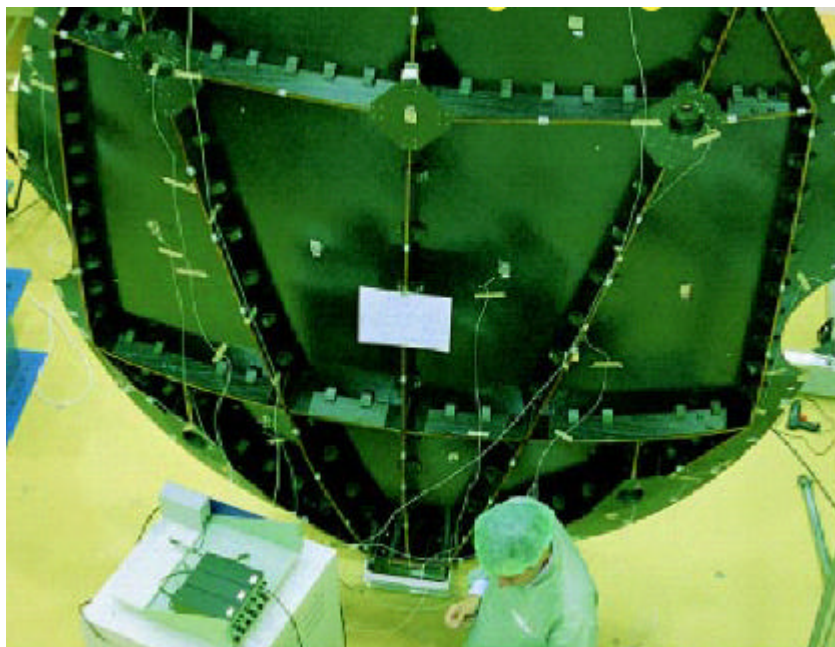


Figure 2.12 Satellite dish with constrained support

The appropriate supporting condition should be selected according to the needs and practical facilities. It is not feasible to support a large machine weighing several tons in free test. On the contrary, it may not be possible to attach a very small device to ground. In addition to these, both of these conditions should be provided for satellite vibration tests since it is free in its operating environment and it is attached to spacecraft while launching the satellite. Also for FEM correlation, the same boundary conditions should be provided.

2.2.2 Exciting the structure

The next step in vibration testing is to choose the excitation function. According to the type of excitation function, type of excitation system is selected. The excitation function is the mathematical signal used as input and the excitation system is the physical mechanism used to create the vibration corresponding to this signal.

Steady-state, periodic, random or transient excitation functions can be obtained using shaker, impactor, step relaxation or self-operation for excitation mechanism. In choosing the excitation function, dynamics of the structure plays an important role. Since it is not possible to measure the force when exciting the structure in its actual operating conditions, self-operating has limited use. Shakers and impact hammers are most commonly used in vibration tests. Step relaxation can be used to excite the structure with higher loads.

Impact hammer excitation is attractive because it requires very little hardware and provides shorter measurement times. However, it is difficult to obtain consistent results from impact hammer testing. The force applied to structure is measured from the force transducer attached at the tip of the impact hammer. Since the frequency range of excitation depends on the stiffness contacting surfaces, using harder or softer tips the frequency content can be determined during testing. The harder the tip, the shorter the pulse duration and thus the higher the frequency content. Impact hammer excitation of Taurus launch vehicle is shown in Figure 2.13.

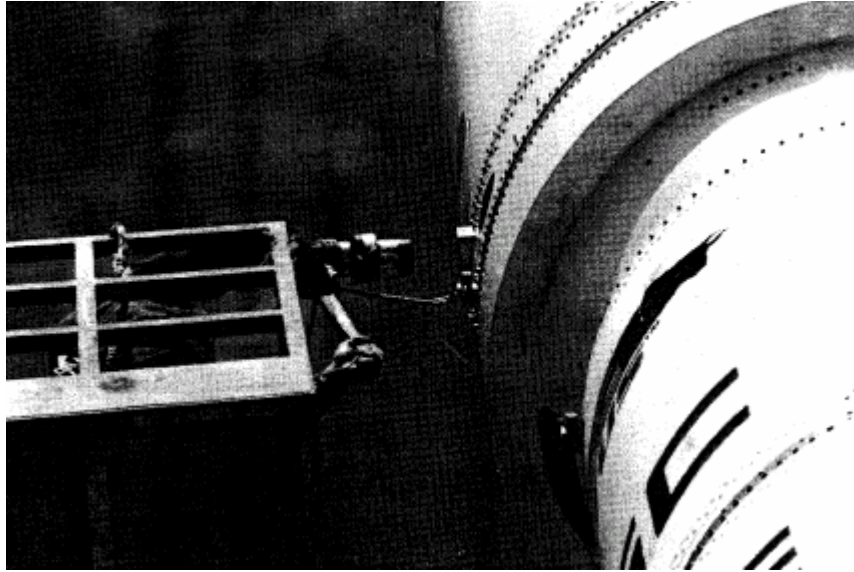


Figure 2.13 Impact hammer excitation of Taurus launch vehicle [14]

Unlike the impact hammers, shakers are attached type of exciters. An attachment device is used to apply the required excitation force to the structure. Electromagnetic (electrodynamic) and hydraulic types are commonly used. They operate in wide frequency ranges depending on the size. Smaller shakers have higher frequency range and lower force ratings. The applied force is measured using force transducers attached to structure at the end of the attachment device.

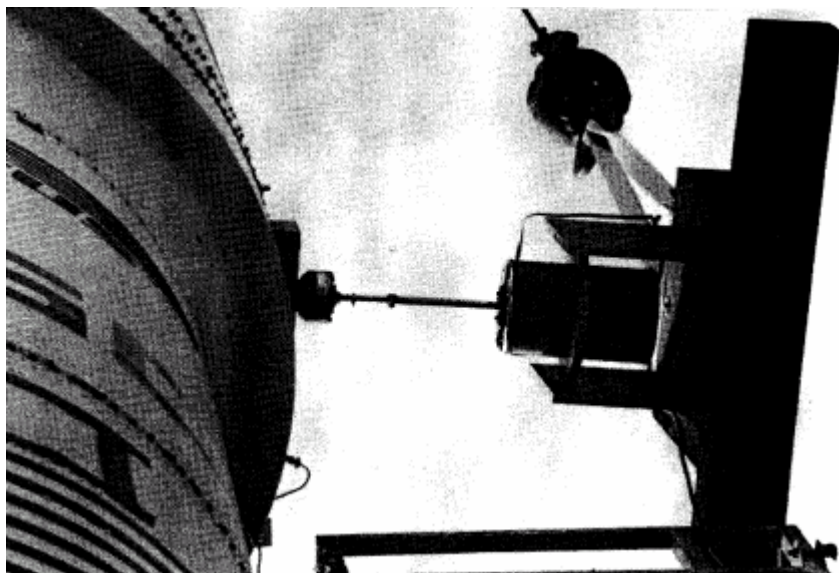


Figure 2.14 Shaker excitation of Taurus launch vehicle

Shaker excitation of Taurus launch vehicle is shown in Figure 2.14.

Step relaxation involves preloading the structure with a measured force through a cable then releasing the cable and measuring the transients. This excitation method is shown in Figure 2.15.

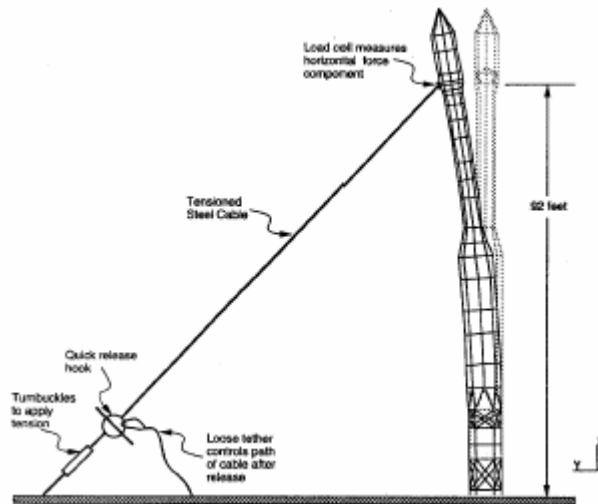


Figure 2.15 Step relaxation excitation of Taurus launch vehicle

2.2.2.1 Shaker testing

Electromagnetic or electrohydraulic shakers are widely used to excite the test structure with various types of excitation functions such as fixed sine, random noise and swept sine. Since the frequency response is a single input function, the shaker should submit only one component of force in line with the main axis of the force transducer.

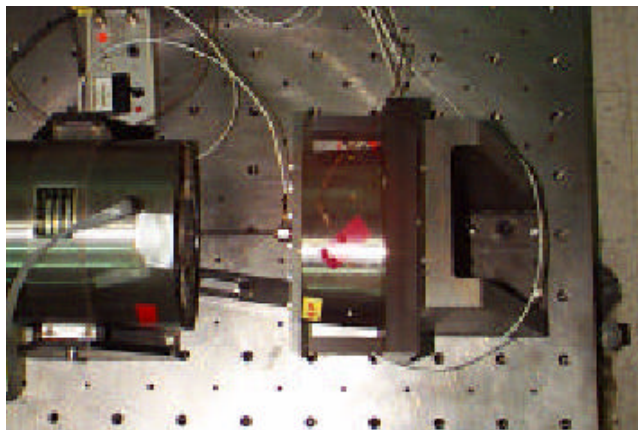


Figure 2.16 Shaker attachment to structure (shaker-left) [15]

To minimize the problem of forces being applied in other directions, the shaker is connected to the structure through a slender rod which is called ‘stinger’. The stinger used for testing of Hubble Telescope solar array damper is shown in Figure 2.16.

The main body of the shaker must be isolated from the structure to prevent any reaction forces being transmitted through the base of the shaker back to the structure. This can be achieved by mounting the shaker on a solid floor and structure from above. Also the shaker can be suspended. Suspended shakers for airplane testing are shown in Figure. 2.17.



Figure 2.17 Suspended shakers (inside the circles) [16]

2.2.3 Data acquisition

Sensing devices for applied force and motion in vibration testing are transducers. There are various types of transducers. But the most commonly used ones are piezoelectric type transducers. The piezoelectric transducer is an electromechanical sensor that generates an electrical output when subjected to vibration.

Force transducers or impedance heads are used to measure the force applied with shaker. These transducers are attached to structure with studs from

one end. And from the other side they are connected to the stinger. Impedance head used to measure the force applied a bridge base model is shown in Figure 2.18.



Figure 2.18 Impedance head connected to bridge base model [17]

Impedance head is a special type of transducer which measures force and acceleration at the same point and it generates two different signals.

To measure the response of the structure accelerometers are used. Accelerometers measure the acceleration at the measurement location. The velocity or displacement at this location can be obtained by electrical integration using the analyzer. Most commonly used types are piezoelectric ones.

Mounting technique for accelerometer is important for best accelerometer performance [18]. Different types of mounting methods are shown in Figure 2.19. The useful frequency range is the range where the sensitivity graph shown in the figure is straight line. For all mounting methods, the useful frequency ranges are given in the figure. The best mounting technique is to use a threaded steel stud. However, this method is not always convenient. The most common and practical mounting method is to use a thin layer of bees-wax. Having applied the bees-wax to the base of the accelerometer, it is firmly pressed on to the structure. Figure 2.20 shows how to mount an accelerometer using bees-wax. This mounting technique produces good results also. Mass loading from accelerometer and useful frequency range are important subjects in vibration measurements. The mass of the accelerometer should be less than one-tenth of the mass of the test

structure. As a rule of thumb, maximum frequency of the test should be set no more than one-tenth of the mounted natural frequency of the accelerometer. The mounted natural frequencies and other technical properties of accelerometers are given in calibration charts provided by the manufacturer of the accelerometer.

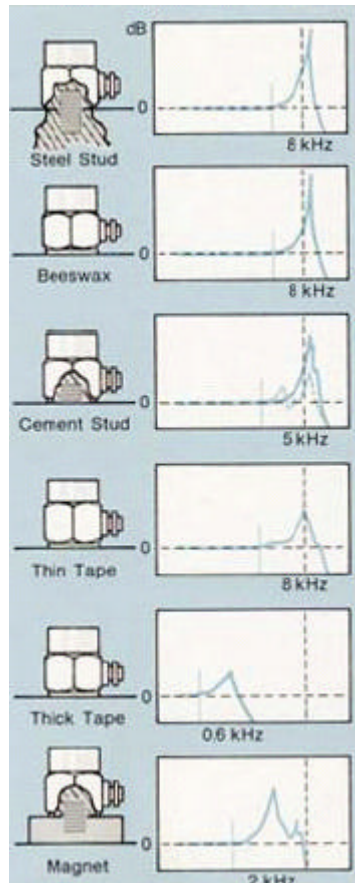


Figure 2.19 Accelerometer mounting methods [19]

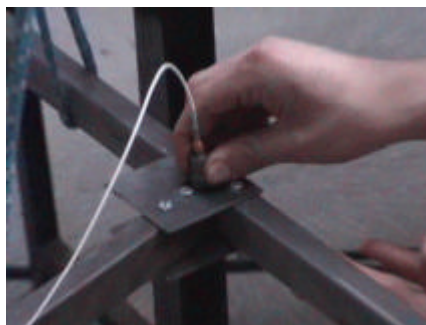


Figure 2.20 Accelerometer mounting using bees-wax

Vibration test setup for bridge base model is shown in Figure 2.21. The structure is suspended using elastic ropes. Shaker is attached to one corner of the structure (at the back). The accelerometer is attached to the structure using beeswax (on the right bottom). Impedance head and accelerometer are connected to charge amplifiers shown on the left. Performing the same sine sweep excitation from the same shaker location, acceleration values are measured at different positions on the structure. The next step is to process the data obtained from the tests.

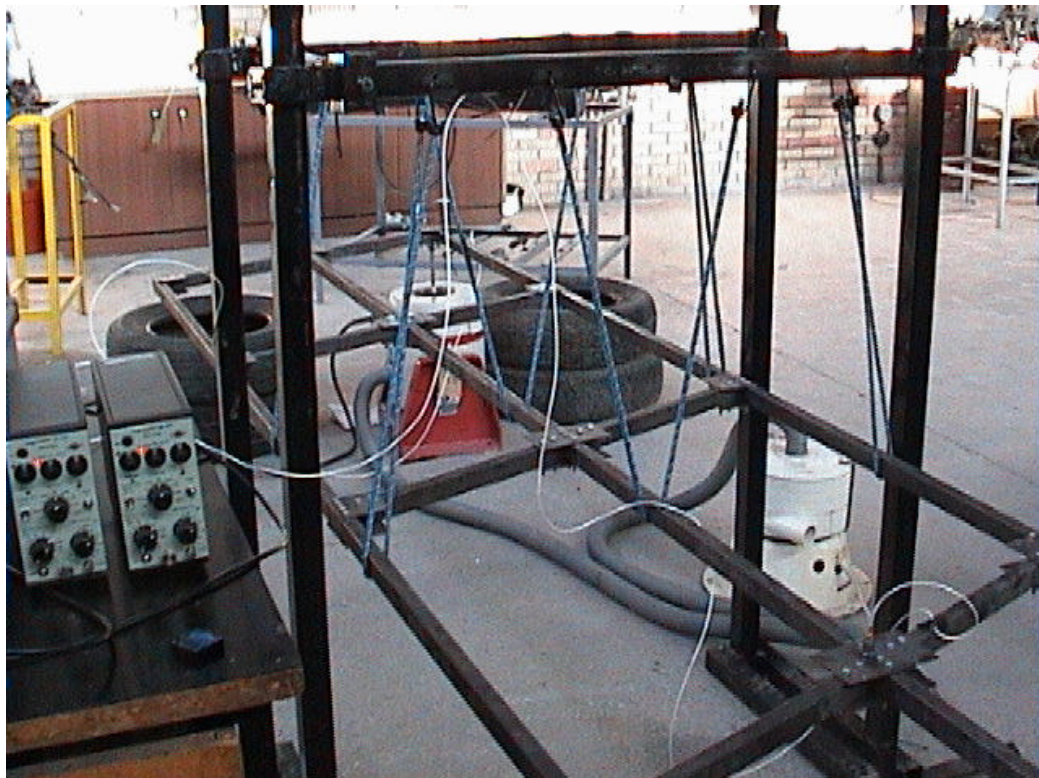


Figure 2.21 Freely suspended structure, shaker testing

2.2.4 Data implementation

After the structure has been supported and instrumented for the tests, the necessary test adjustments are done on the analyzer. For FRF measurements, at least two channels are used. One of the channels is used to get the force data and

the other one is used to get the acceleration data. From these two input channels; FRF can be obtained making the necessary mathematical calculations in the analyzer or using a PC. But the input ranges of these two input channels should be arranged. In sine sweep testing the levels for these channels are adjusted automatically. Frequency resolution in the frequency range affects the results of the tests. Thus, the resolution should be kept high as much as possible.

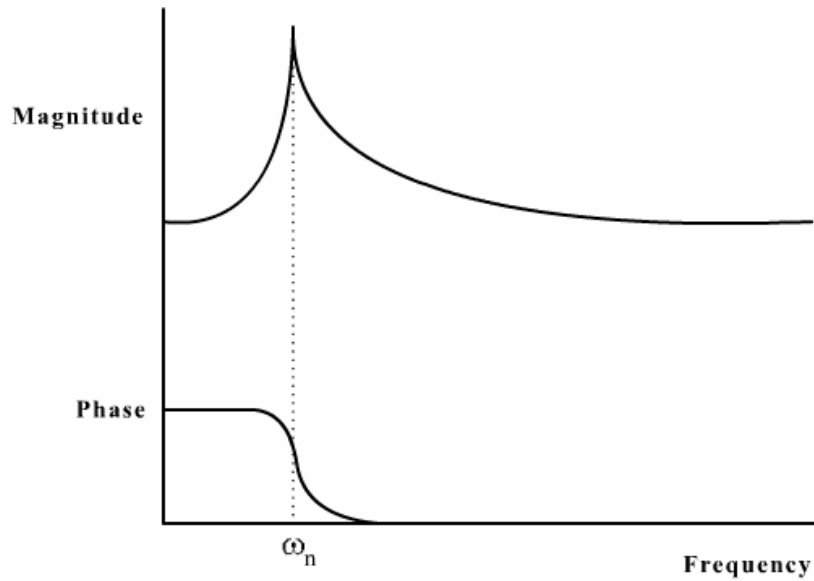


Figure 2.22 FRF, magnitude and phase

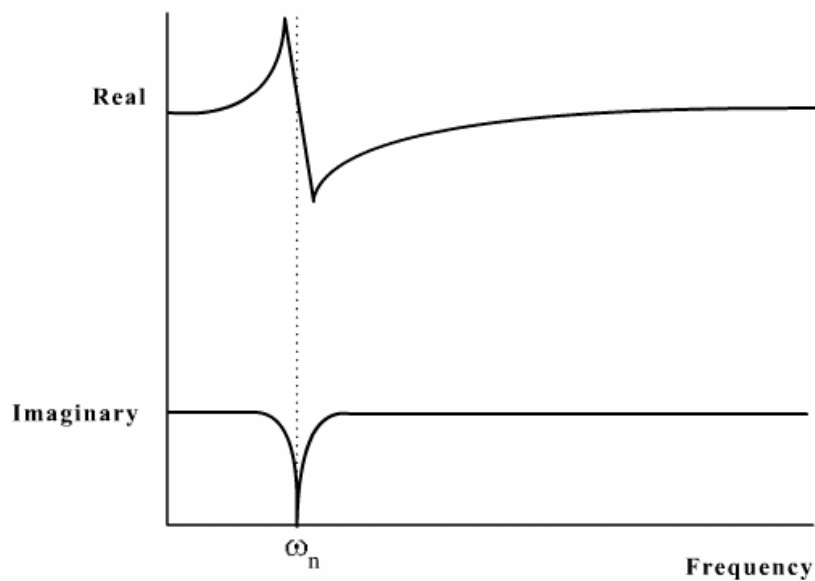


Figure 2.23 FRF, real and imaginary parts

After frequency response functions are being acquired and stored, natural frequencies and the mode shapes are determined. The resonant frequencies are estimated from the frequency response data by observing the frequency at which any of the following occur, as shown in Figures 2.22 and 2.23:

- The magnitude of the FRF is a maximum.
- The imaginary part of the FRF is a maximum or minimum.
- The real part of the FRF is zero.
- The response lags the input by 90° phase.

The magnitude of the response for the known input is determined from the modal coefficient of FRF. In order to determine the mode shape, the mode shape factor, which is proportional to modal coefficient, is estimated. One of the simplest mode shape factor estimation techniques is “quadrature peak picking” method. Mode shape factors are estimated from the imaginary part of the frequency response as shown in Figure 2.24. As mentioned above, the imaginary part reaches a maximum at the natural frequency. The magnitude of the mode shape factor is simply taken as the value of the imaginary part at resonance. The sign is taken from the direction that the peak lies along the imaginary axis. Using the mode shape factors for each measurement locations on the structure, the deformed shapes (mode shapes) at each natural frequency can be illustrated.

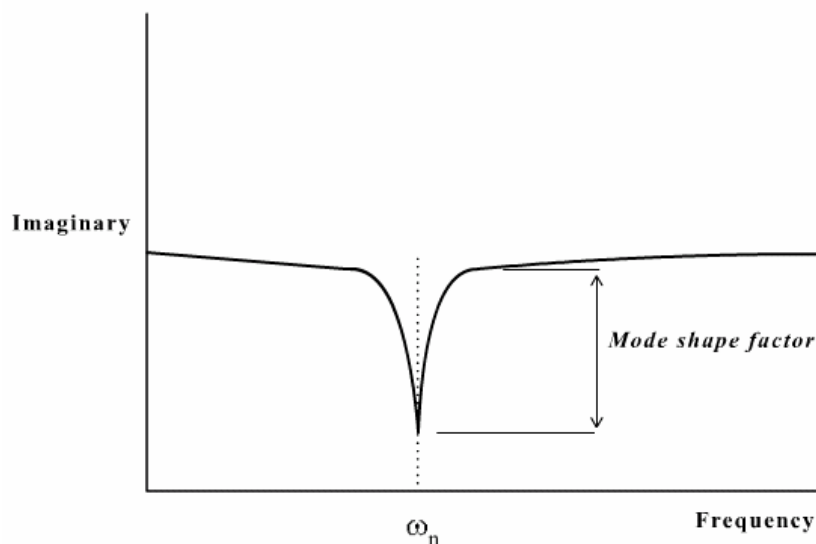


Figure 2.24 *Quadrature peak picking method*

Another mode shape factor estimation technique is “circle fit method”. This method is based upon the fact that the frequency response of a mode traces out a circle in the imaginary plane. The method fits a circle to the real and imaginary part of the frequency response data. The mode shape factor is then determined from the diameter of the circle as shown in Figure 2.25. This method usually results in better estimates than obtained by quadrature. However, it requires much more user interaction than the quadrature peak method and results with errors when fitting closely spaced modes.

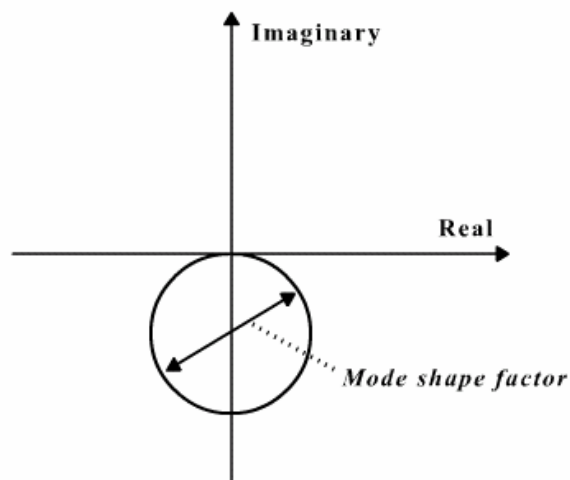


Figure 2.25 Circle fit method

2.2.5 An application of quadrature peak picking method

A freely supported rectangular plate model is given in Figure 2.26 [20].

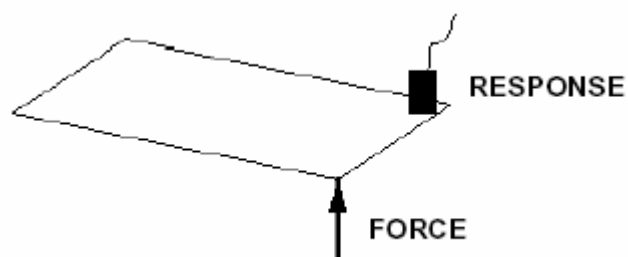


Figure 2.26 Freely supported plate

A constant force is applied to one corner of the plate. The response of the plate due to the excitation is measured with an accelerometer attached to one corner of the plate. FRF obtained from the measurement is shown in Figure 2.27. Natural frequencies can be estimated from the peaks in FRF.

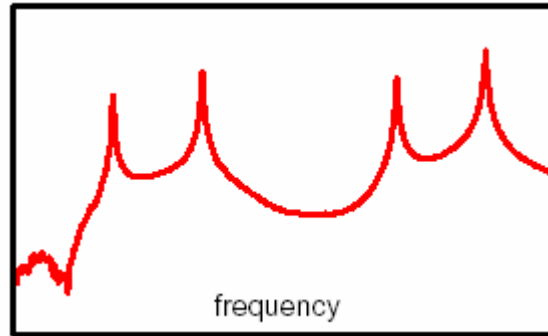


Figure 2.27 Plate FRF

In order to obtain the mode shapes of the plate at these natural frequencies frequency response measurements are made through the plate applying the same force. The plate measurement locations are shown in Figure 2.28.

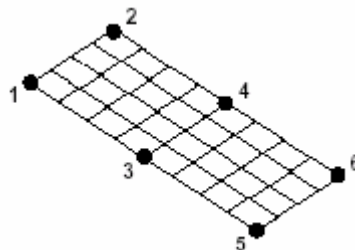


Figure 2.28 Measurement locations on plate

Total number of six FRFs, at the four corners and the two mid-points are obtained from the measurements. This type of test is called Single Input Single Output (SISO) test. The force is applied from one point and measurement is taken from another point on the test structure. Using the quadrature peak picking method, first two modes of the plate can be obtained. These mode shapes are shown in Figures 2.29 and 2.30.

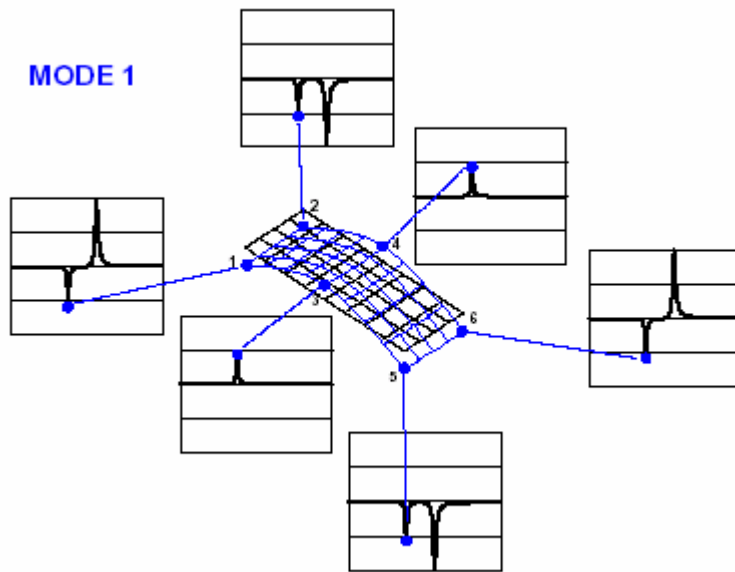


Figure 2.29 Mode 1

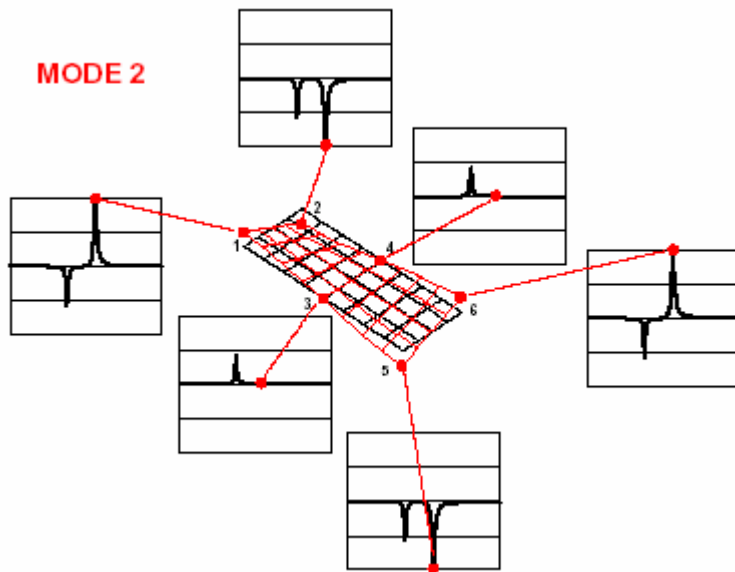


Figure 2.30 Mode 2

Using the same procedure for the resonances of FRF, all flexible modes of the plate can be estimated.

CHAPTER 3

TEST SETUP

The general test configuration for frequency response measurement is mentioned in Chapter 2. First of all the structure should be supported in some manner. Then, it should be excited in the frequency range of interest. And the resultant vibration data should be collected to obtain the necessary information about the dynamic characteristics of the structure. Exploring the past vibration tests performed for car bodies and searching their feasibility with the facilities of METU Mechanical Engineering Automotive Laboratory, the optimum test conditions are prepared. The general view of test setup planned before tests is shown in Figure 3.1. The necessary mechanical attachment equipments and devices are produced using the Machine Shop manufacturing facilities. The electronic devices are present in Automotive Laboratory.

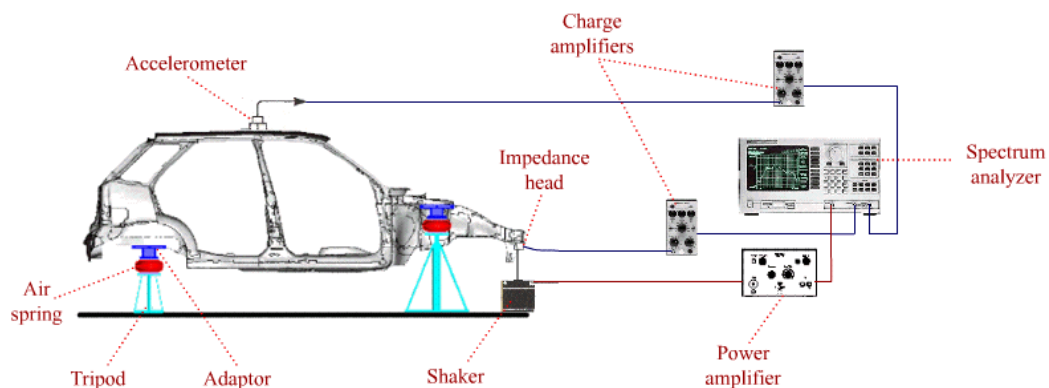


Figure 3.1 Planned test setup configuration

The car body-in-white is supported on air springs to simulate free-free boundary conditions. An electrodynamic shaker excites the body-in-white. The excitation function signal is provided from the analyzer. In addition the analyzer collects the force and response data coming from the impedance head and accelerometer. The signals created by impedance head and accelerometer are amplified using two charge amplifiers. Shaker uses its own power amplifier to excite the structure according to the signal provided by the analyzer source channel.

3.1 SUPPORTING THE STRUCTURE

Supporting large structures such as car bodies with air springs has been used for a long time for vibration tests. This kind of support is more practical and safe than elastic rope support for large structures like car bodies. In 1979, J.W. Dunn used air springs to support the car body-in-white for frequency response measurements [21]. Air spring support idea is originated from this study.

There are many air spring manufacturers and many types of air springs. The air springs used to suspend the truck seats are most useful ones for car body support. Therefore, CONTI single convoluted air spring FS 70-7 produced by ContiTech Luftfedersysteme GmbH is selected for supporting the body.



Figure 3.2 ContiTech air spring type FS 70-7

Technical details of air springs are given in Appendix 1. Body-in-white is attached to four air springs from the suspension attachment points. In order to place the body on to these air springs, some attachment devices should be produced. Having the CAD model of the body-in-white, the connection parts for

air spring attachment are designed easily. After determining the correct geometry and dimensions, the necessary parts are produced.

Different support parts for air springs are designed and manufactured since the front and rear suspension attachments are different in body-in-white. In front, air springs are placed on tripods (metallic part of stool) using an adaptor part. Another adaptor part is used to attach the air spring to tripod from its bottom. The front assembly parts for air springs are shown in Figure 3.3. The final assembled front support is shown in Figure 3.4.



Figure 3.3 Front air spring support parts together

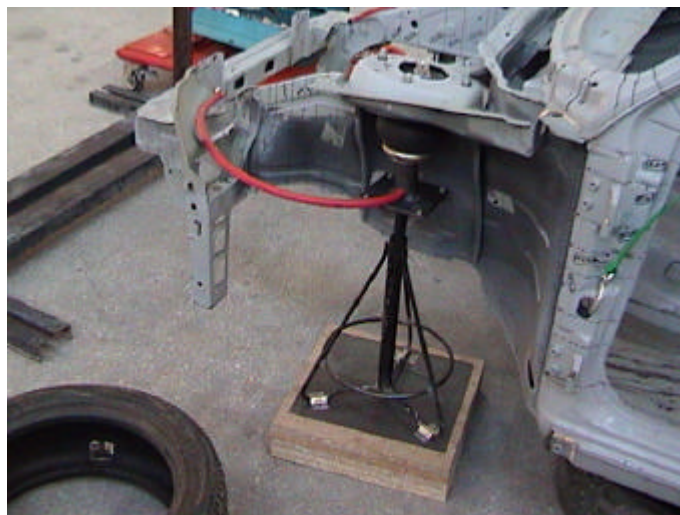


Figure 3.4 Front support assembled

In rear, smaller base is used since the height is lower than front. Also the adaptor to attach the air spring to body is a simple small part. Rear support assembly parts are shown in Figure 3.5. The final assembled rear support is shown in Figure 3.6. Air is supplied through the air-compressor hoses.



Figure 3.5 Rear air spring support parts together



Figure 3.6 Rear support assembled

All attachment parts are produced stiff enough to prevent any effect on body dynamic characteristics. Body-in-white is shown with air spring supports in Figure 3.7, just after the hydraulic lifting jack is unloaded.



Figure 3.7 Body-in-white with air spring supports

3.2 EXCITING THE STRUCTURE

Shaker excitation location is selected as the front left suspension attachment point, since dynamic analysis in FEA for the car body-in-white is performed applying a harmonic force from this point. However, the body is supported with air spring from left front suspension attachment point. So the shaker is suspended and it is connected to body suspension attachment point from above as shown in Figure 3.8. Four same kind of elastic ropes are used to hang the shaker. A mechanical jack is used to adjust the height of the shaker since the height of the body-in-white changes with the air pressure inside the air springs. These ropes, mechanical jack and shaker from side are shown in Figure 3.9. Alignment of the shaker is adjusted and necessary security precautions are prepared. These arrangements are shown in Figure 3.10.

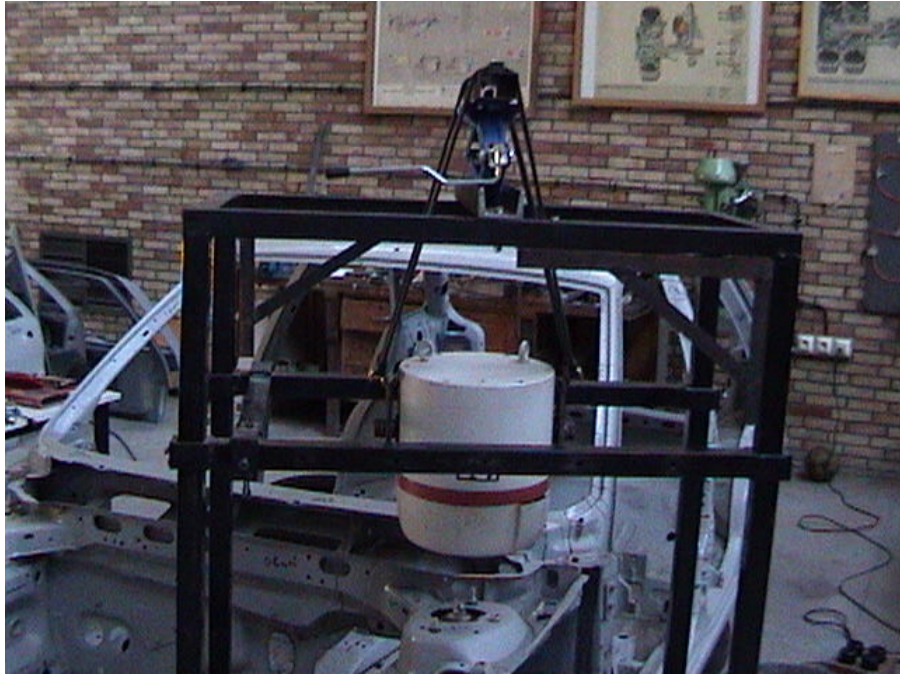


Figure 3.8 Shaker suspended



Figure 3.9 Elastic ropes and mechanical jack



Figure 3.10 Alignment adjustments for shaker

As mentioned in Chapter 2, excitation is applied to test structure through a stinger in shaker applications. The stinger used in the experiments is shown in Figure 3.11. Stinger is connected to shaker from one side and to the force transducer from the other side. The length and the diameter for the stinger are important parameters. The necessary dimensions for the stinger can be calculated using the axial stiffness and material properties [22]. The dimensions for the stinger, 200 mm length and 3 mm diameter, used in the tests are determined from B&K Modal Exciter Configuration guide for car body-in-white [23].



Figure 3.11 Stinger and its connections

Excitation function signal is fed to the shaker through the power amplifier. Signal is generated by the analyzer and using the source channel sent to the power amplifier. The required excitation force is applied to the body-in-white by the shaker according to the input coming from the power amplifier. Instruments used to excite the body-in-white are shown in Figure 3.12.

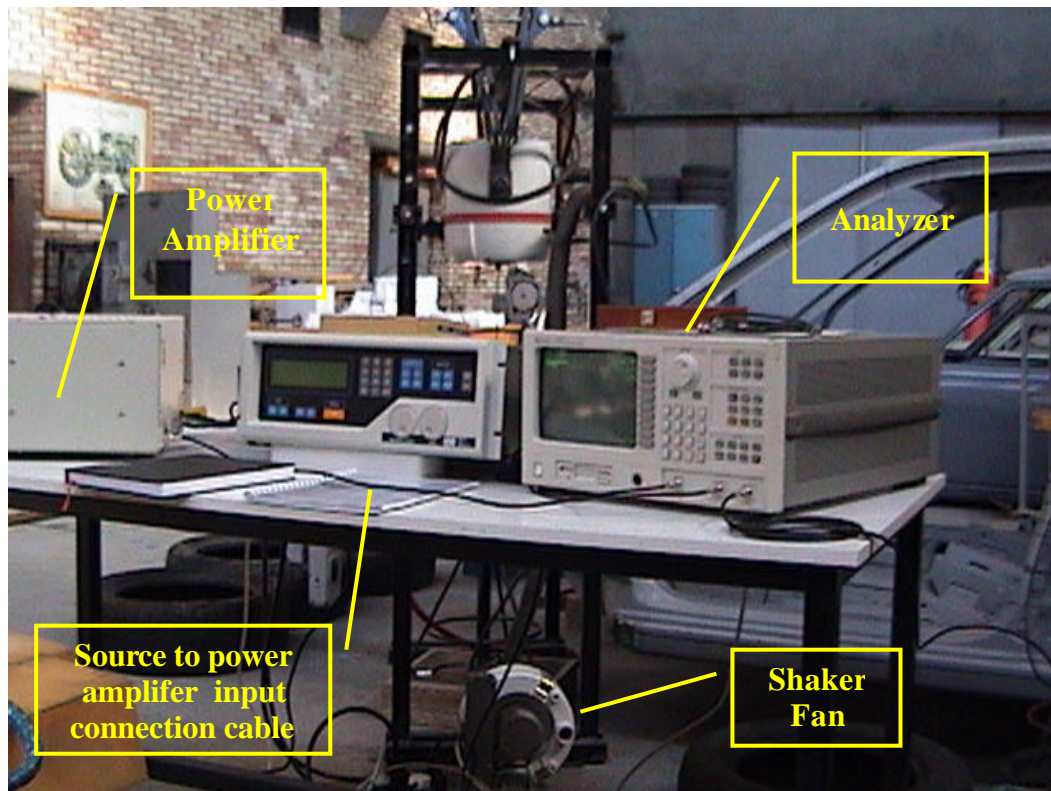


Figure 3.12 Excitation instruments and source signal transmission

3.3 DATA ACQUISITION AND SIGNAL CONDITIONING

Force applied to body is measured using an impedance head. Because of insufficient work space in front left support attachment area, impedance head is attached to the adaptor, which is used to connect air spring to body-in-white, before the front left support is assembled to body. Then, the front left support is attached to body-in-white. The impedance head attached to adaptor part is shown

in Figures 3.13. In Figure 3.14, the adaptor is connected to body-in-white suspension attachment area. Stinger is connected to impedance head using the nuts and bolts as shown in Figure 3.15. Force and acceleration outputs of impedance head are connected to charge amplifiers using special cables.



Figure 3.13 Impedance head attached to front top adaptor part



Figure 3.14 Impedance head in place



Figure 3.15 Stinger and cable connections to impedance head

The response of the body-in-white is measured using accelerometer. Accelerometer is mounted to body using bees-wax. It is shown in Figure 3.16.



Figure 3.16 Accelerometer mounted on body using bees-wax

Outputs of both impedance head and accelerometer are amplified using charge amplifiers shown in Figure 3.17. Outputs of charge amplifiers are connected to two input channels present on analyzer as shown in the figure. Two BNC cables are used to connect these instruments.



Figure 3.17 Charge amplifiers connected to two input channels of analyzer

3.4 INSTRUMENTS

3.4.1 Shaker

An electrodynamic shaker Vibrator-Model V450 Series produced by Ling Dynamic Systems Ltd is used in this study. The Ling Dynamic Systems 450 Series Vibrator is a wide frequency band electro-dynamic shaker, capable of producing a sine vector force of 311 N (70 lb force), when force cooled. The 450 Series Vibrator is designed for structural and environmental vibration testing by converting electrical current into mechanical force. Technical properties of this shaker is given in Appendix 2.



Figure 3.18 LDS V450 electrodynamic shaker

A remote fan unit to obtain maximum efficiency from the shaker is supplied by Ling Dynamic Systems Ltd which is shown in Figure 3.19.



Figure 3.19 LDS V450 electrodynamic shaker fan unit

The model 450 Vibrator is fitted with a low impedance armature and is suitable for use with the Ling Dynamics Systems Ltd. PA500 amplifier. This amplifier is shown in Figure 3.20.



Figure 3.20 LDS PA 500 power amplifier

3.4.2 Signal analyzer

The analyser used in the experiments is 35665A 2-Channel DC to 102.4 kHz Dual Channel Dynamic Signal Analyzer. The Agilent 35665A is a 2-channel Dynamic Signal Analyzer providing measurement solutions in vibration, acoustics, and control systems. Its major options are computed order tracking, real-time octave, swept sine, curve fit and synthesis, arbitrary source, and Instrument BASIC. Technical properties are given in Appendix 3.



Figure 3.21 Agilent 35665A 2-channel dynamic signal analyzer

3.4.3 Impedance head

B&K Impedance Head Type 8001 is used in this thesis study for force measurements. This impedance head is for general purpose measurements on light structures. Technical properties of this type of impedance head is given in Appendix 4.



Figure 3.22 B&K impedance head type 8001

3.4.4 Accelerometer

B&K Accelerometer Type 4384 is used in this thesis study for response measurements. These 17 gram accelerometers are used for acceleration measurements in 0-10 kHz range. Technical specifications of B&K Type 4384 accelerometer are given in Appendix 5.



Figure 3.23 B&K accelerometer type 4384

3.4.5 Charge amplifiers

B&K Charge Amplifier Type 2635 is used for signal amplification purpose and power supply for transducers. These amplifiers are used for general vibration measurements with a piezoelectric accelerometers and sound measurements with piezoelectric underwater probes. Technical details are given in Appendix 6 for this type of charge amplifiers.



Figure 3.24 B&K charge amplifier type 2635

3.4.6 Microphone and preamplifier

SPL measurements are taken using the B&K Microphone Type 4165 and B&K Microphone Preamplifier Type 2660. Technical properties of microphone and preamplifier used in the tests are given in Appendix 7 and Appendix 8, respectively.

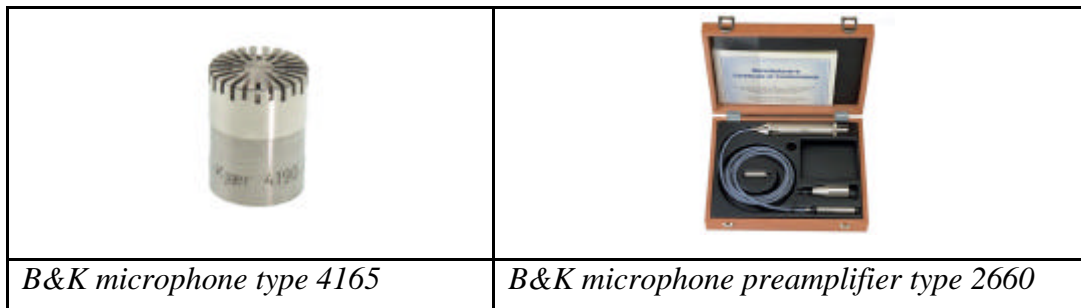


Figure 3.25 Microphone and preamplifier used for SPL measurements

3.4.7 General view of setup and instruments

A general view from the test setup is shown in Figure 3.26.



Figure 3.26 General view of setup and instruments

CHAPTER 4

EXPERIMENTAL PROCEDURE AND TEST RESULTS

4.1 EXPERIMENTAL PROCEDURE

The car body-in-white has been suspended using air springs and the shaker has also been suspended using elastic ropes. The connections between instruments have been arranged.

Before the experiments some of the instruments should be checked for errors. In order to see if the connection elements are functioning correctly, the cables are connected to charge amplifiers from one end and to analyzer from the other. Using the reference signal at 159 Hz ($\omega = 1000\text{rad/s}$), the cables are checked if they are sending the correct signal to analyzer. After this check some of the useless cables are set apart. Also the accelerometers are controlled using reference vibration at 159 Hz ($\omega = 1000\text{rad/s}$) Bruel&Kjaer calibration exciter type 4294. Having checked the connection elements and instruments, necessary adjustments for charge amplifiers are done according to the sensitivities of impedance head and accelerometers used.

Excitation of the system will be sine sweep for frequency range of 10-100 Hz. The lower limit for the frequency is determined from NVH studies and the similar experiments done with same boundary conditions in the world. Upper limit is selected to have 10-15 numbers of flexible modes of the body in the frequency range.

Since the body is suspended on air springs, these air springs give the body to move freely in vertical direction only, i.e. in z direction. As a result of this suspension the body will have three rigid body frequencies and three rigid body modes. These modes are body bounce, body pitch and body roll. These frequencies should be kept as low as possible. The air springs used have different stiffness values under different load and pressure conditions. Before taking measurements the air pressure inside the air springs should be arranged such that the body will have its lowest rigid body frequencies. To see the effects and to have lower rigid body frequencies the inflation pressures of the air springs are changed. It is observed that lowering the pressure results in lower rigid body frequencies. The pressure level for tests is determined as 1 bar. At 1 bar and under the load of 69 kg (that is the 1/4th of the body weight), the stiffness value for each air spring is found as 603.52 N/cm from the technical properties of the air springs given in Appendix 1. And the corresponding body bounce frequency is calculated as 4.7 Hz. In order to see the decrease in rigid body frequencies, air springs are inflated to 1 bar (test pressure) and 1.8 bar (maximum pressure) and two FRF measurements are taken for each pressure. The resultant frequency response functions are given in Figure 4.1.

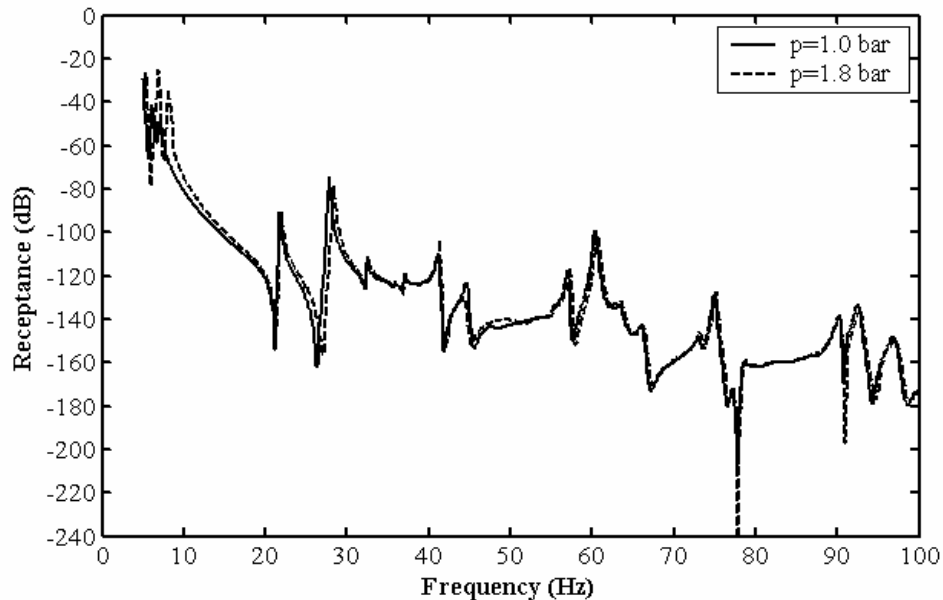


Figure 4.1 FRF measurements for two different air spring pressures

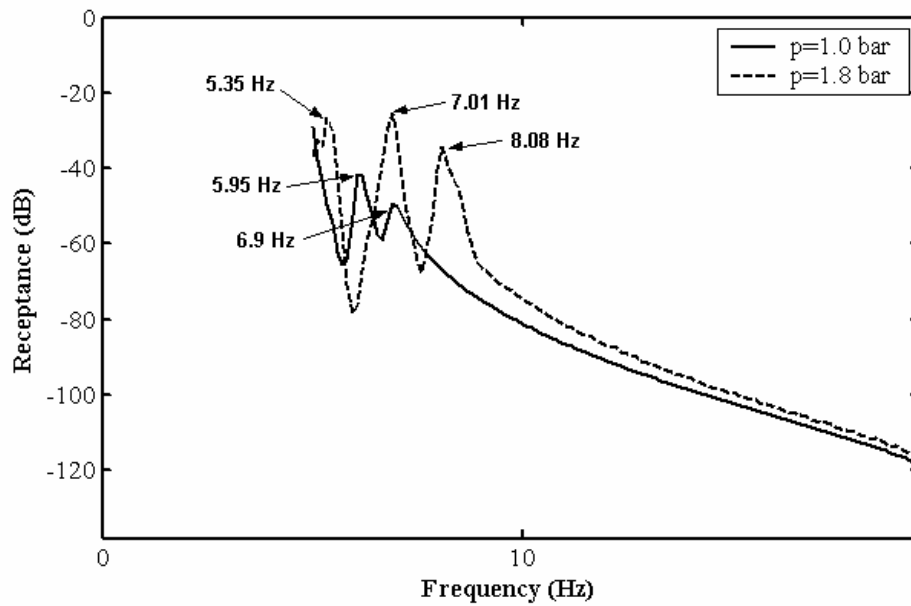


Figure 4.2 Rigid body frequency change by changing air spring pressure
(zoom in rigid body frequencies region)

Starting frequency is taken as 5 Hz since it has been calculated 4.7 Hz for body bounce frequency at 1 bar. From the technical properties, the body bounce frequency for 1.8 bar is calculated as 5.4 Hz, which is very close to the experimental result 5.35 Hz. From figure 4.1 it can be observed that the higher natural frequencies for flexible modes do not change by changing the pressure. On the other hand, there is a decrease in rigid body frequencies more than 1 Hz. At 1.8 bar, 5.35 Hz, 7.01 Hz, 8.08 Hz are body bounce, body pitch and body roll frequencies respectively. At 1 bar, 5.95 Hz, 6.9 Hz are body pitch and body roll frequencies, respectively. Body bounce frequency is below 5 Hz which is expected according to calculations. One thing to notice for FRF at 1 bar is that at 6 Hz there is also shaker bare table resonance. In addition, if the suspension springs are soft enough, it will be possible to have the rigid body frequencies less than 10-20 % of that for the lowest bending mode. If this is achieved than the suspension system approximates the truly free support condition for the test structure. This condition should be checked after the modes are identified.

The experiments are carried out at air spring pressures of 1 bar. Excitation signal is sent to the shaker using the ‘source’ option in the analyzer. The source is linear and up sine sweep from 10 Hz to 100 Hz with 500ms and 1s integration and settling times respectively. Resolution is arranged as 801 points/sweep (maximum). Using ‘overloaded data rejection’ prevents to have overloaded data in measurements. Estimated sweep time, i.e. time for one FRF measurement at one location, is about half an hour. The source level is kept low to protect the setup and the body-in-white from any damage which may occur during resonances. The applied source level is 14.227 mV_{peak} (10 mV_{rms}).

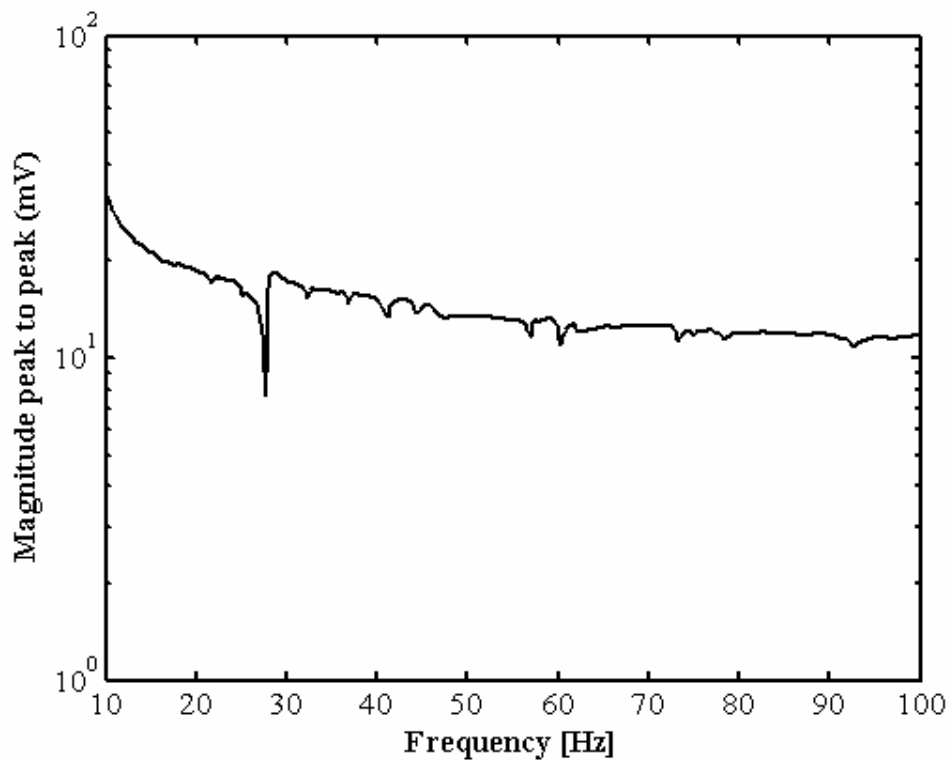


Figure 4.3 Input force spectrum used in the tests

Input should be checked if it is placing any resonance into output examining the force spectrum and point mobility. It is important to keep the force constant in the frequency range for this kind of FRF measurements in vibration tests. From Figure 4.3, it can be observed that the force is almost constant in the frequency region where the flexible modes lie. Point mobility at shaker excitation

point is measured from impedance head. Point mobility plot is given in Figure 4.4.

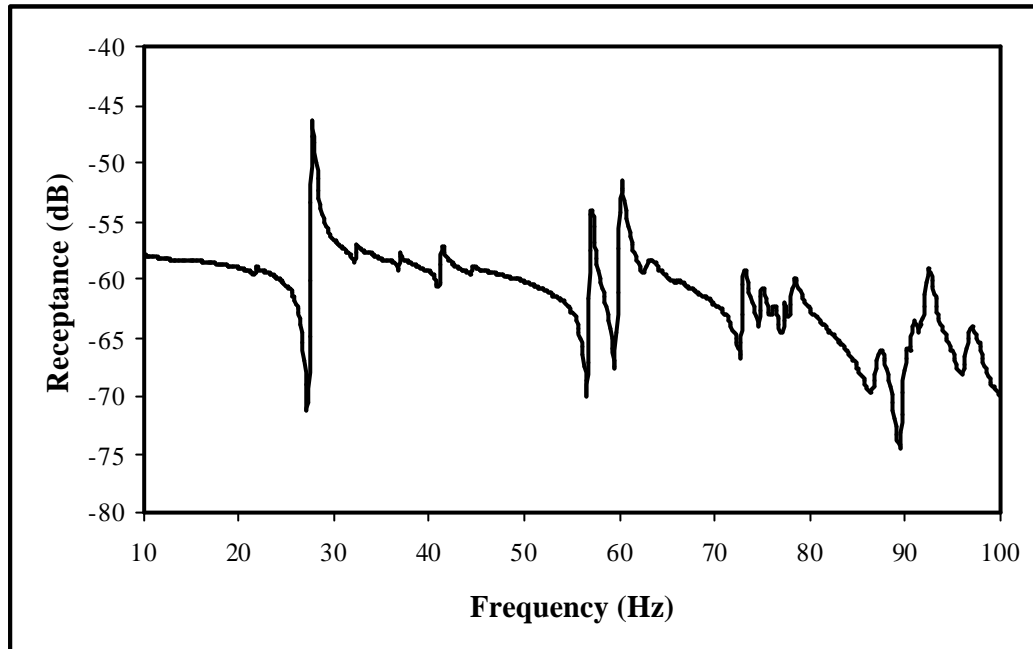


Figure 4.4 Point mobility @ shaker excitation location

This point mobility plot should be checked if the resonances occur at the same frequencies after the resonance frequencies of the body are determined from the transfer mobility plots obtained from sine sweep tests. This will verify that the resonances occur due to the structural response characteristics of body-in-white without any contribution from input force.

4.2 TEST RESULTS

Measurements are performed after everything is correctly adjusted. The measurement locations are shown in Figure 4.5. In all of these locations, the accelerometer is attached to the body vertically, i.e. in z-direction and also vertical to earth. Force level is the same for all measurements; it is shown in Figure 4.3 above. Force application point is shown with letter “o”.

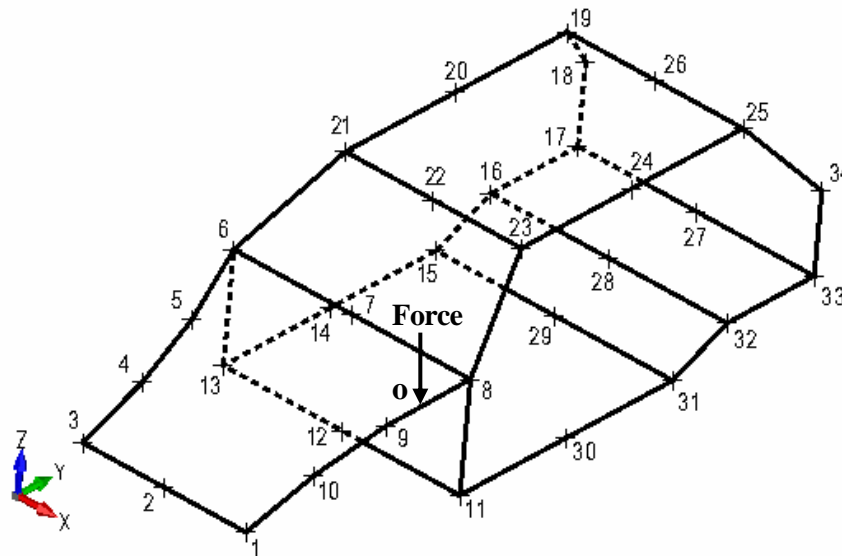


Figure 4.5 Measurement and force application locations on body-in-white

4.2.1 Frequency Response Functions

The measurements give the frequency response functions as inertance, i.e., acceleration divided by force on analyzer screen. This FRF is divided by $(j\omega)^2$ using the operations defined in the analyzer's analysis tools. The receptances are taken from the analyzer into a diskette with file extensions 'dat'. For a typical frequency response function measurement, this file contains the frequency and complex value of FRF information. Using the programs provided with the analyzer, the files are converted to text file (*.txt) and to matlab data file (*.mat) to plot the results. FRF magnitudes versus frequency plots are presented. The magnitude of the FRF is given in decibel using the reference value of 1 mm/N. All of 34 measurement locations are shown in Figure 4.5.

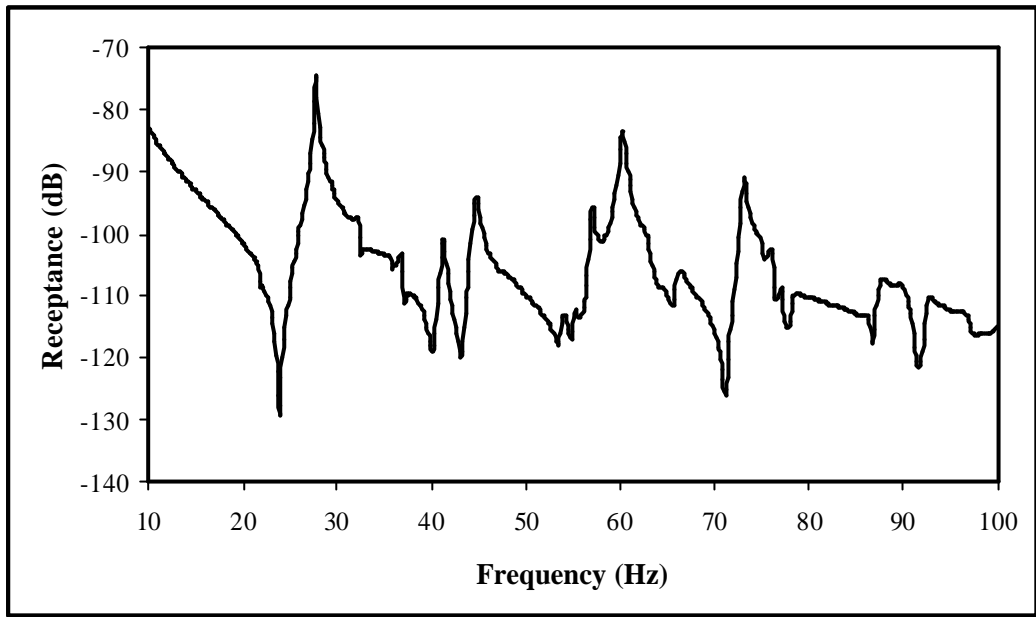


Figure 4.6 FRF between force at point 0 and response location 1

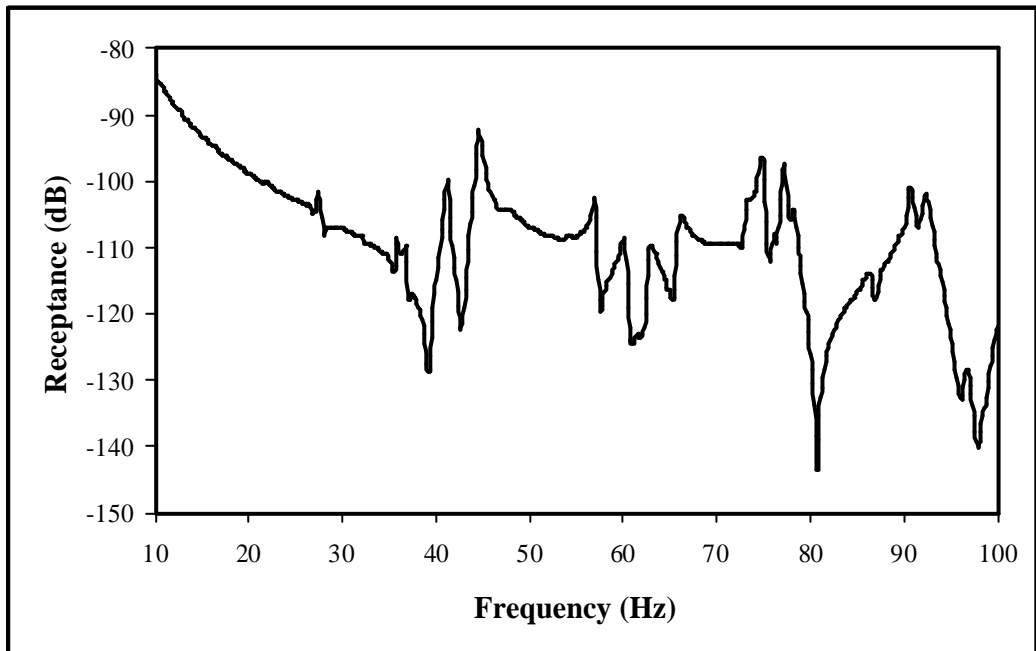


Figure 4.7 FRF between force at point 0 and response location 2

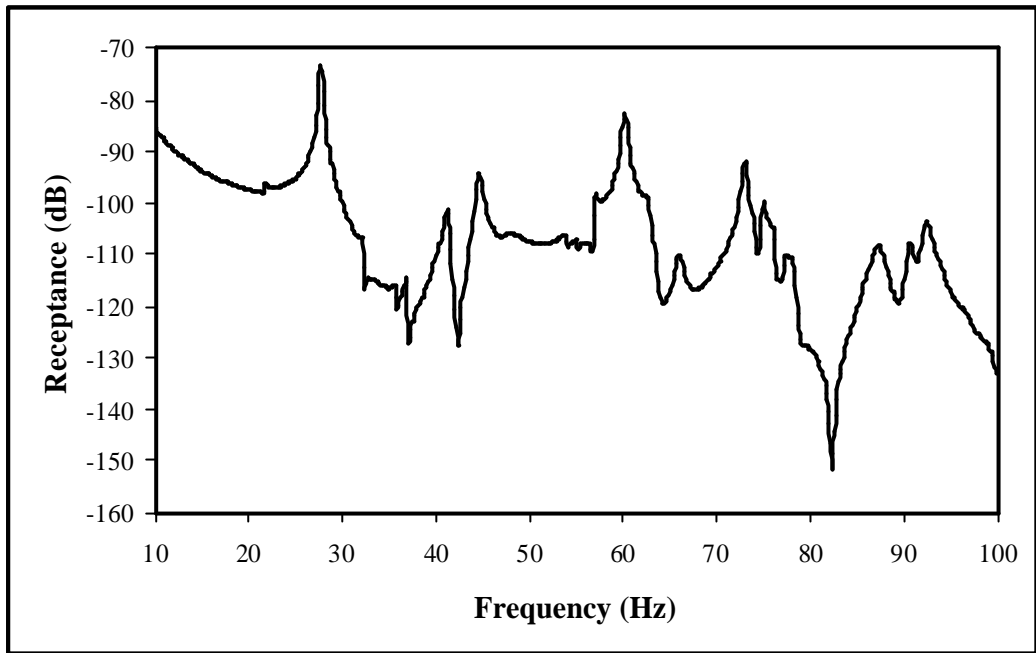


Figure 4.8 FRF between force at point o and response location 3

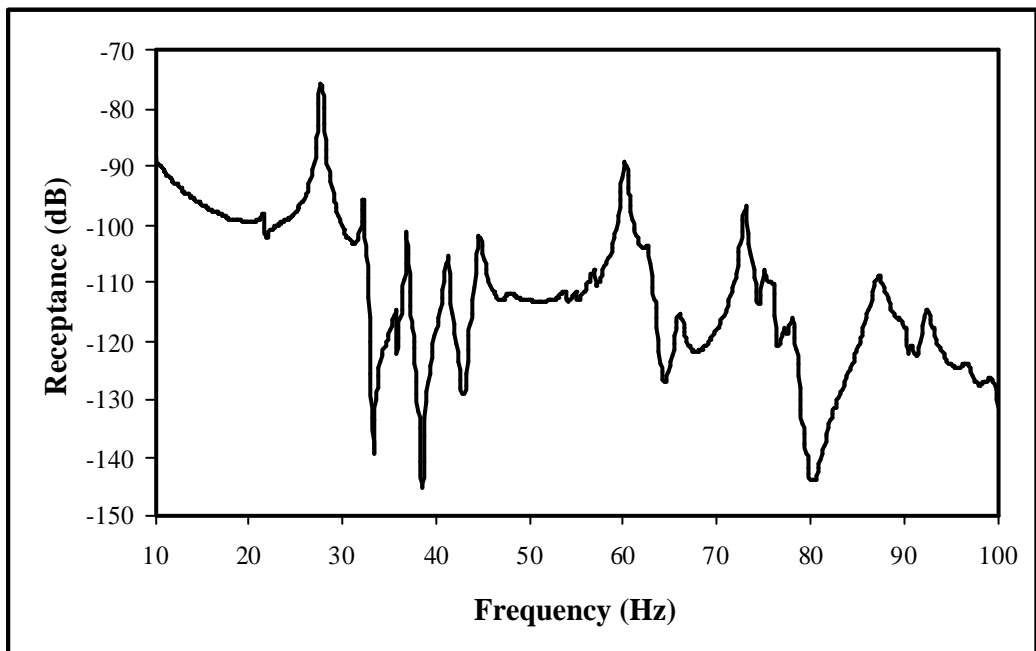


Figure 4.9 FRF between force at point o and response location 4

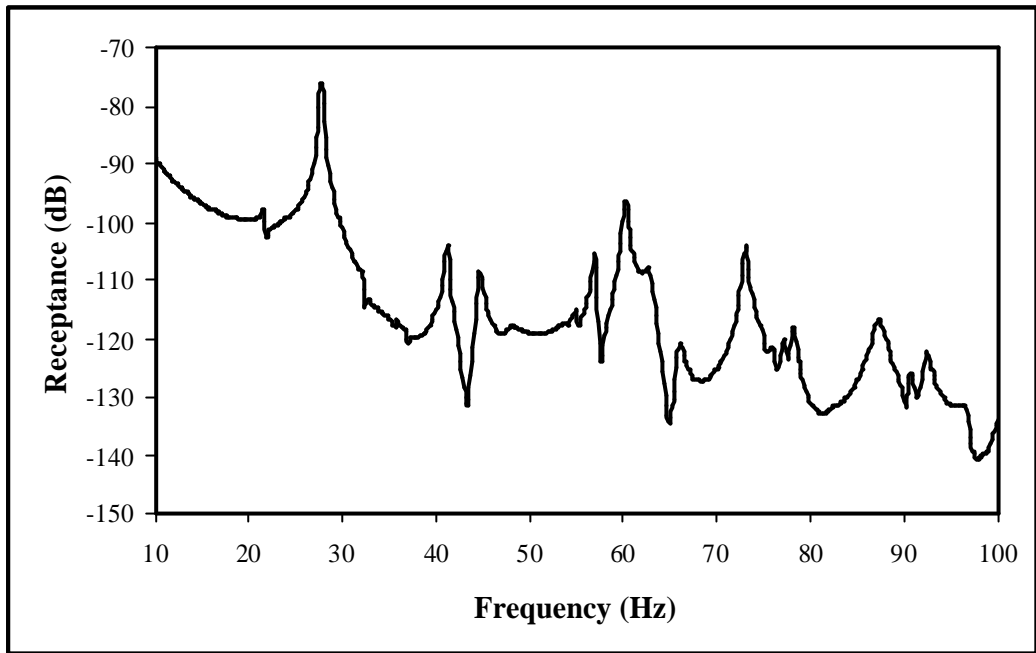


Figure 4.10 FRF between force at point o and response location 5

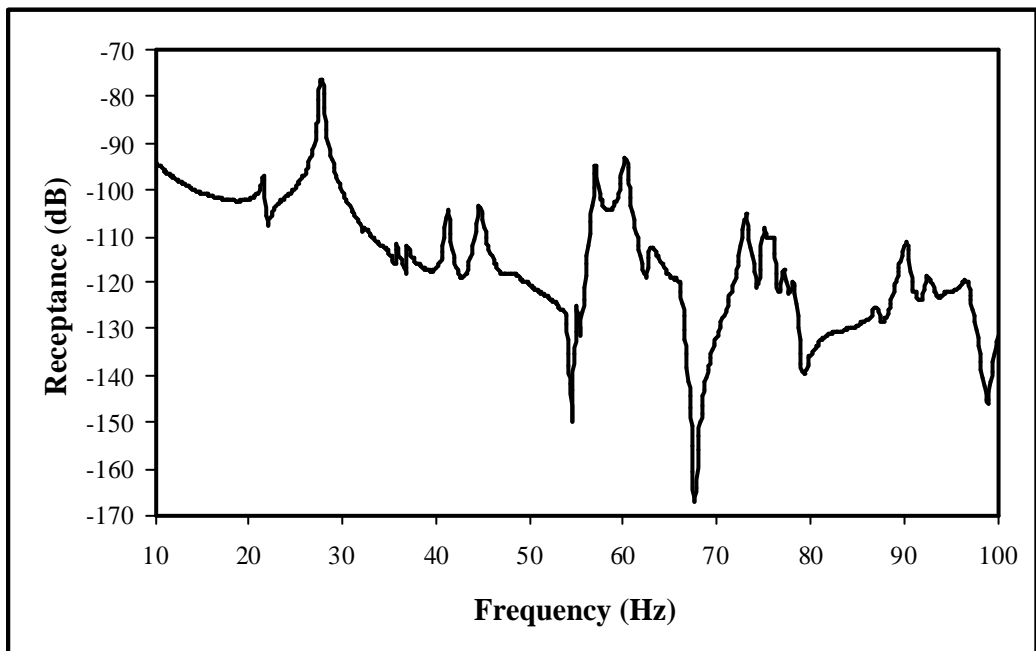


Figure 4.11 FRF between force at point o and response location 6

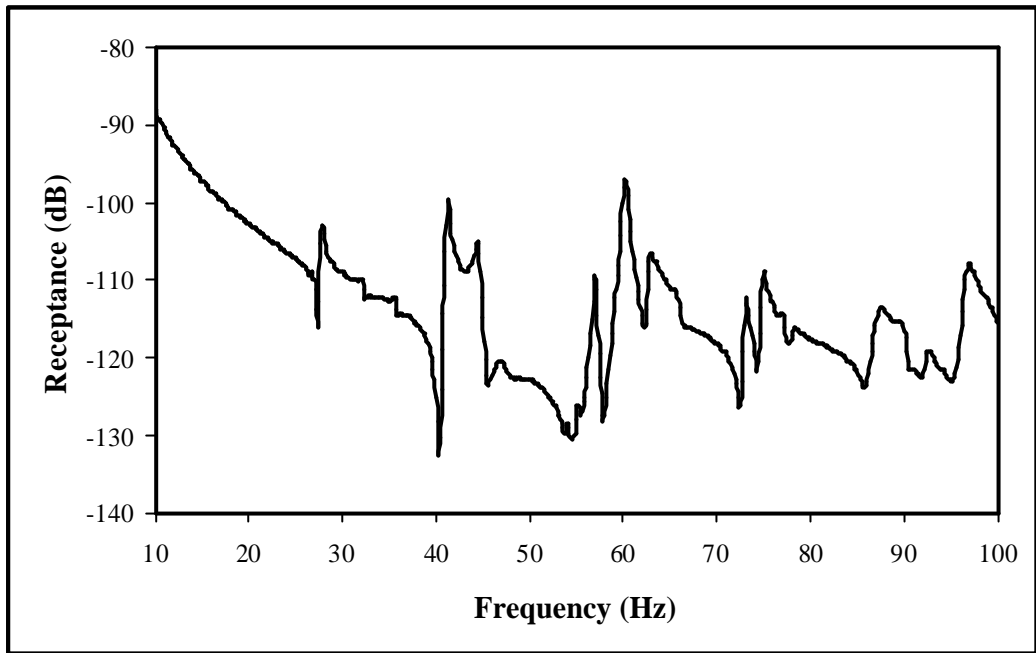


Figure 4.12 FRF between force at point o and response location 7

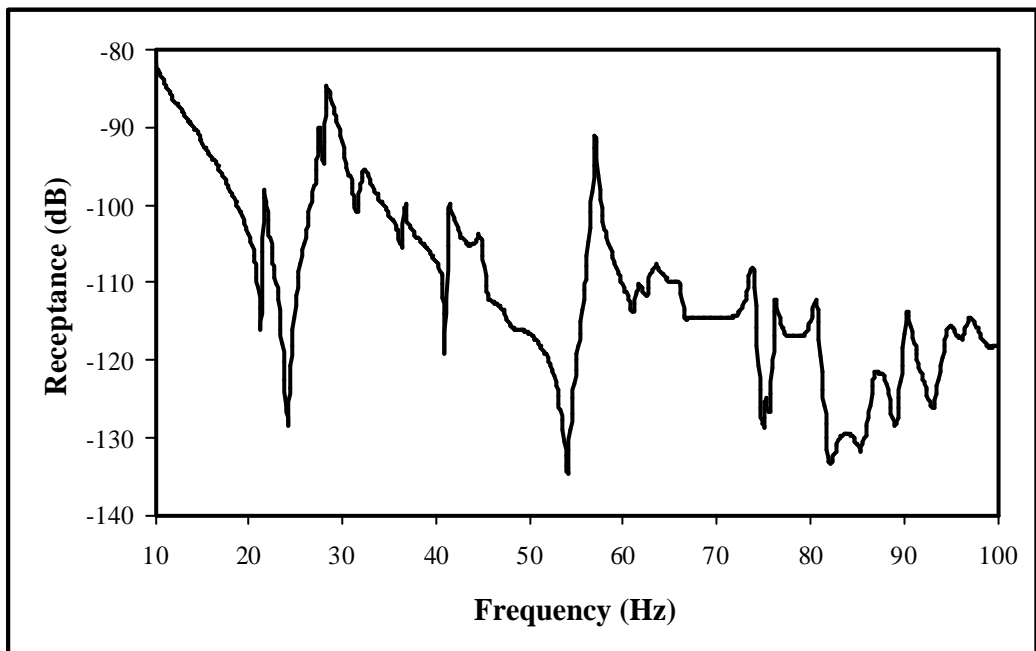


Figure 4.13 FRF between force at point o and response location 8

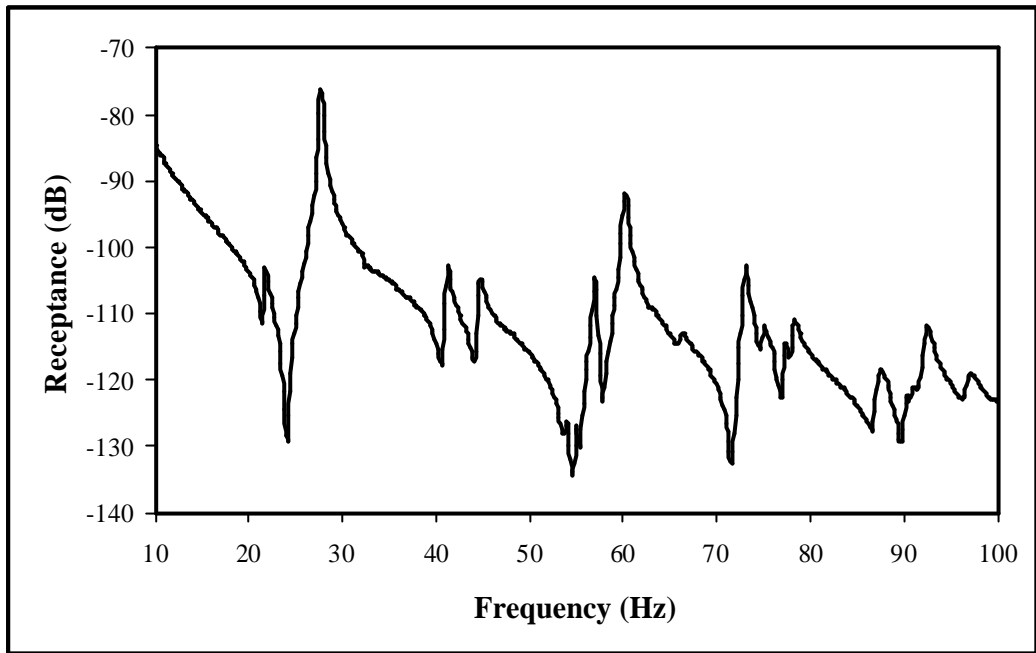


Figure 4.14 FRF between force at point o and response location 9

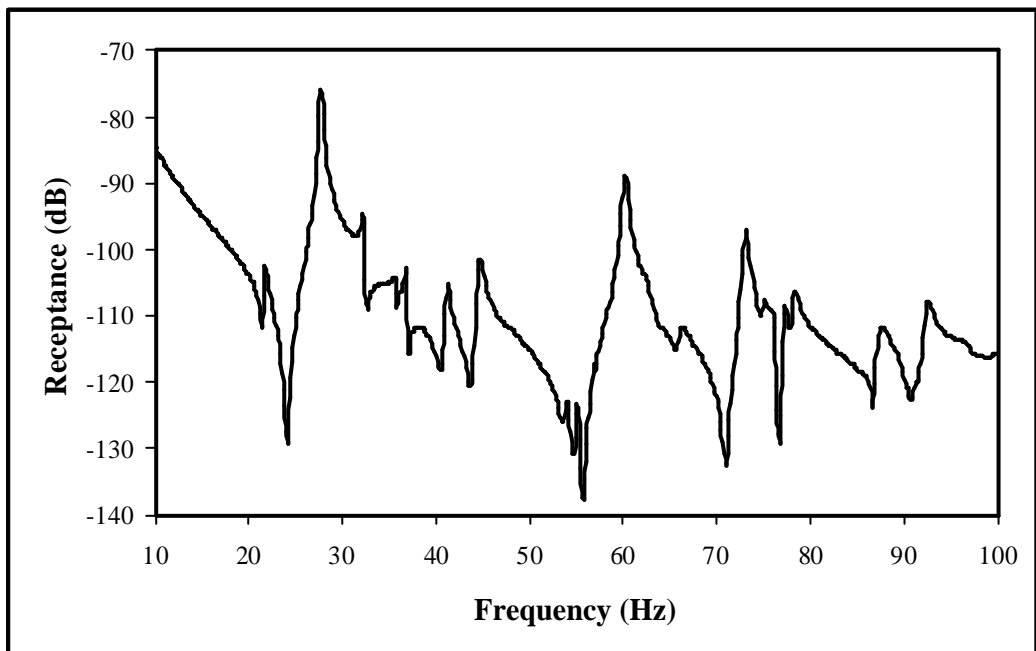


Figure 4.15 FRF between force at point o and response location 10

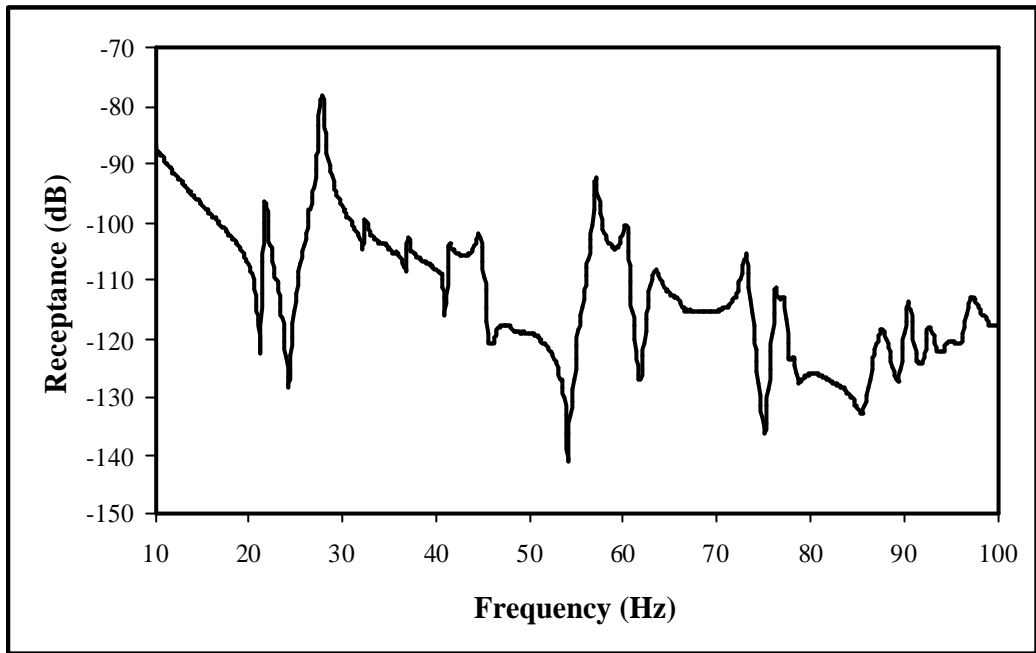


Figure 4.16 FRF between force at point 0 and response location 11

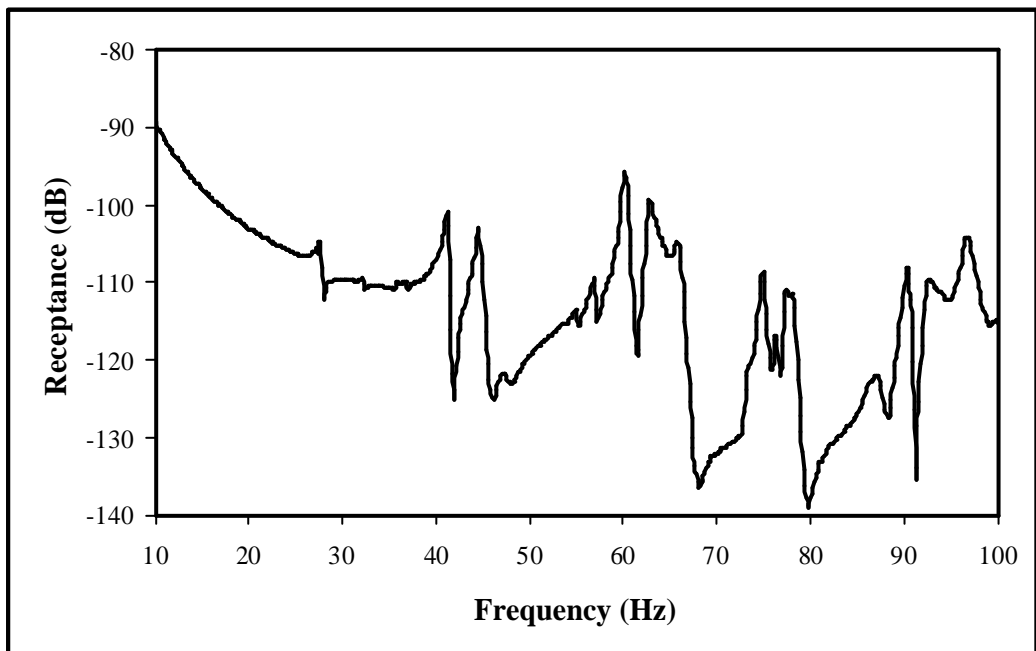


Figure 4.17 FRF between force at point 0 and response location 12

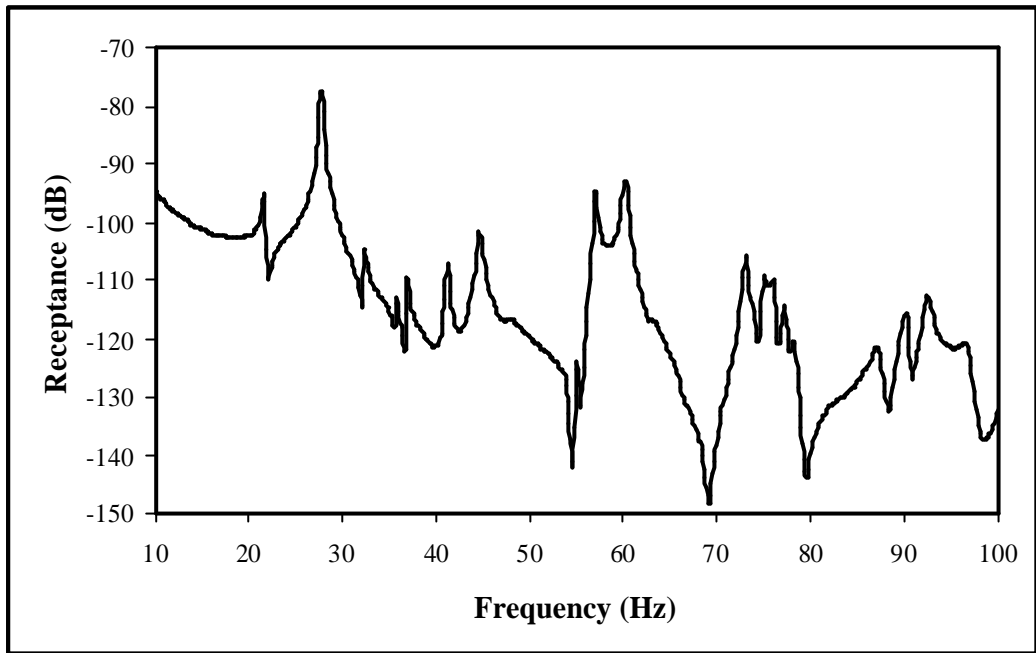


Figure 4.18 FRF between force at point o and response location 13

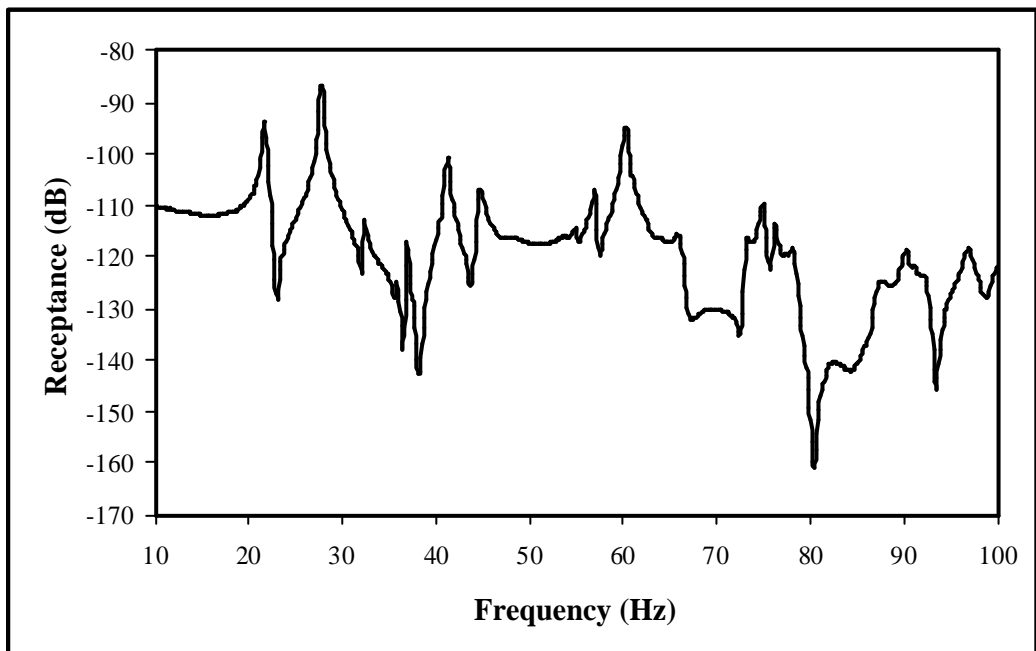


Figure 4.19 FRF between force at point o and response location 14

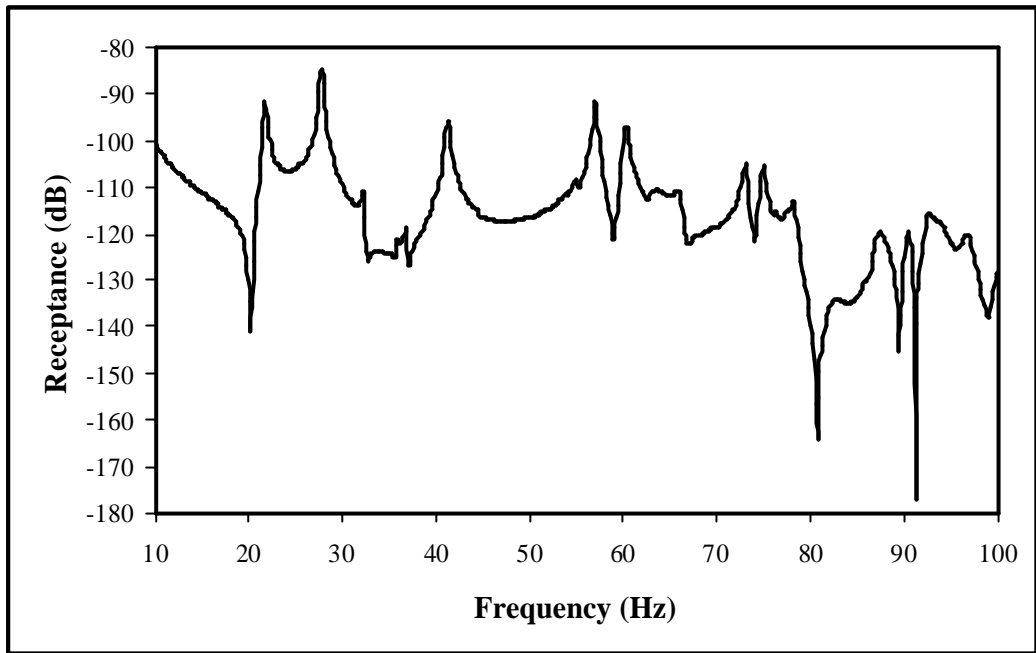


Figure 4.20 FRF between force at point o and response location 15

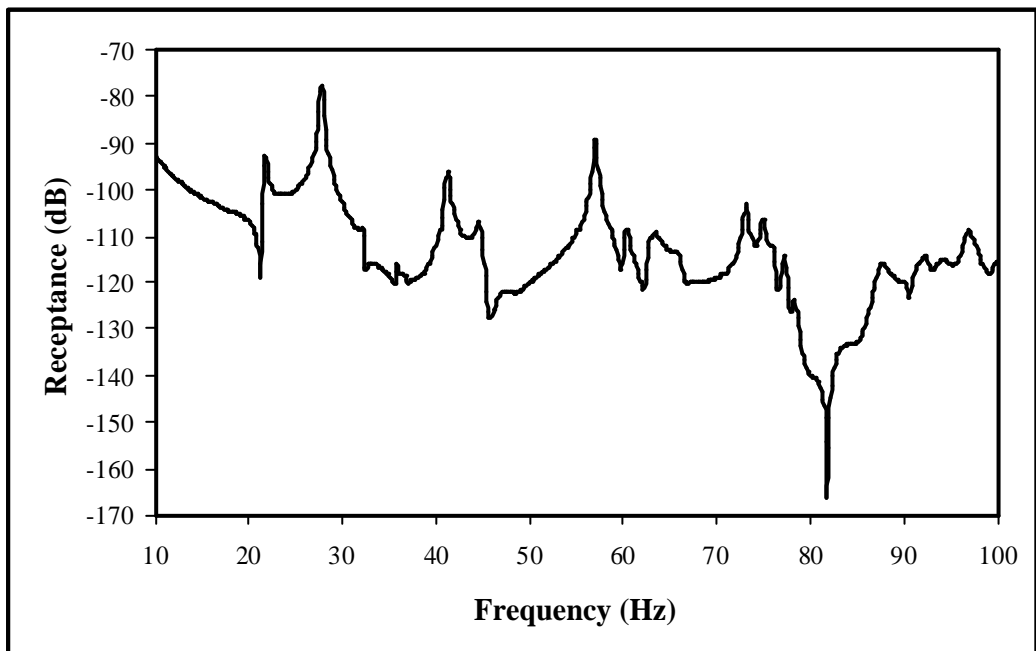


Figure 4.21 FRF between force at point o and response location 16

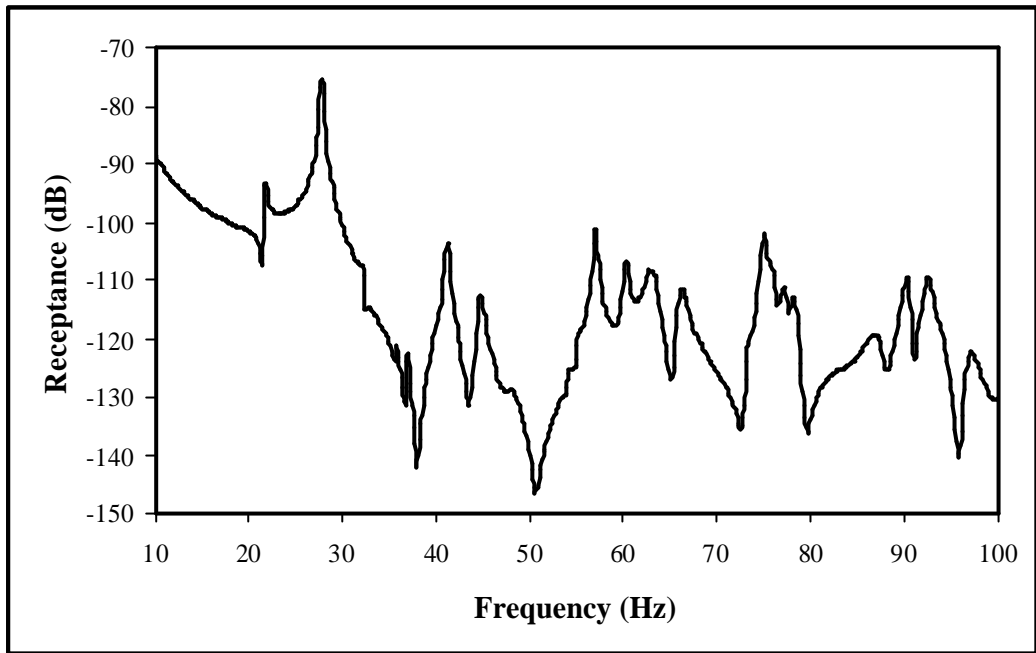


Figure 4.22 FRF between force at point o and response location 17

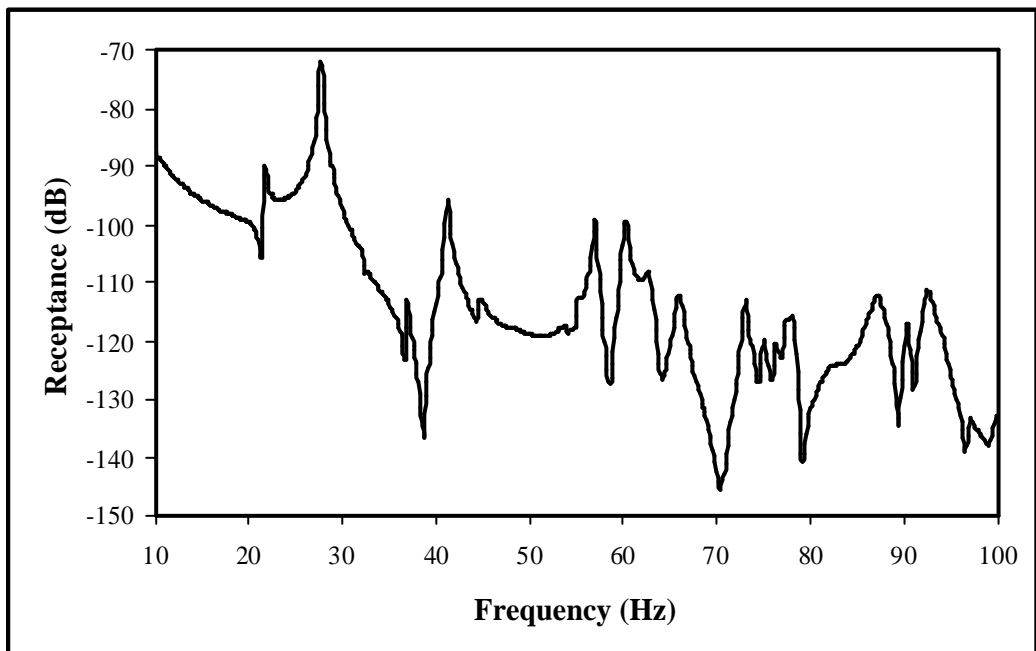


Figure 4.23 FRF between force at point o and response location 18

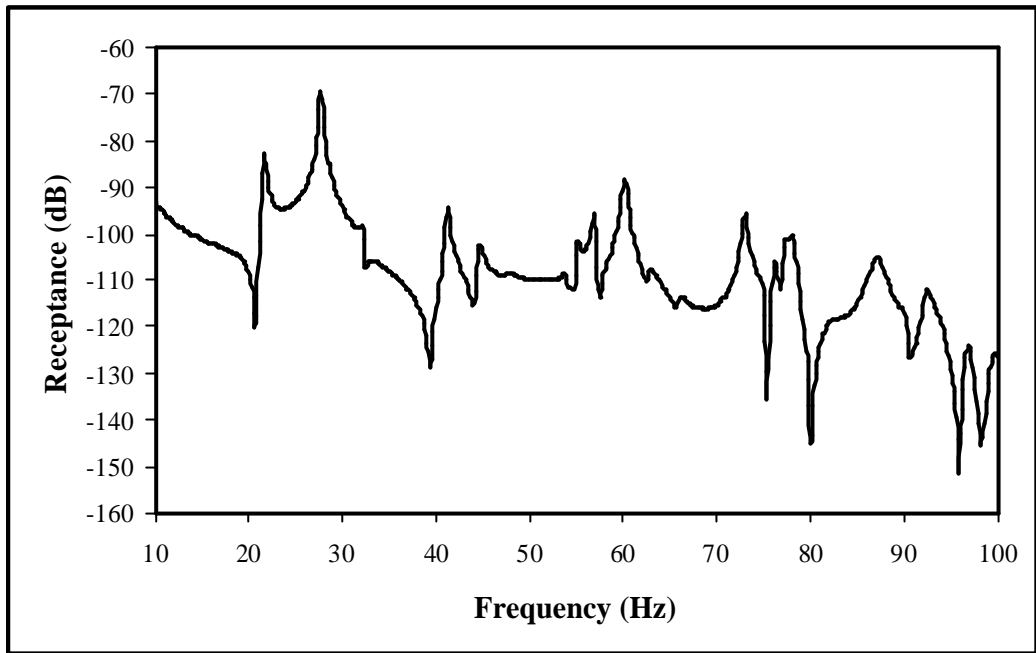


Figure 4.24 FRF between force at point o and response location 19

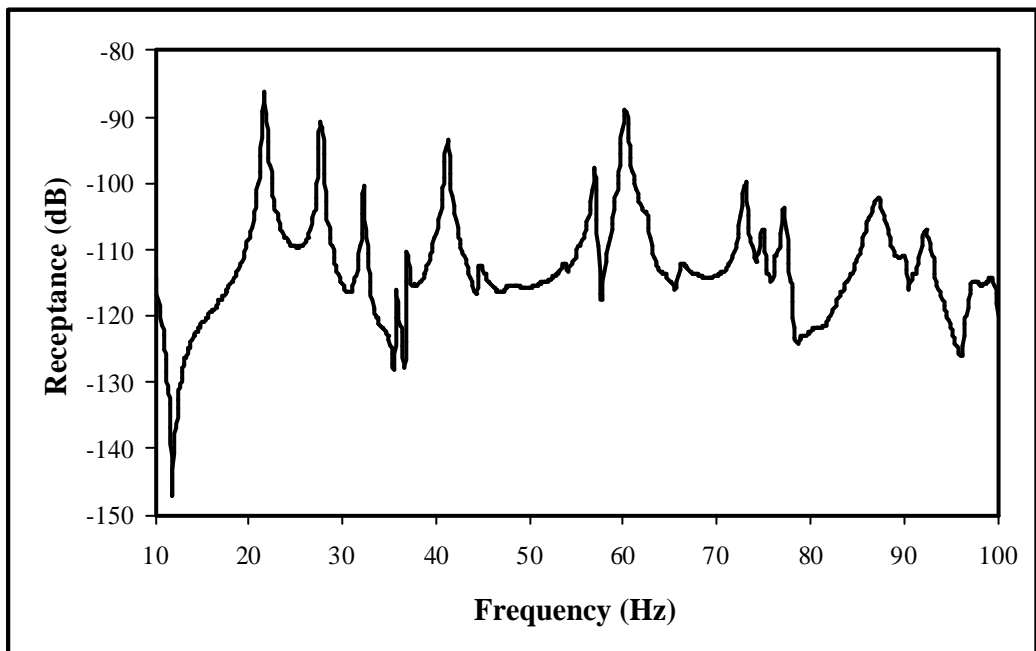


Figure 4.25 FRF between force at point o and response location 20

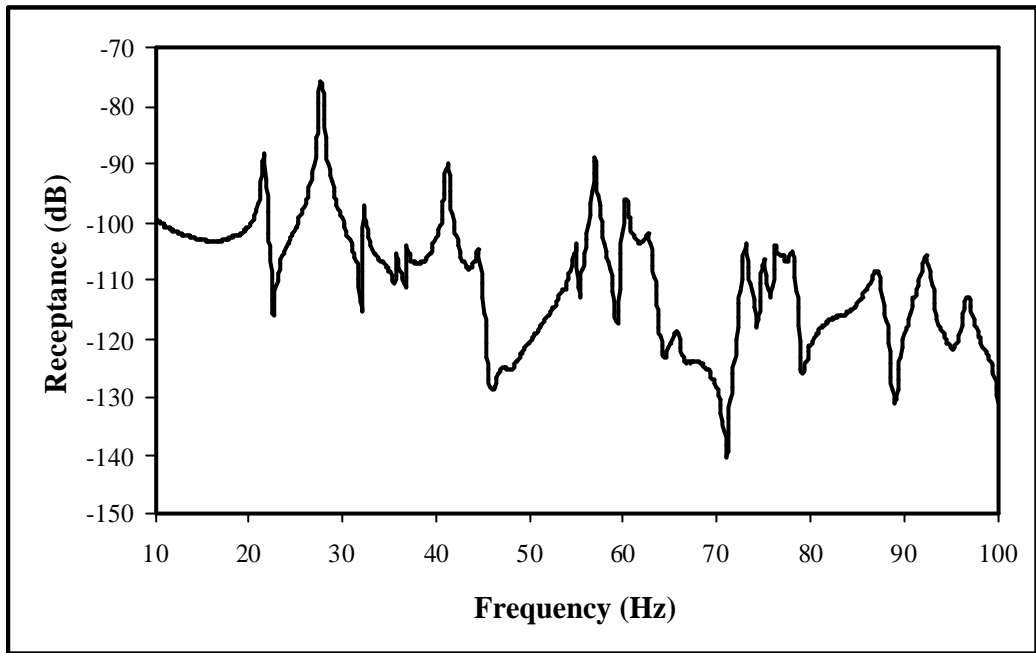


Figure 4.26 FRF between force at point o and response location 21

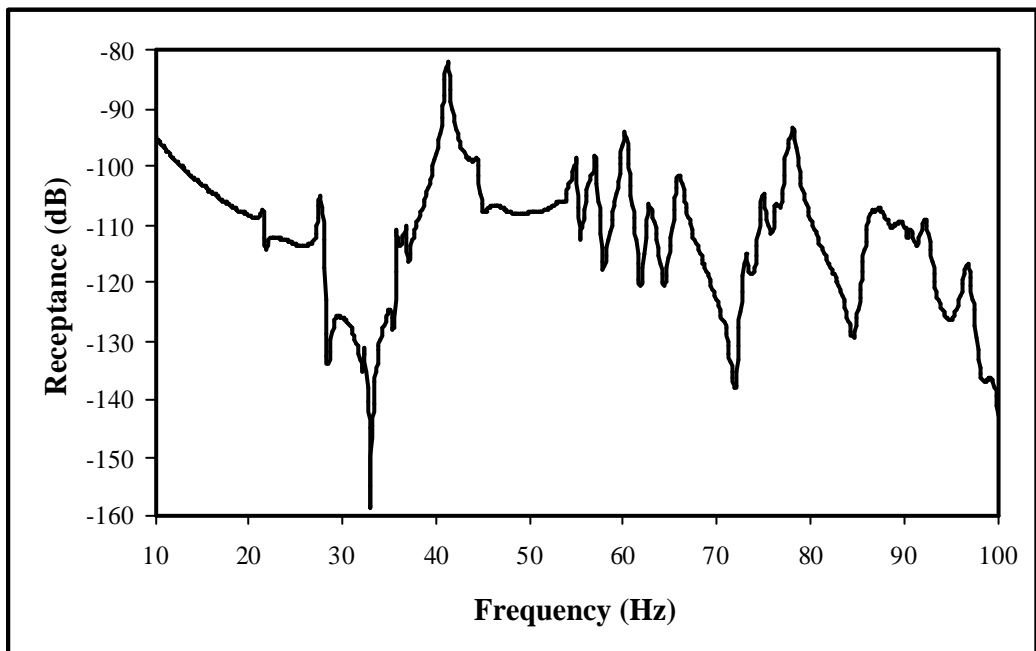


Figure 4.27 FRF between force at point o and response location 22

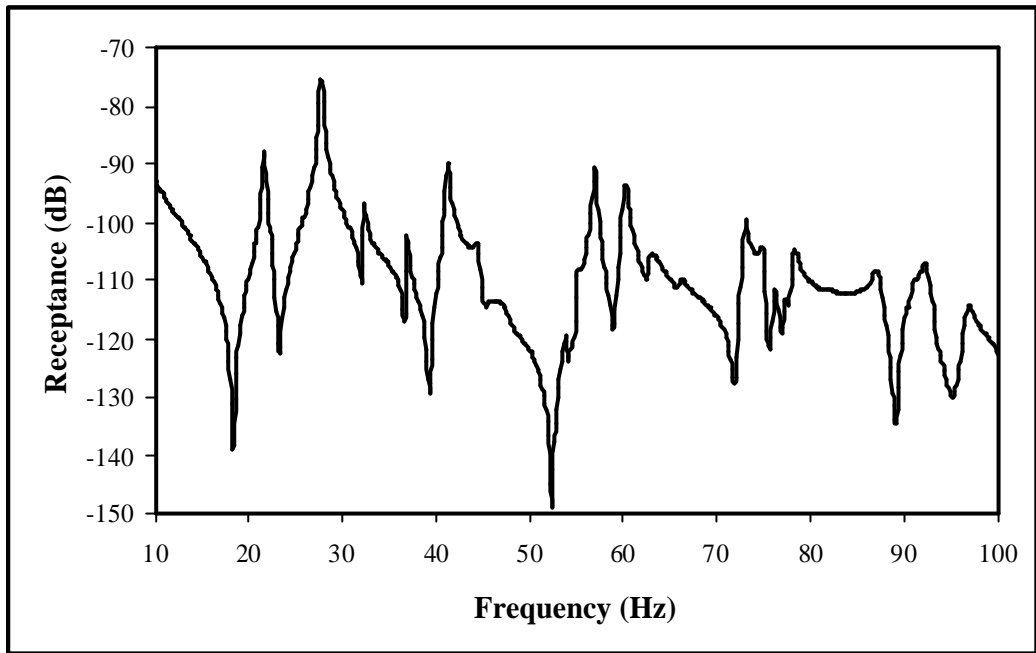


Figure 4.28 FRF between force at point 0 and response location 23

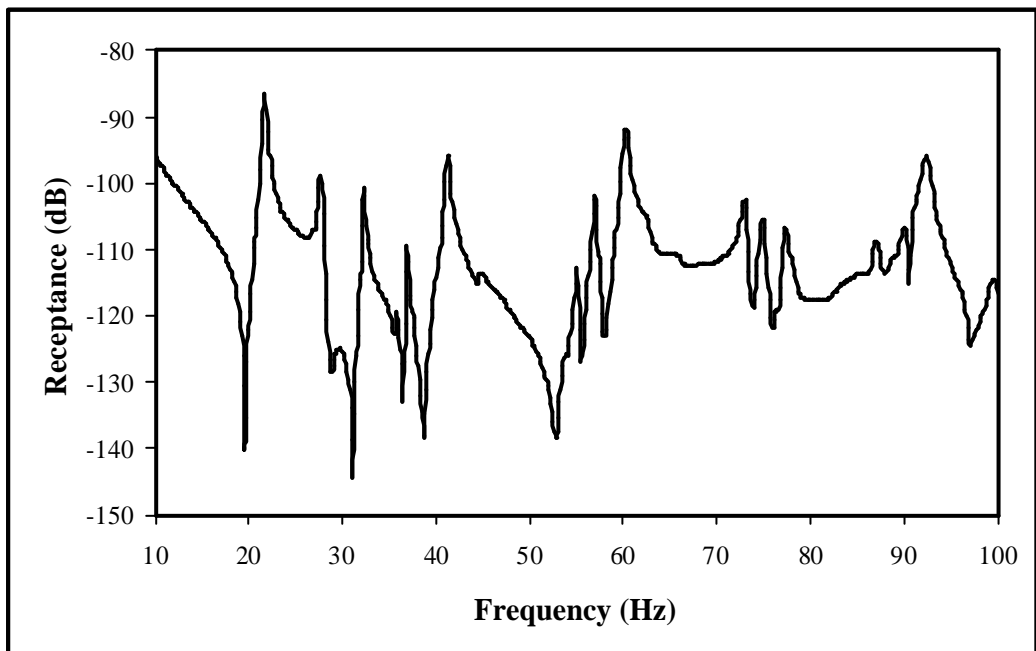


Figure 4.29 FRF between force at point 0 and response location 24

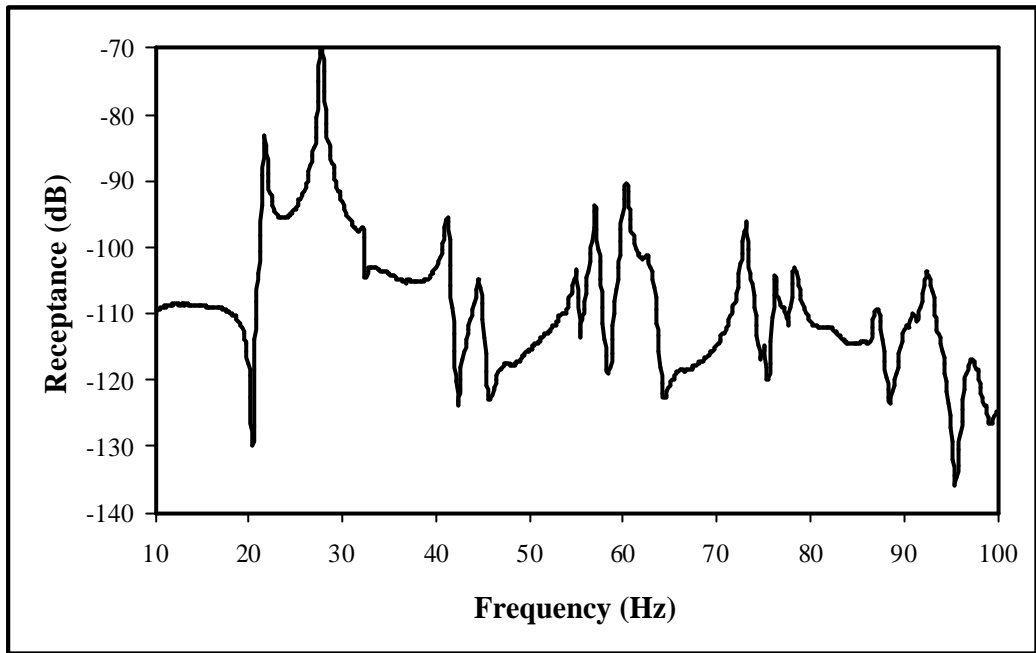


Figure 4.30 FRF between force at point o and response location 25

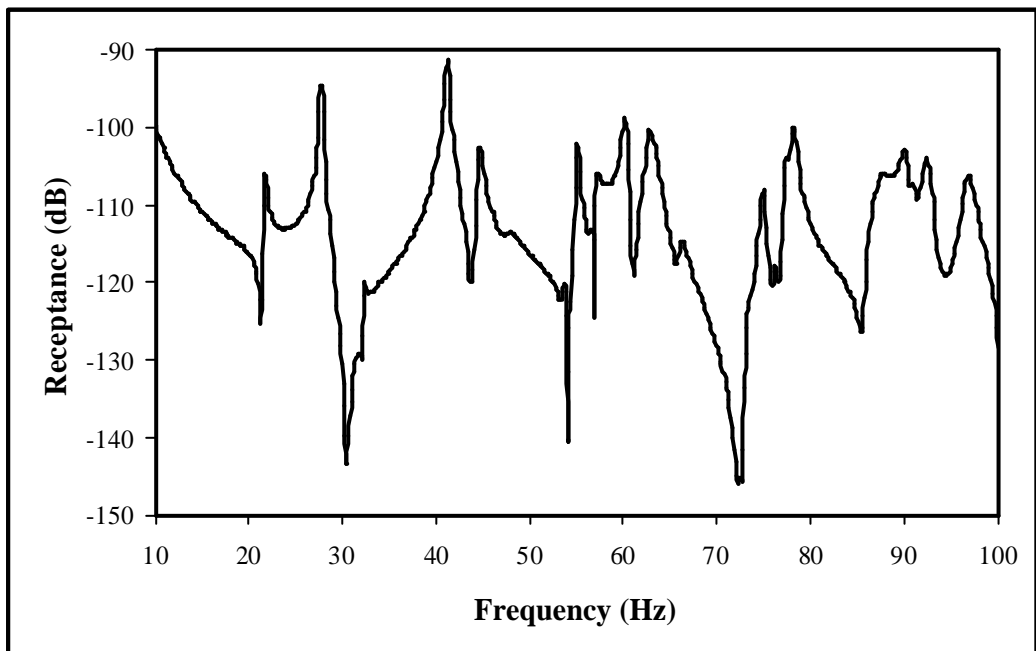


Figure 4.31 FRF between force at point o and response location 26

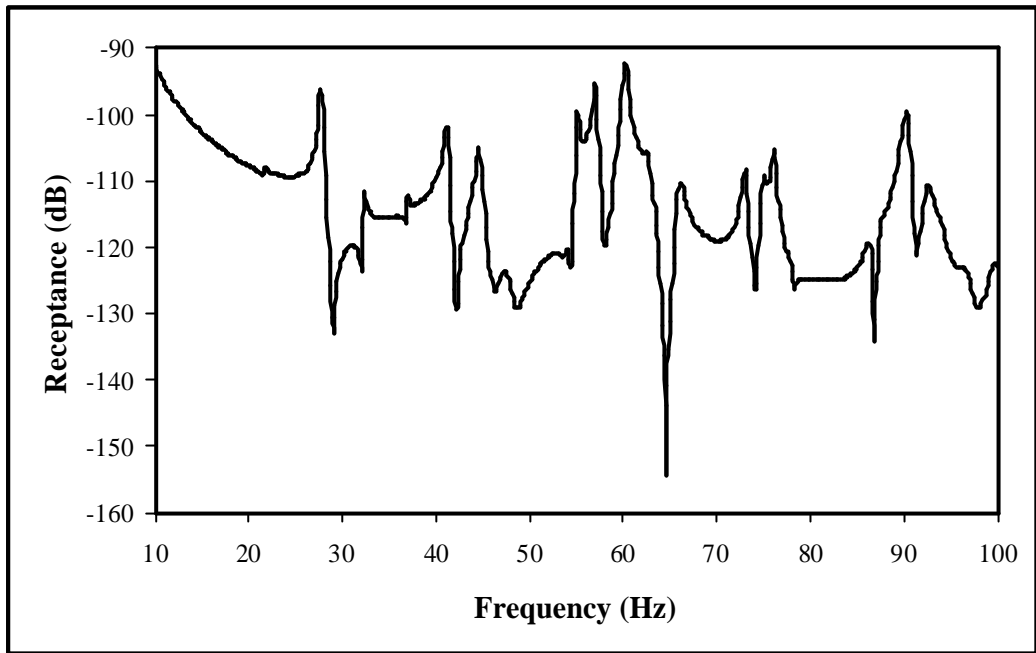


Figure 4.32 FRF between force at point 0 and response location 27

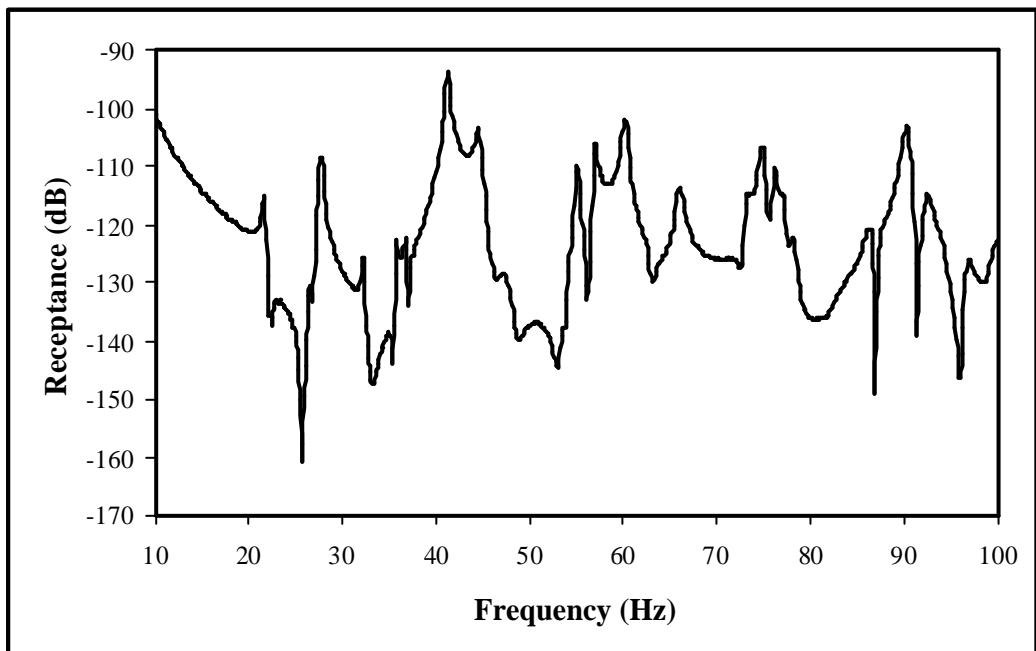


Figure 4.33 FRF between force at point 0 and response location 28

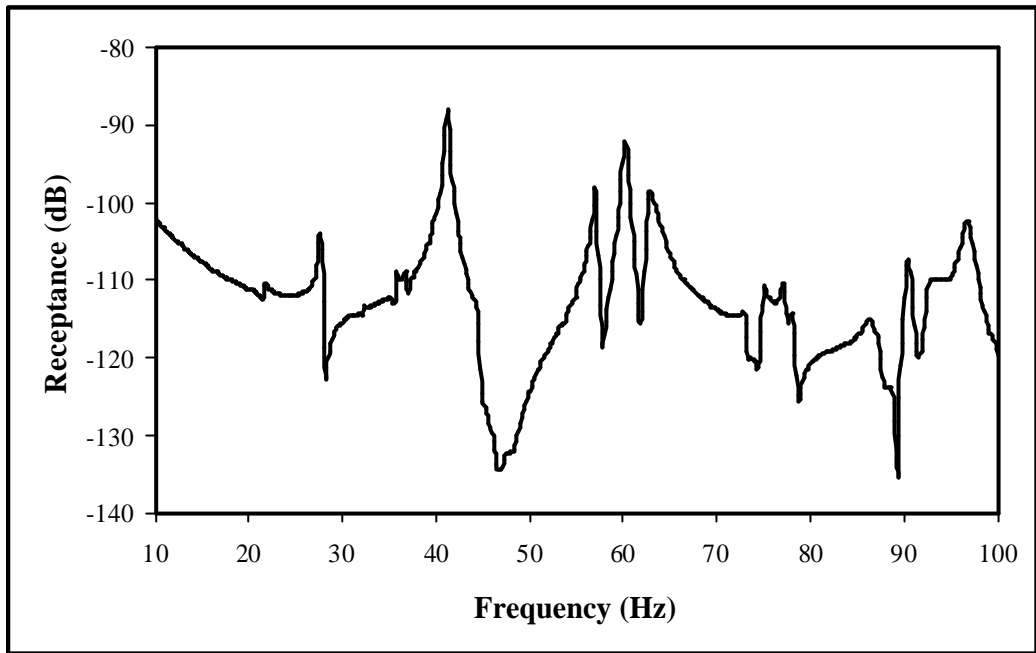


Figure 4.34 FRF between force at point o and response location 29

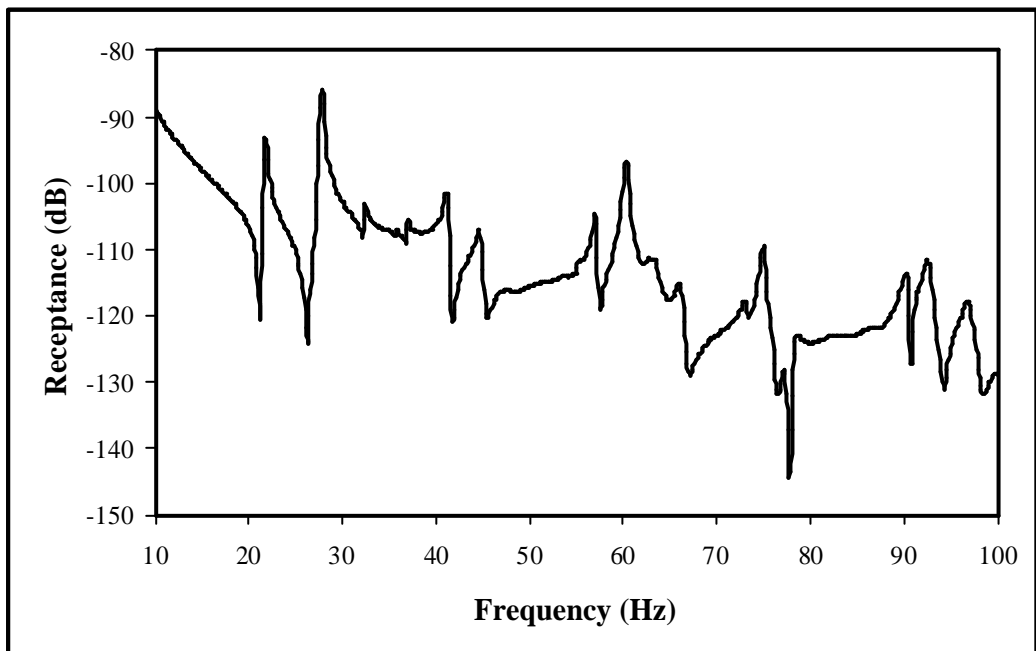


Figure 4.35 FRF between force at point o and response location 30

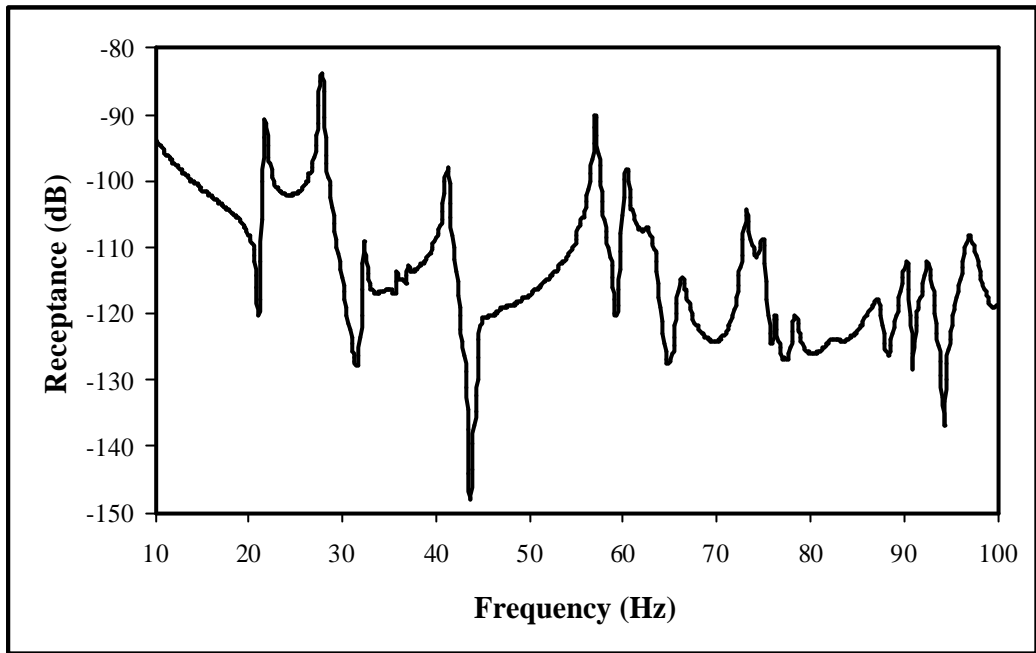


Figure 4.36 FRF between force at point 0 and response location 31

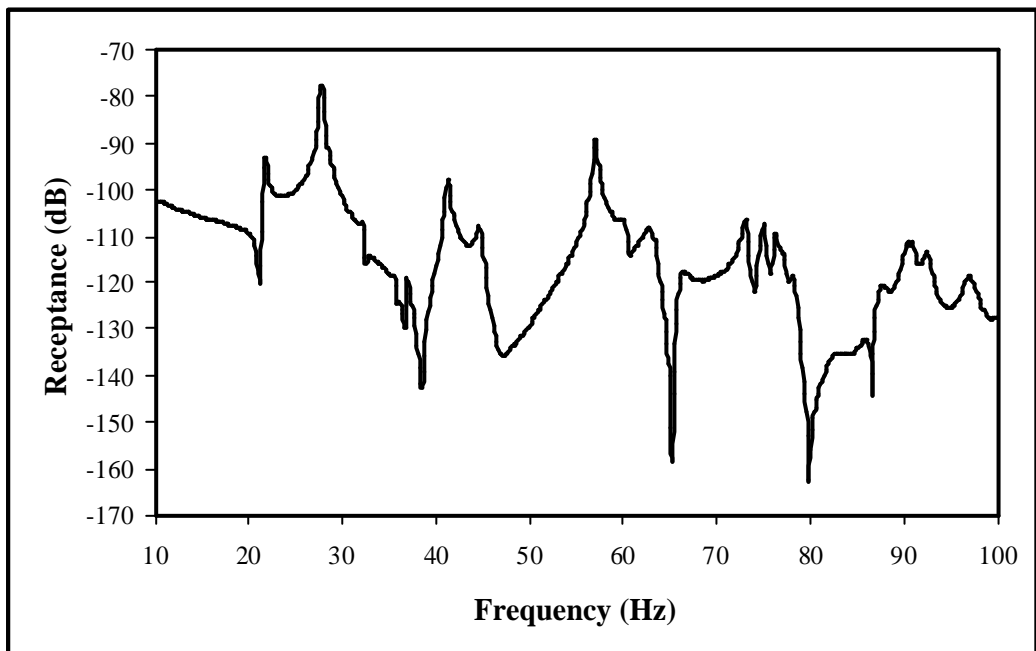


Figure 4.37 FRF between force at point 0 and response location 32

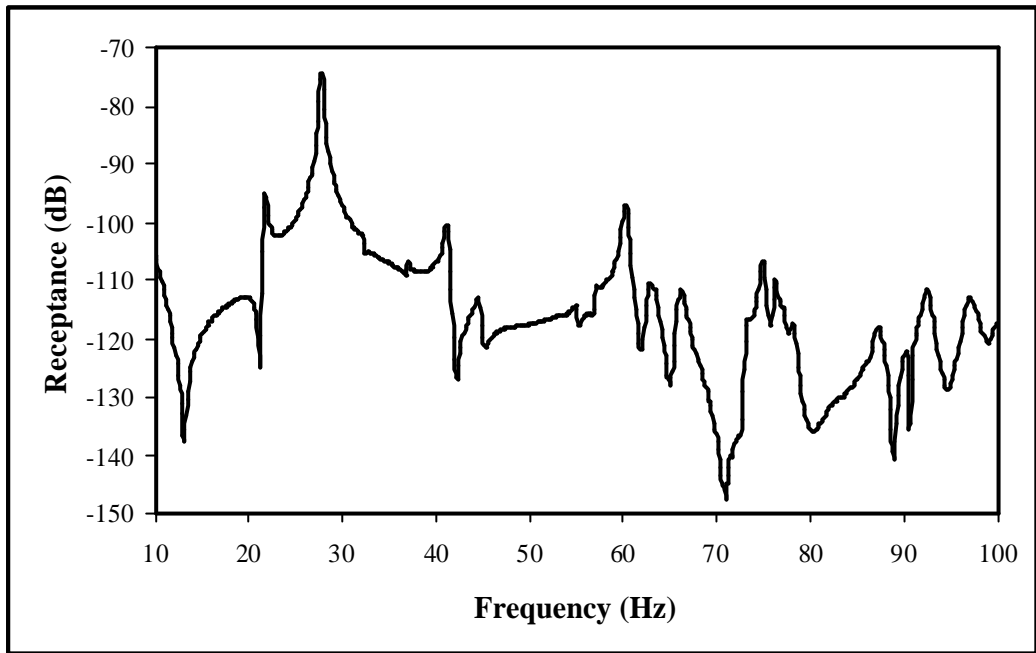


Figure 4.38 FRF between force at point o and response location 33

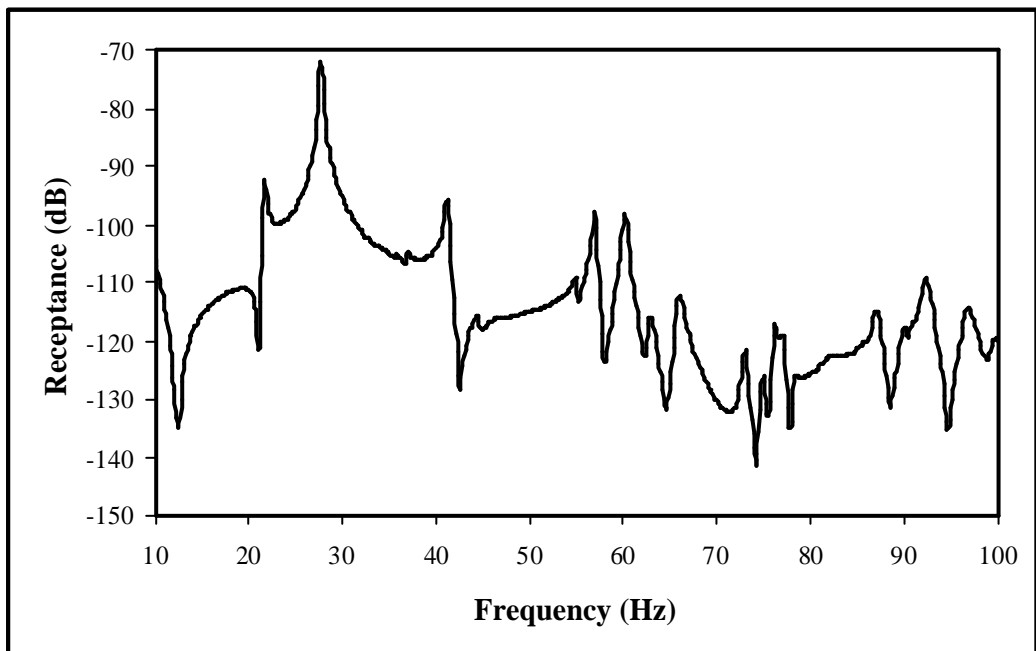


Figure 4.39 FRF between force at point o and response location 34

4.2.2 Natural Frequencies of body-in-white

Natural frequencies of car body-in-white are easily determined from the peaks observed in FRF plots. At these peaks the response is observed to have maximum corresponding to the excitation frequency.

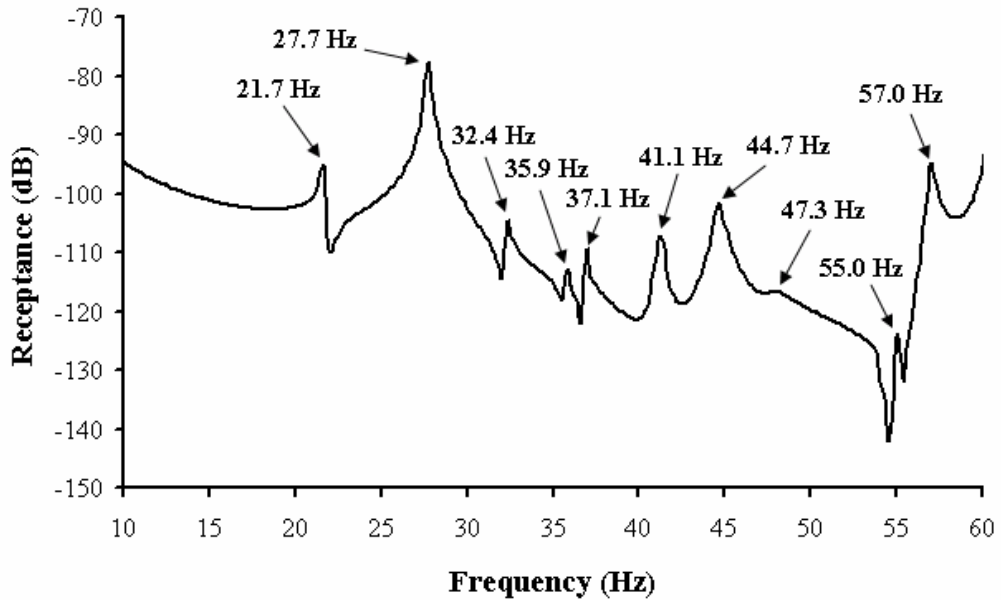


Figure 4.40 Natural frequencies from FRF plot @ location 13, 10-60 Hz

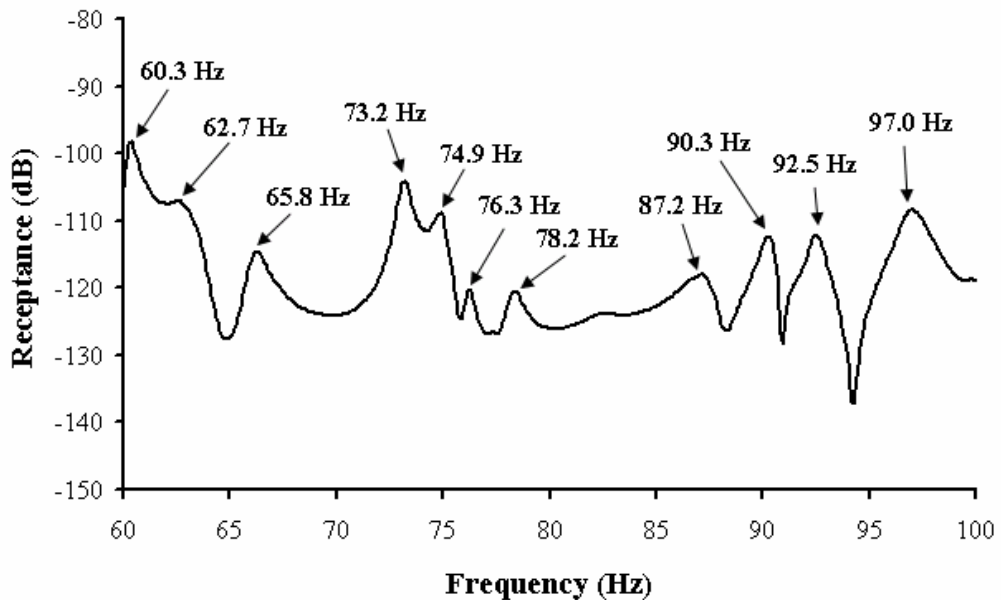


Figure 4.41 Natural frequencies from FRF plot @ location 31, 60-100 Hz

In FRF measurements, it is necessary to check the coherence. Coherence is a function of frequency with values between 0 and 1 that indicate how well the input corresponds to the output at each frequency. If measurement is good, then the coherence is unity. For a typical FRF measurement, coherence is good everywhere except near resonances and antiresonances. Coherence for the FRF given in Figure 4.40 is shown in Figure 4.42. Since the coherence values are good except the near resonances, FRF measurements are acceptable for natural frequency and mode shape determination.

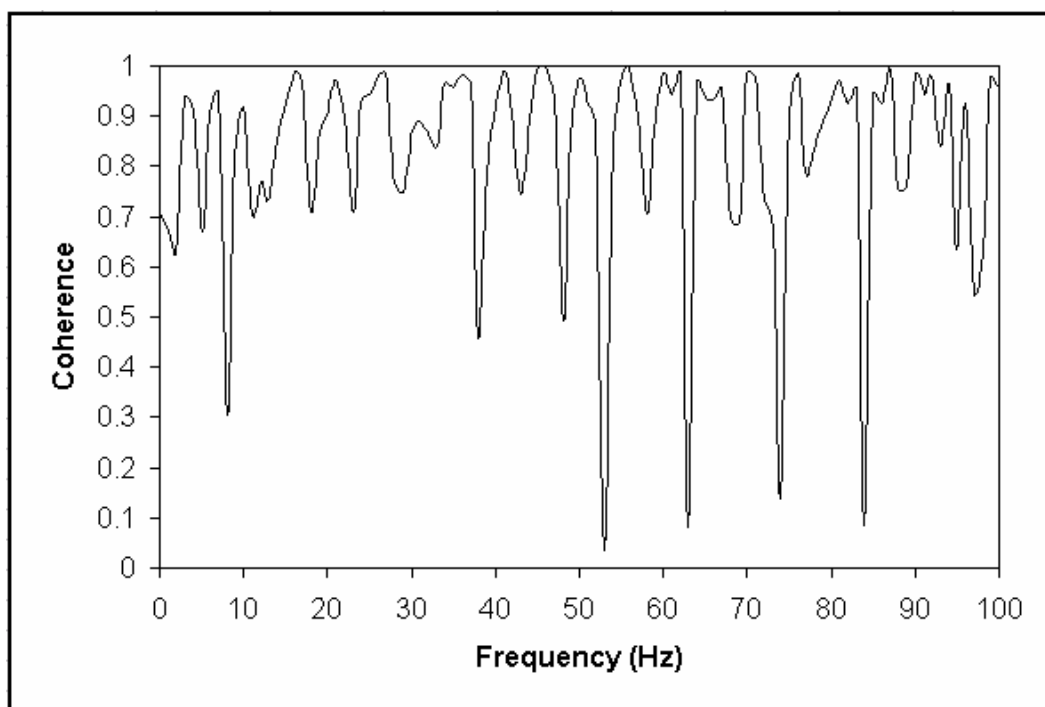


Figure 4.42 Coherence for FRF measurement @ location 13

The body-in-white has 21 resonances in the frequency range 10-100 Hz. The frequencies corresponding to the FRF peak values are shown in Figure 4.40 and Figure 4.41. The natural frequencies of the body are listed in Table 4.1.

Table 4.1 Natural frequencies of body-in-white

| | Natural frequencies (Hz) |
|-----------|---------------------------------|
| 1 | 21.7 |
| 2 | 27.7 |
| 3 | 32.4 |
| 4 | 35.9 |
| 5 | 37.1 |
| 6 | 41.1 |
| 7 | 44.7 |
| 8 | 47.3 |
| 9 | 55.0 |
| 10 | 57.0 |
| 11 | 60.3 |
| 12 | 62.7 |
| 13 | 65.8 |
| 14 | 73.2 |
| 15 | 74.9 |
| 16 | 76.3 |
| 17 | 78.2 |
| 18 | 87.2 |
| 19 | 90.3 |
| 20 | 92.5 |
| 21 | 97.0 |

4.2.3 Mode shapes of body-in-white

The natural frequencies of the body-in-white have been determined in the frequency range of interest. The body has specific mode shapes for each of these natural frequencies. Since there are 21 natural frequencies, the body will have 21

flexible modes between 10-100 Hz. Since frequency response functions are given as displacement divided by force, mode shape factors in transfer functions will give the displacements for applied force inputs. Using the 'quadrature peak picking' method, mode shape factors are estimated from the imaginary part of the frequency response as mentioned in Chapter 2. For measurement points, the displacements are determined from the value of imaginary parts of the FRF at resonances and these values are used to draw the mode shape. Frequency versus imaginary part of FRF at location 1 is shown in Figure 4.43.

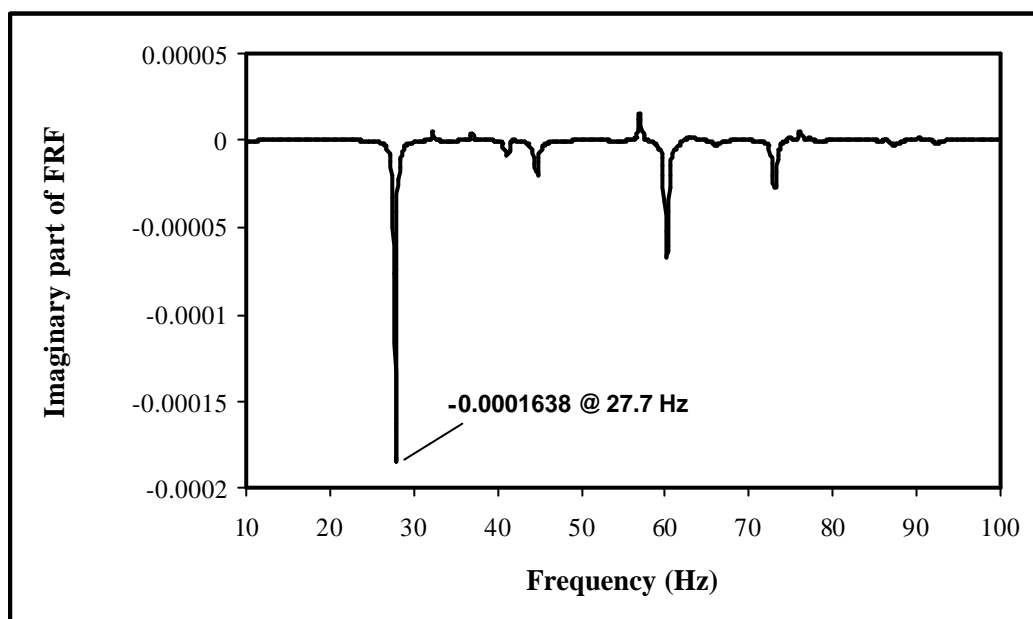


Figure 4.43 Imaginary part of FRF @27.7 Hz, location 1

Since imaginary parts are so small, a multiplier is used to make the modes more apprehensible in figures. At location 1, the displacement is taken as -0.0001638 as shown in Figure 4.43. In order to make it more sensible in figure, the value is multiplied by 10^6 and displacement at this location for 27.7 Hz is shown in Figure 4.44.

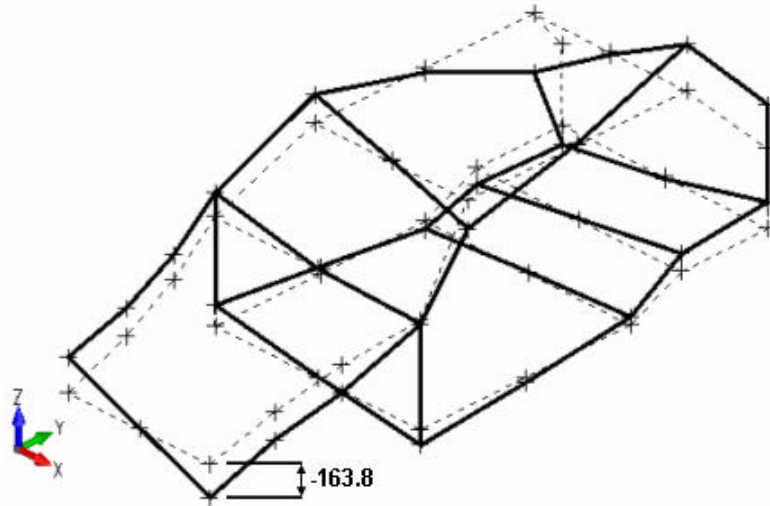


Figure 4.44 Displacement @ location 1, 27.7 Hz

It is possible to use circle fit method to determine the mode shape factor in frequency response function. For the same location, location 1, the FRF and the circle fit region for resonance at 41.1 Hz is shown in Figure 4.45.

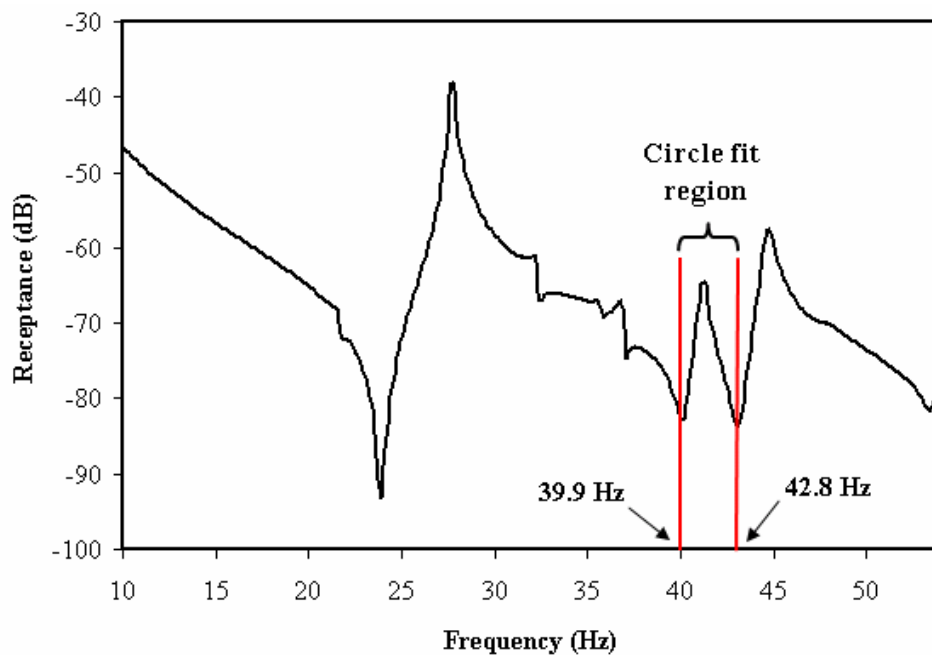


Figure 4.45 Circle fit region @ location 1, 41.1 Hz

The magnitude of mode shape factor is taken as the diameter of the circle fitted to real part versus imaginary part of FRF plot as shown in Figure 4.46. The

sign of mode shape factor is determined from the phase of FRF, it is positive if the phase at 41.1 Hz is between 0° - 180° , and it is negative if the phase is between -180° - 0° [24].

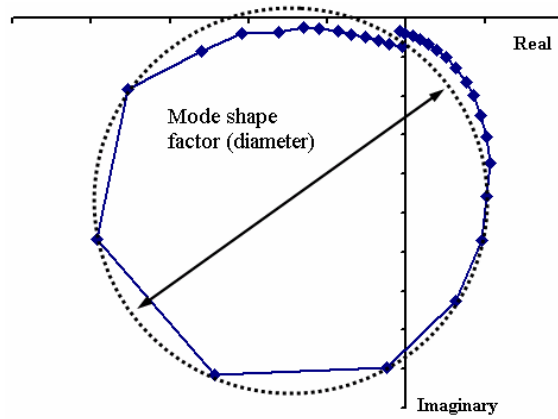


Figure 4.46 Mode shape factor estimation by circle fit @ location 1, 41.1 Hz

The mode shapes for each natural frequency are plotted using the imaginary parts of FRF data taken at 34 points (peak picking method), shown in Figure 4.5. All modes are shown between Figures 4.47-4.67.

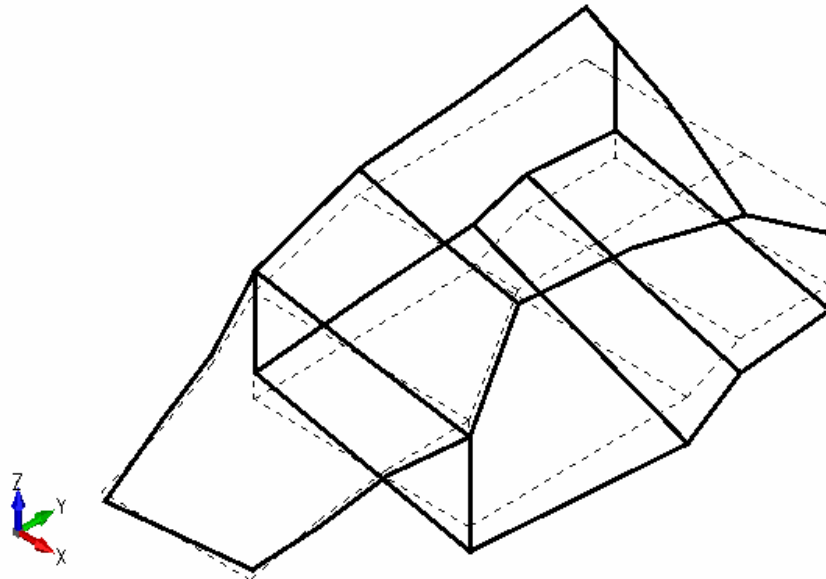


Figure 4.47 Mode shape @ 21.7 Hz

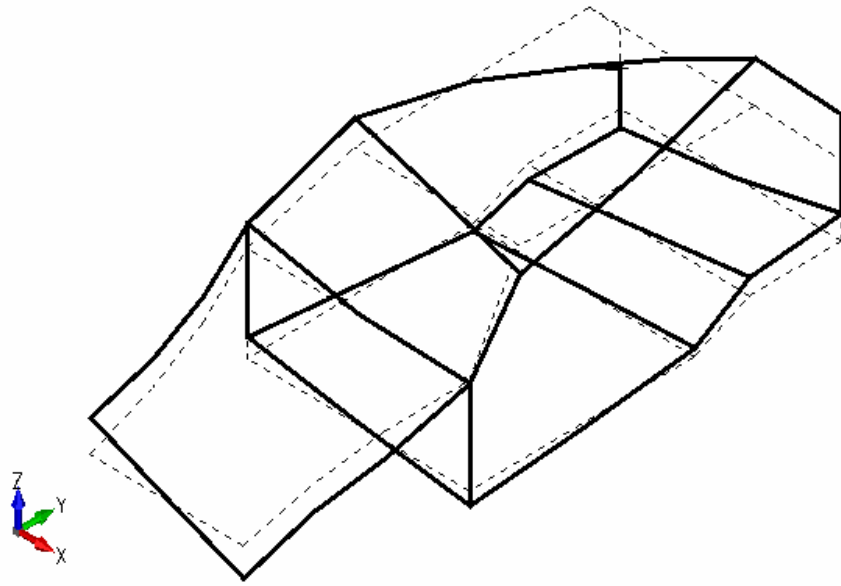


Figure 4.48 Mode shape @ 27.7 Hz

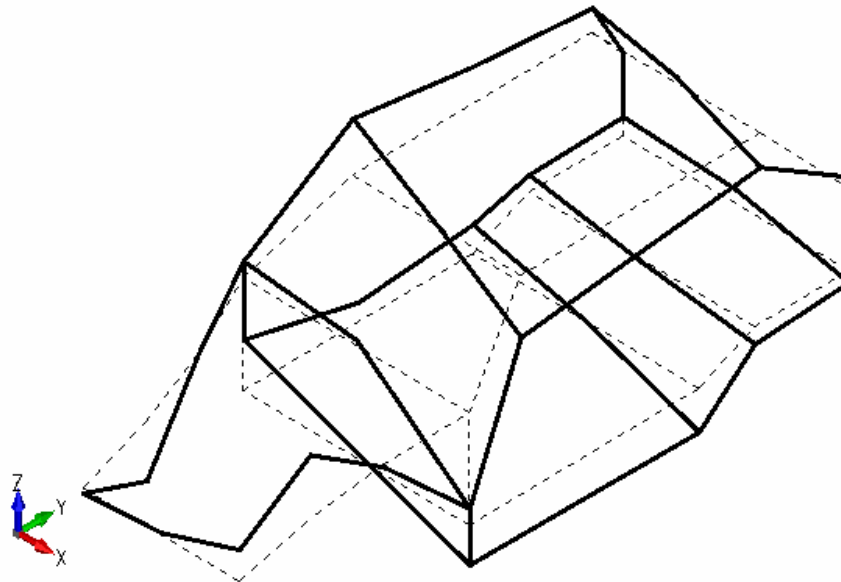


Figure 4.49 Mode shape @ 32.4 Hz

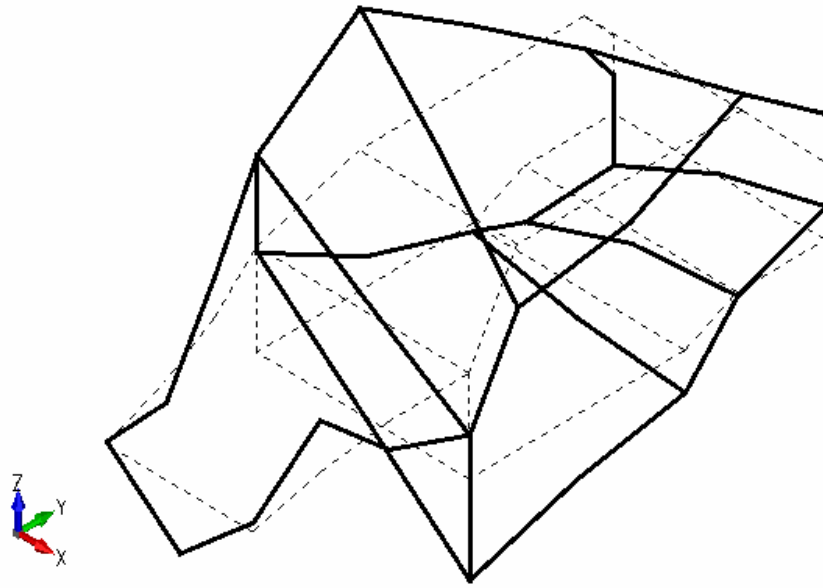


Figure 4.50 Mode shape @ 35.9 Hz

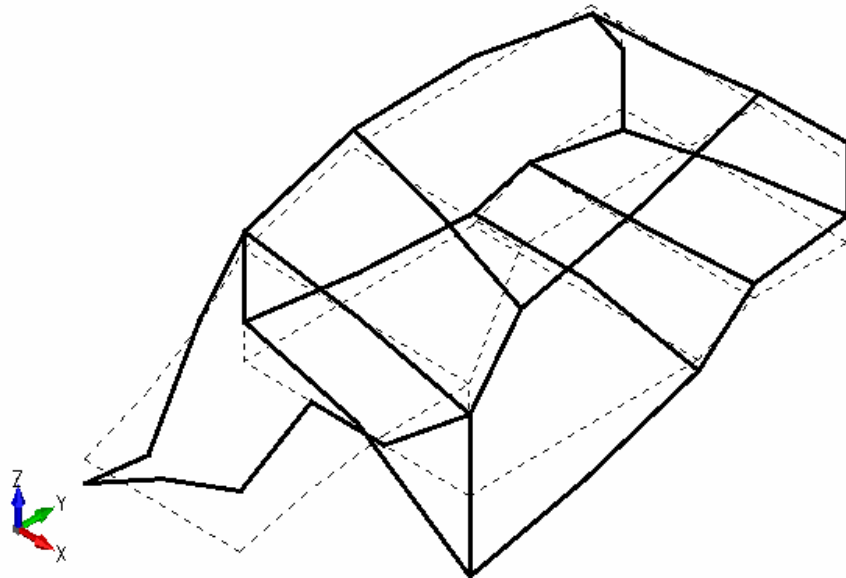


Figure 4.51 Mode shape @ 37.1 Hz

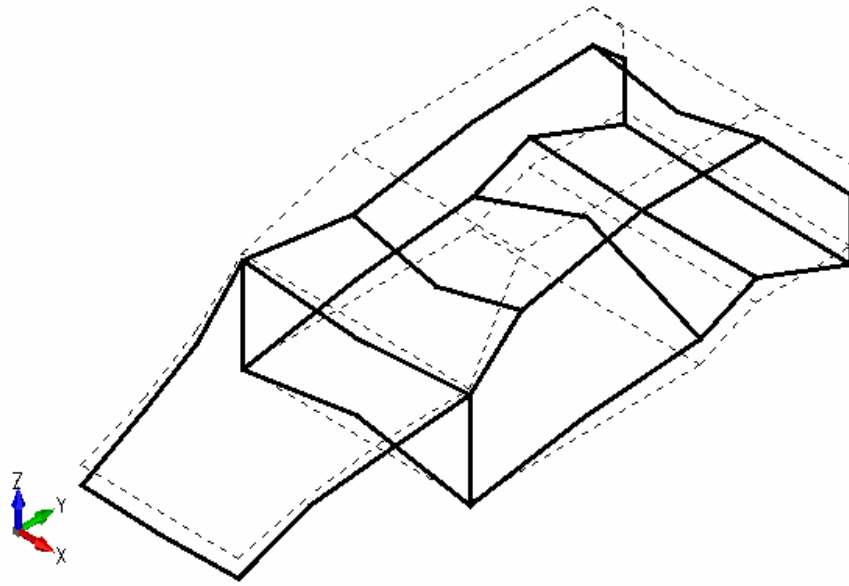


Figure 4.52 Mode shape @ 41.1 Hz

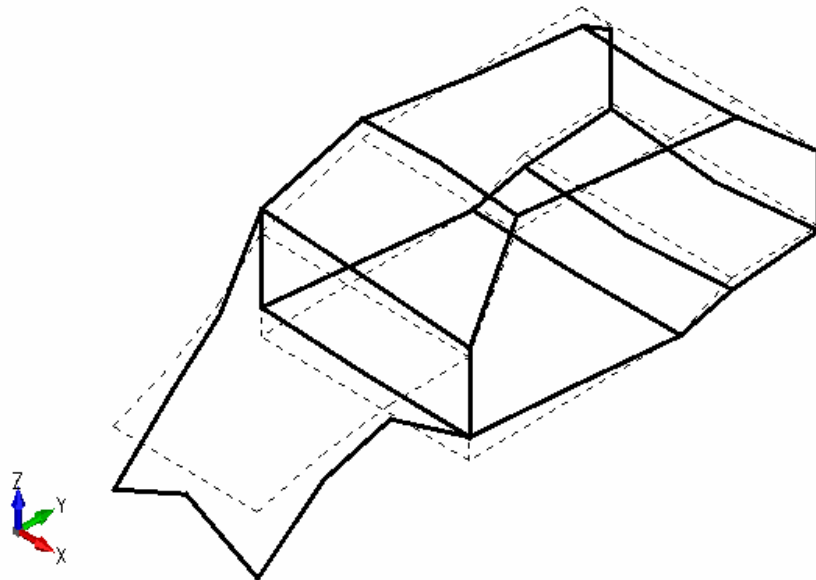


Figure 4.53 Mode shape @ 44.7 Hz

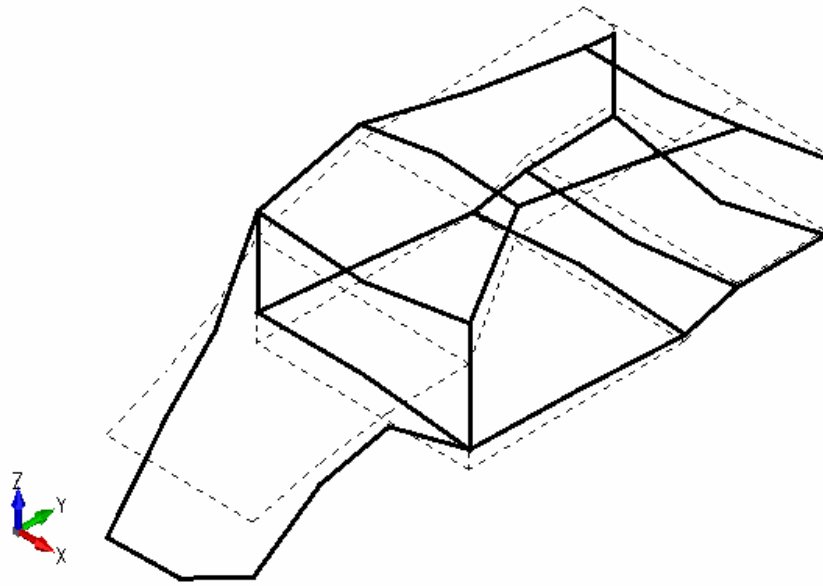


Figure 4.54 Mode shape @ 47.3 Hz

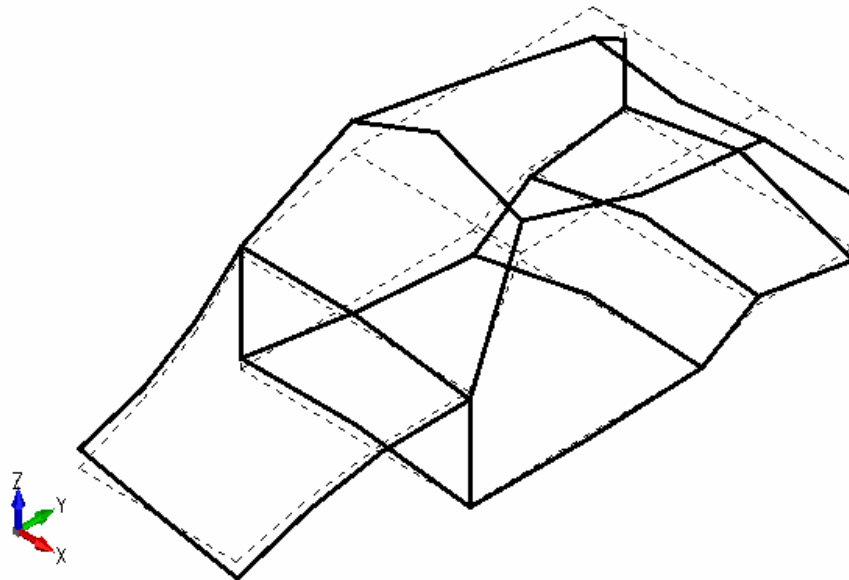


Figure 4.55 Mode shape @ 55.0 Hz

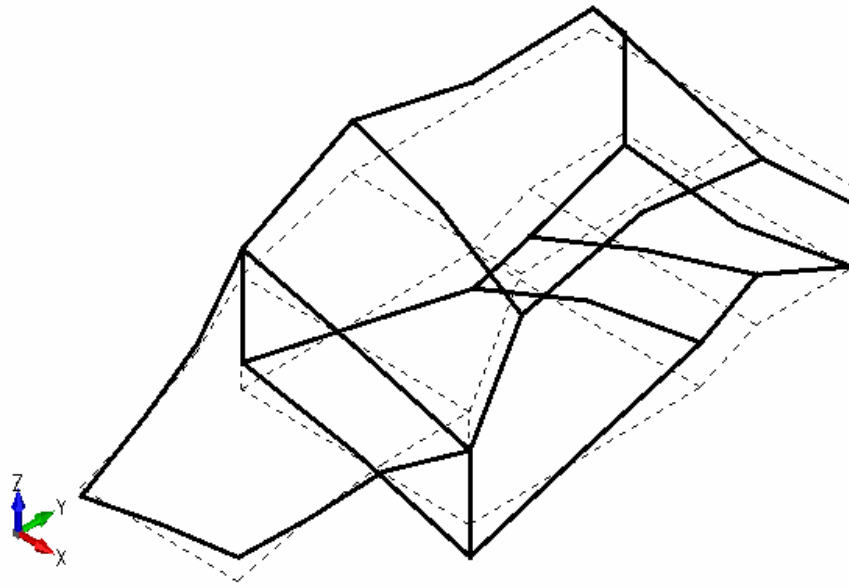


Figure 4.56 Mode shape @ 57.0 Hz

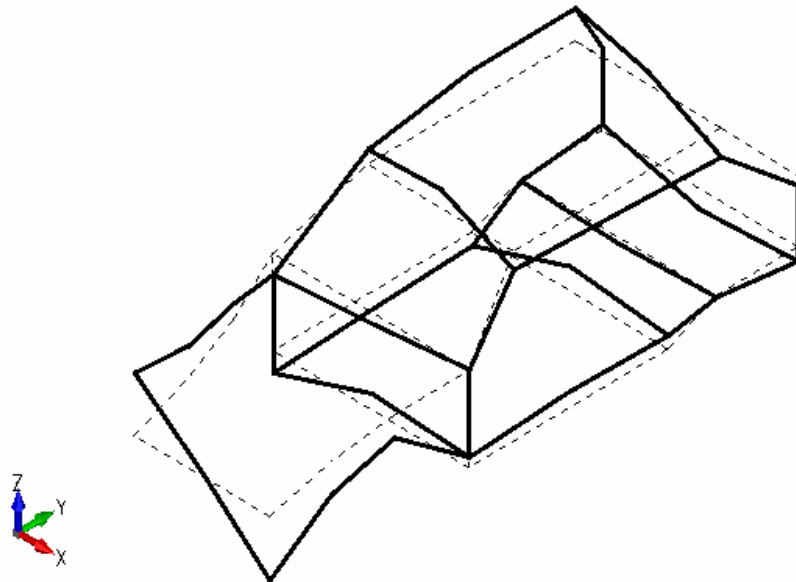


Figure 4.57 Mode shape @ 60.3 Hz

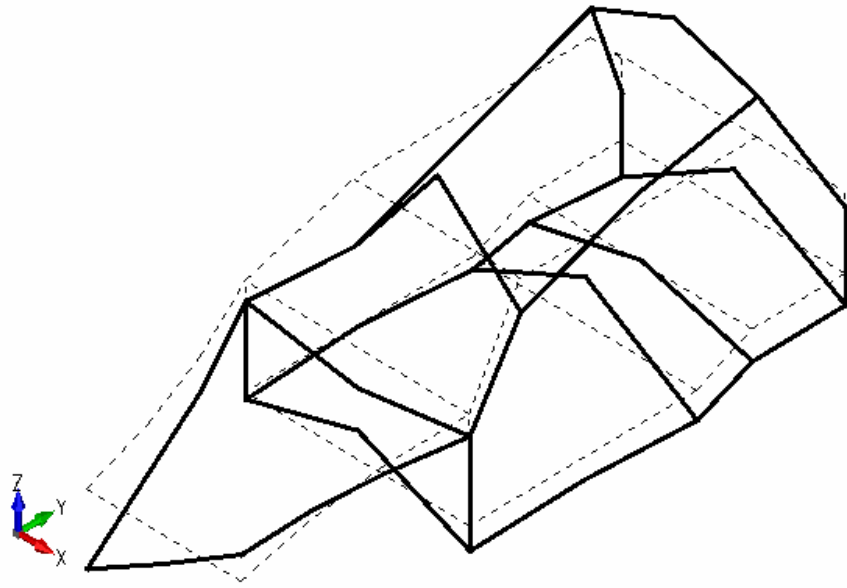


Figure 4.58 Mode shape @ 62.7 Hz

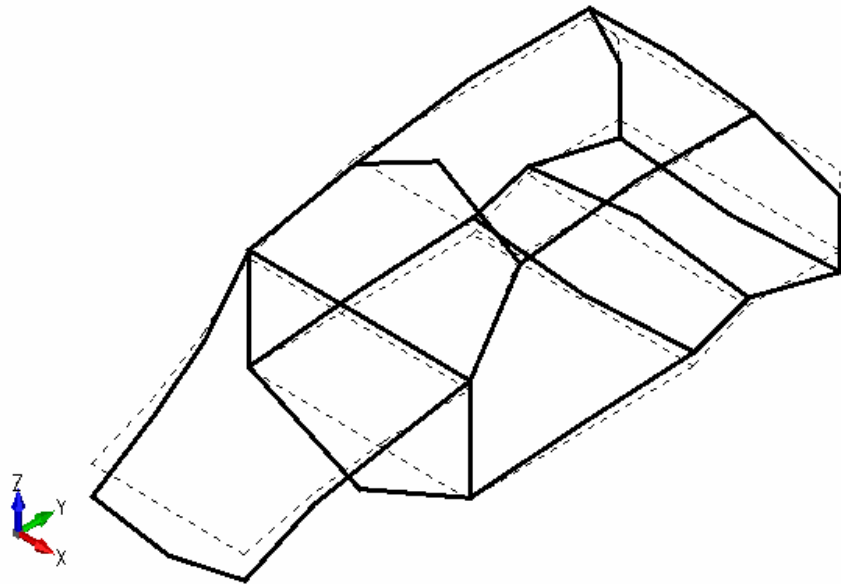


Figure 4.59 Mode shape @ 65.8 Hz

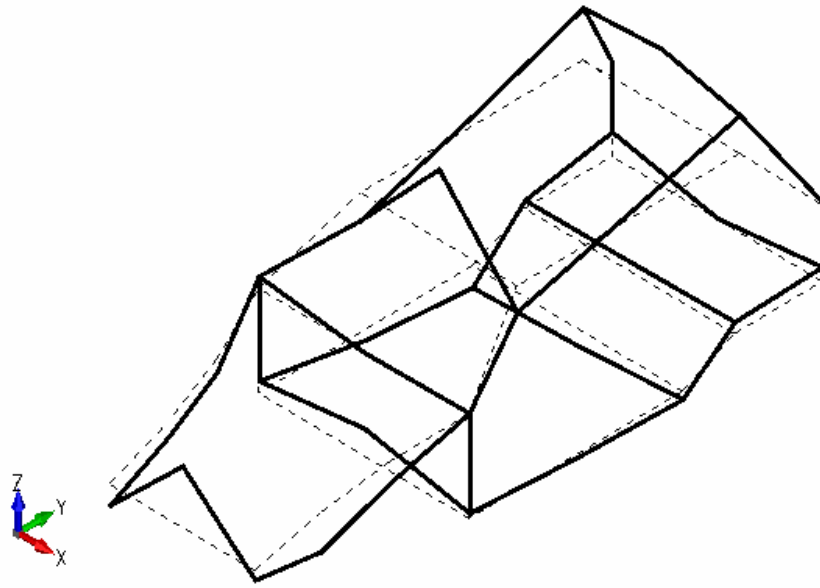


Figure 4.60 Mode shape @ 73.2 Hz

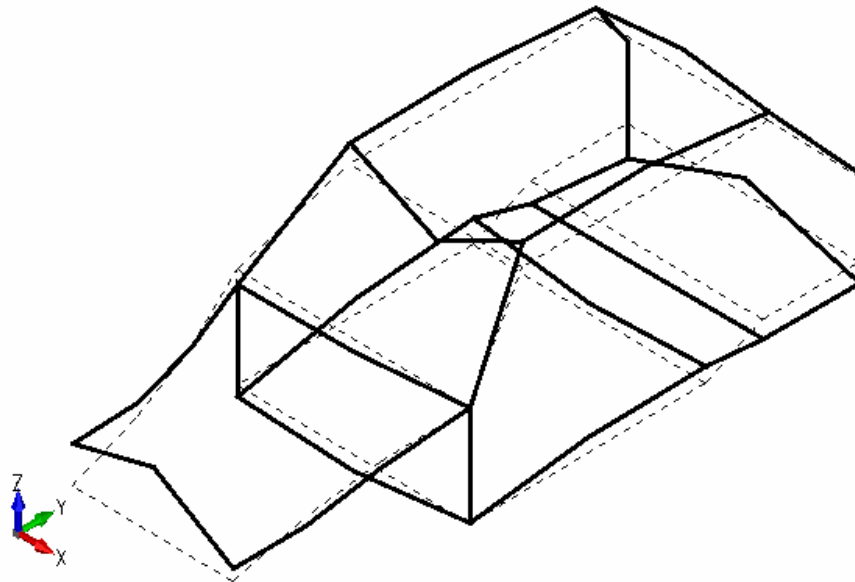


Figure 4.61 Mode shape @ 74.9 Hz

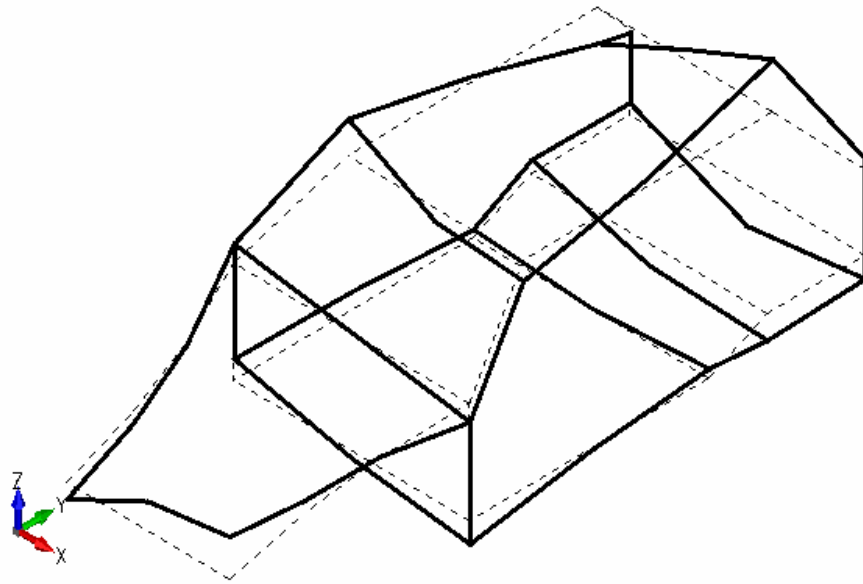


Figure 4.62 Mode shape @ 76.3 Hz

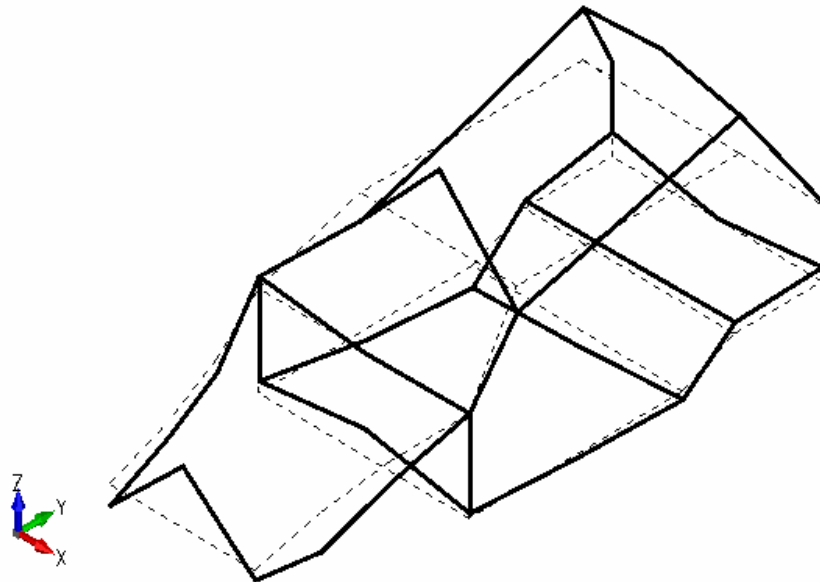


Figure 4.63 Mode shape @ 78.2 Hz

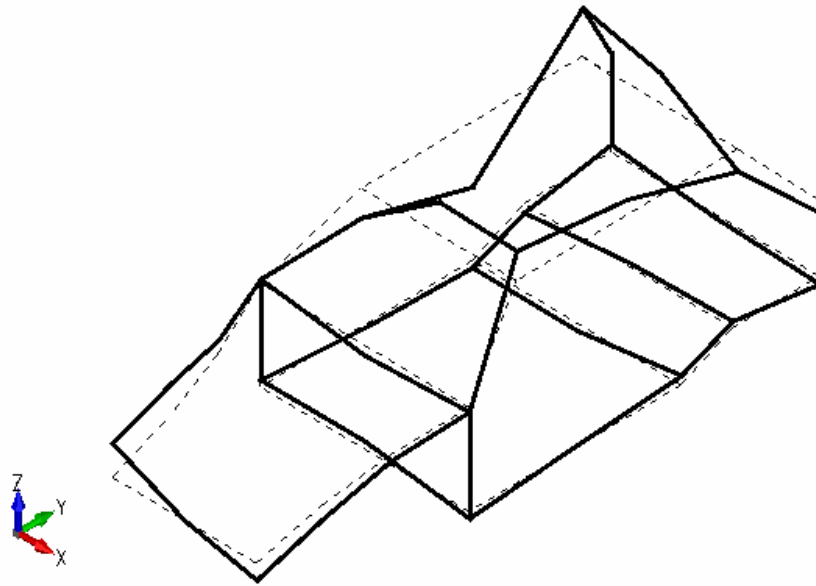


Figure 4.64 Mode shape @ 87.2 Hz

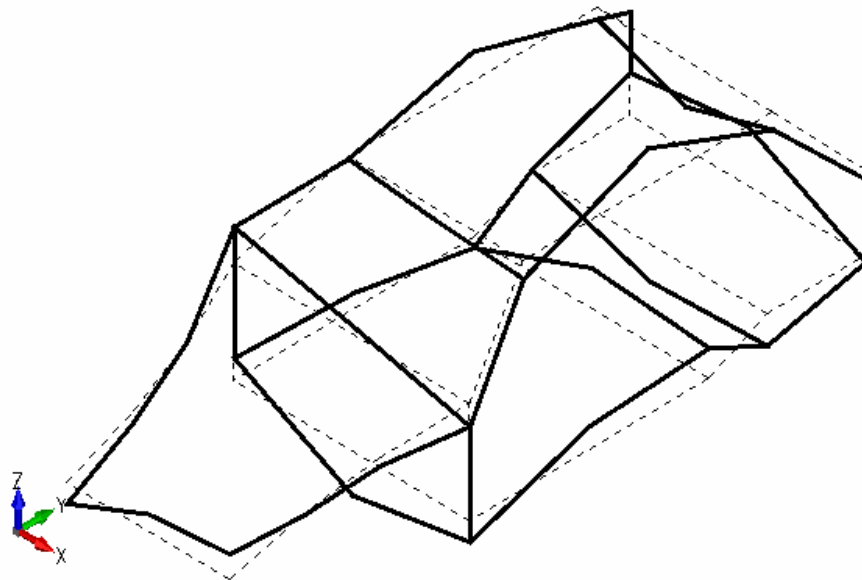


Figure 4.65 Mode shape @ 90.3 Hz

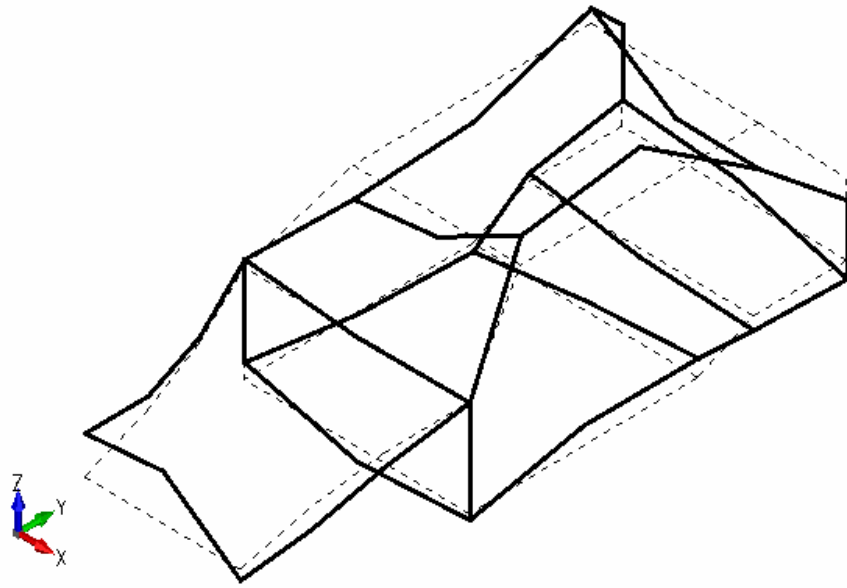


Figure 4.66 Mode shape @ 92.5 Hz

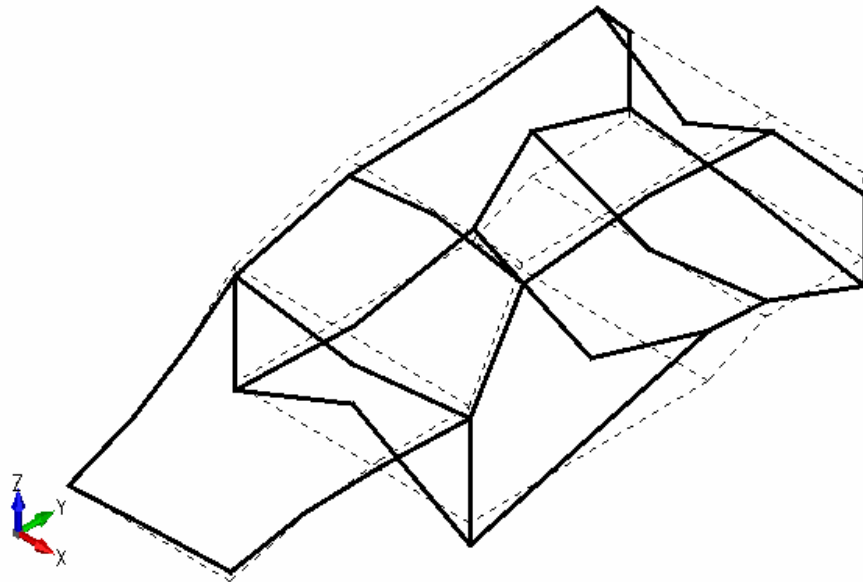


Figure 4.67 Mode shape @ 97.0 Hz

4.2.4 Identification of modes

By studying the mode shapes plotted using the wire frame model of body-in-white, modes are described as pure bending, pure torsional or combination of bending and torsional modes. Descriptions of mode shapes at each natural frequency are given in Table 4.2.

Table 4.2 Identification of modes

| Natural Frequency (Hz) | Description of mode |
|-------------------------------|----------------------------|
| 21.7 | 1 st torsional |
| 27.7 | 2 nd torsional |
| 32.4 | Bending + torsional |
| 35.9 | 3 rd torsional |
| 37.1 | Bending + torsional |
| 41.1 | 1 st bending |
| 44.7 | Bending + torsional |
| 47.3 | 2 nd bending |
| 55.0 | Bending + torsional |
| 57.0 | Torsional |
| 60.3 | Bending + torsional |
| 62.7 | Bending + torsional |
| 65.8 | 3 rd bending |
| 73.2 | Bending |
| 74.9 | Bending |
| 76.3 | Torsional |
| 78.2 | Bending + torsional |
| 87.2 | Torsional |
| 90.3 | Torsional |
| 92.5 | Torsional |
| 97.0 | Bending + torsional |

4.2.5 Sound pressure level

Sound pressure level at driver's ear position is measured in frequency range 10-100 Hz. The purpose of this measurement is to see if the resonances for sound pressure levels occur at the natural frequencies of body-in-white. The result of this measurement is given in Figure 4.68 with 401 points resolution. Sound pressure levels are presented in dB using reference value of $20 \cdot 10^{-5}$ Pa. The peak values for sound pressure level measurements are given in tabular form in Table 4.3.

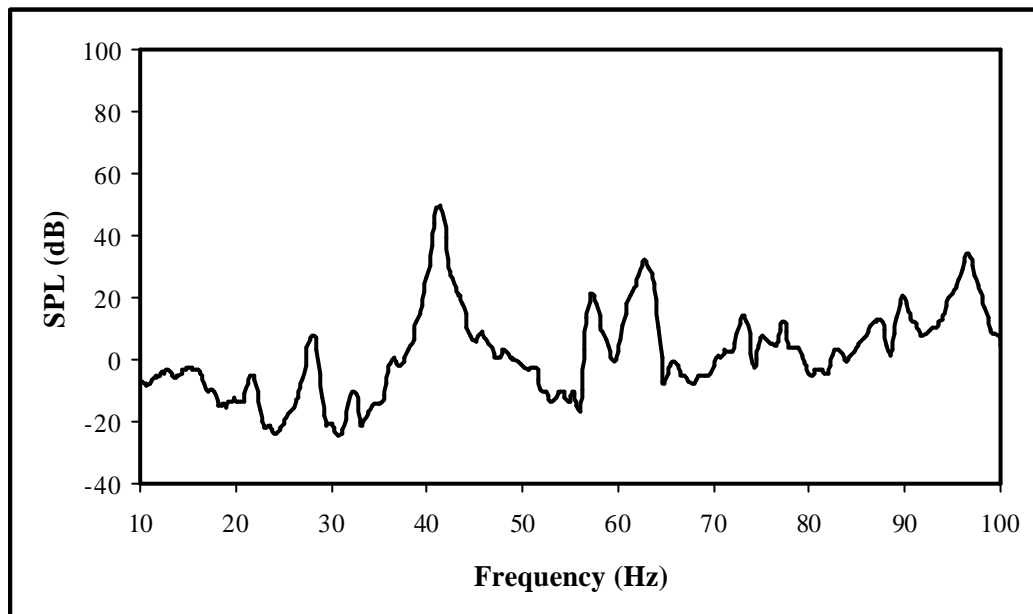


Figure 4.68 SPL, 401 points

Table 4.3 Peak frequencies from SPL measurement

| | | | | | | | | | |
|-----|-----------|-----------|-----------|-----------|-----------|-----------|-----------|-----------|-----------|
| | 1 | 2 | 3 | 4 | 5 | 6 | 7 | 8 | 9 |
| SPL | 21.8 | 28 | 32.3 | 35 | 36.5 | 41.3 | 45.8 | 48 | 54 |
| | 10 | 11 | 12 | 13 | 14 | 15 | 16 | 17 | 18 |
| SPL | 55.3 | 57.3 | 62.8 | 66 | 73.3 | 75.3 | 77.3 | 78.5 | 87.5 |
| | 19 | 20 | 21 | | | | | | |
| SPL | 89.8 | 92.3 | 96.8 | | | | | | |

Table 4.4 Peak frequencies from vibration and sound measurements

| Natural Frequency (Hz) | SPL Peak Frequency (Hz) | Difference (Hz) | Description of mode |
|-------------------------------|--------------------------------|------------------------|----------------------------|
| 21.7 | 21.8 | 0.1 | 1 st torsional |
| 27.7 | 28.0 | 0.3 | 2 nd torsional |
| 32.4 | 32.3 | -0.1 | Bending + torsional |
| 35.9 | 35.0 | 0.9 | 3 rd torsional |
| 37.1 | 36.5 | -0.6 | Bending + torsional |
| 41.1 | 41.3 | 0.2 | 1 st bending |
| 44.7 | 45.8 | 1.1 | Bending + torsional |
| 47.3 | 48.0 | 0.7 | 2 nd bending |
| 55.0 | 54.0 | 1.0 | Bending + torsional |
| 57.0 | 55.3 | -1.7 | Torsional |
| 60.3 | 57.3 | -3 | Bending + torsional |
| 62.7 | 62.8 | 0.1 | Bending + torsional |
| 65.8 | 66.0 | 0.2 | 3 rd bending |
| 73.2 | 73.3 | 0.1 | Bending |
| 74.9 | 75.3 | 0.4 | Bending |
| 76.3 | 77.3 | 1.0 | Torsional |
| 78.2 | 78.5 | 0.3 | Bending + torsional |
| 87.2 | 87.5 | 0.3 | Torsional |
| 90.3 | 89.8 | -0.5 | Torsional |
| 92.5 | 92.3 | -0.2 | Torsional |
| 97.0 | 96.8 | -0.2 | Bending + torsional |

Peak frequencies for both vibration and sound measurements are given in Table 4.4. Peak frequencies for these measurements are very close. It is expected to have peaks for sound measurements at natural frequencies of the body, since the noise generated is expected to be greater for larger displacements of body-in-white at its natural frequencies. Identification of modes is shown in Figure 4.69. Sound pressure levels at each peak frequency are plotted and the mode descriptions are given in Figure 4.70.

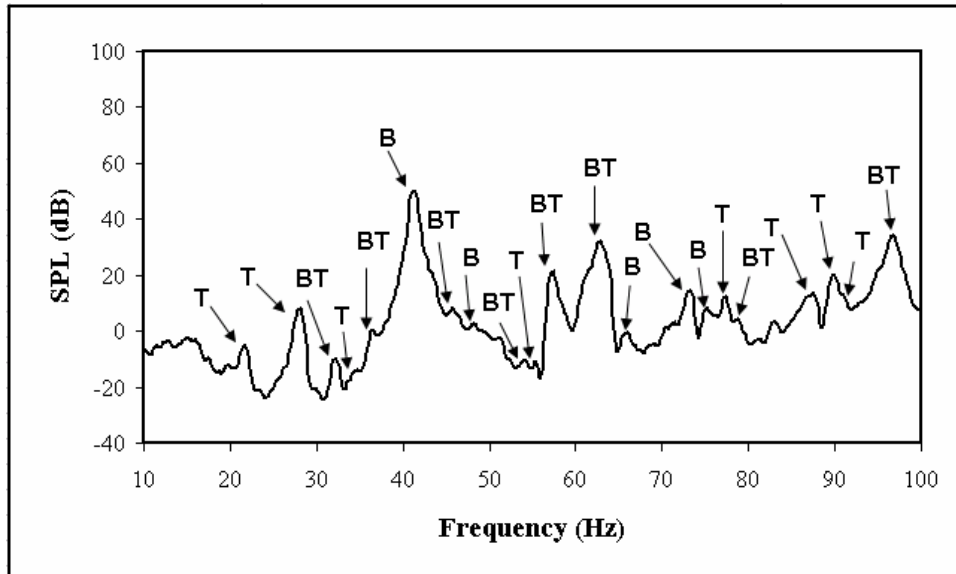


Figure 4.69 Mode descriptions (*T: Torsional, B: Bending, BT: Bending+Torsional*)

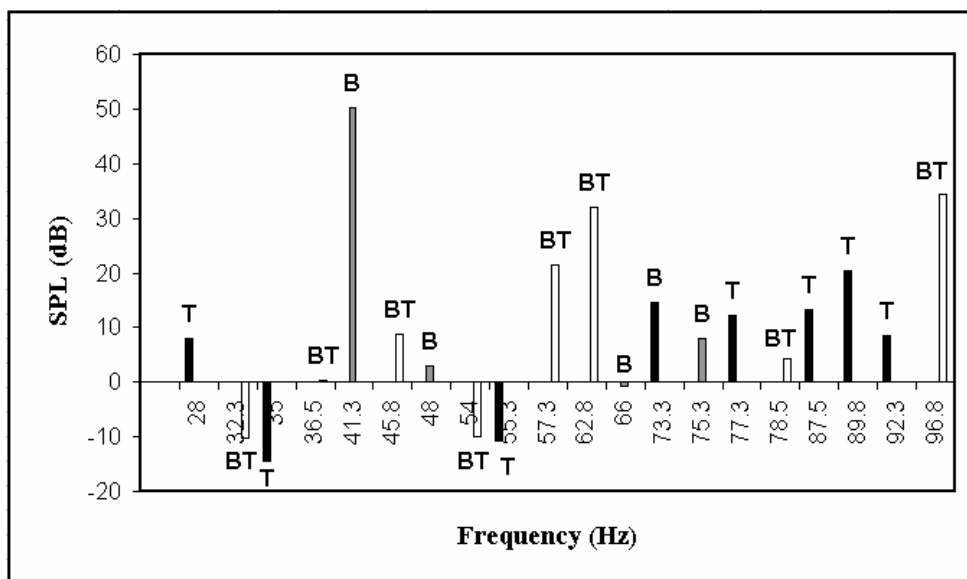


Figure 4.70 Sound pressure levels at peaks (*T: Torsional, B: Bending, BT: Bending+Torsional*)

From figure 4.70, it may be concluded that the noise levels for bending modes are greater than that of torsional modes since the highest level is observed for bending. In addition, noise levels for combination of bending and torsional modes are greater than that of pure torsional modes.

CHAPTER 5

COMPARISON OF TEST AND FINITE ELEMENT ANALYSIS RESULTS

5.1 FINITE ELEMENT MODEL

In the previous thesis study, completed by Özgen [25] in August 2001, first a CAD model and then the FE model was created for the car body-in-white which is used in this thesis study. The surface model of the body-in-white is shown in Figure 5.1 and the FE model is shown in Figure 5.2.

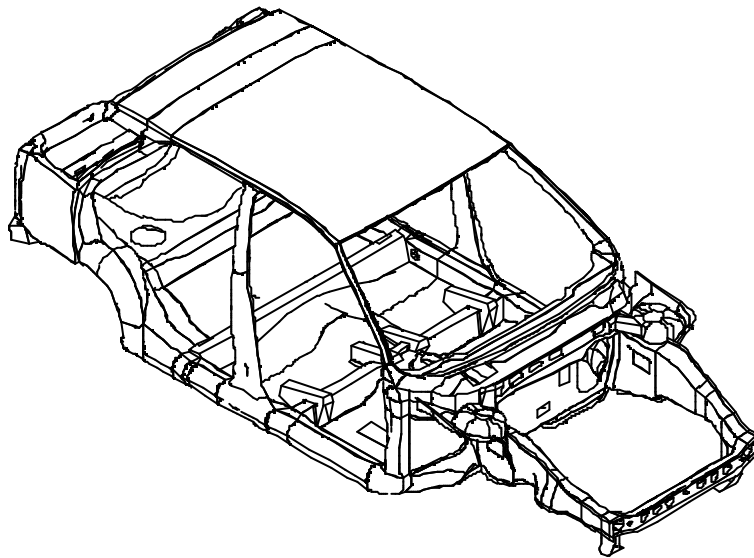


Figure 5.1 Surface model of body-in-white

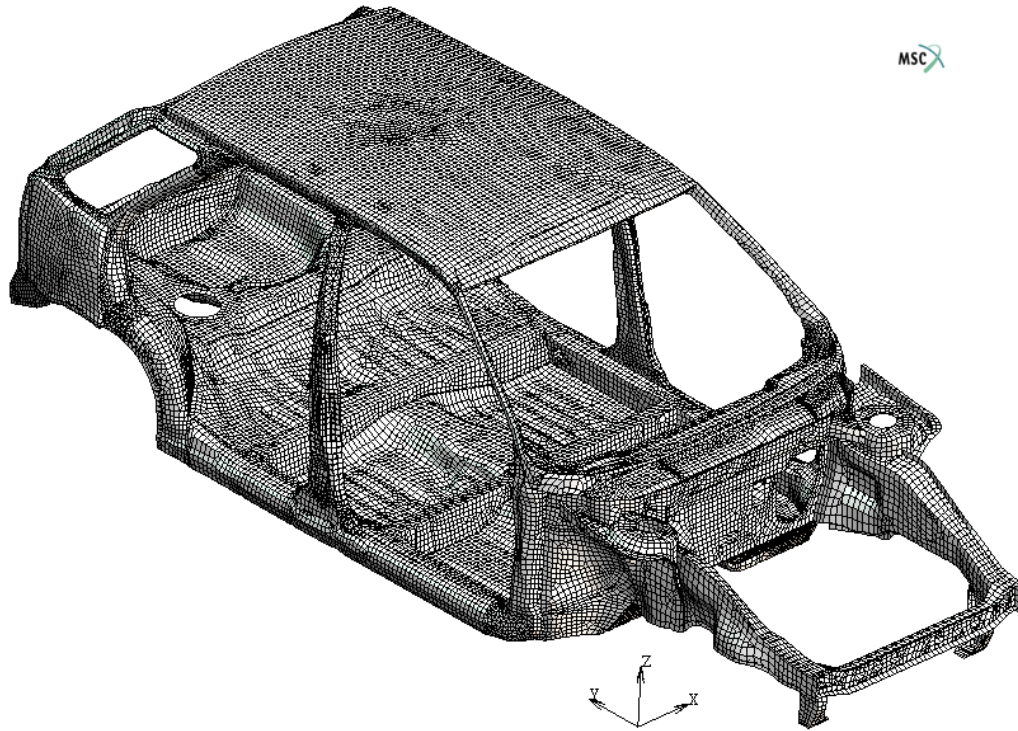


Figure 5.2 FE model of body-in-white

FE model contains 60962 elements and 54207 nodes.

5.2 FINITE ELEMENT ANALYSIS

Bending and torsional stiffness analyses have been performed as a part of static analysis using the FE software MSC.Marc. In dynamic analysis studies, first 10 undamped natural frequencies of body-in-white were found and the harmonic analysis was performed to find the frequency response of the body in the frequency range 5-54 Hz.

Performing a fully free vibration analysis, first 10 natural frequencies of the body has been calculated. Major structural modes and corresponding natural frequencies are given in Table 5.1.

Since the model is large, dynamic analysis has been performed dividing the frequency range into smaller parts.

Table 5.1 Natural frequencies and modes from FEA

| Mode number | Natural Frequency (Hz) | Description of mode |
|--------------------|-------------------------------|----------------------------|
| 1 | 24.2 | 1 st torsional |
| 2 | 30.1 | 2 nd torsional |
| 3 | 31.2 | - |
| 4 | 36.0 | 3 rd torsional |
| 5 | 42.2 | 1 st bending |
| 6 | 47.2 | - |
| 7 | 49.2 | 2 nd bending |
| 8 | 51.5 | - |
| 9 | 53.2 | - |
| 10 | 56.2 | - |

Mode shape figures and frequency response results from finite element analysis are given in Chapter 5.3.

5.3 FEA AND TEST RESULTS

Both experimental and analytical results for natural frequencies and mode shapes of car body-in-white are available to make a comparison. FRF plots from experiments are available for 34 points on the body. Nine points from the body are selected to compare the frequency responses. In order to have the transfer functions from FEA at these points, the job results files of harmonic analysis are opened in MSC.Marc and the data are collected.

5.3.1 Natural frequencies

First 10 natural frequency results of both FEA and tests are given in Table 5.2.

Table 5.2 Natural frequencies

| Mode number | FEA (Hz) | Test (Hz) | Difference % |
|--------------------|-----------------|------------------|---------------------|
| 1 | 24.2 | 21.7 | +10.3 |
| 2 | 30.1 | 27.7 | +7.9 |
| 3 | 31.2 | 32.4 | -3.8 |
| 4 | 36.0 | 35.9 | +0.3 |
| 5 | 42.2 | 37.1 | +12.1 |
| 6 | 47.2 | 41.1 | +12.9 |
| 7 | 49.2 | 44.7 | +9.1 |
| 8 | 51.5 | 47.3 | +8.1 |
| 9 | 53.2 | 55.0 | -3.4 |
| 10 | 56.2 | 57.0 | +1.4 |

An average of 6.9% change is observed between the natural frequencies found from FEA and tests. The basic reason to have such a difference in natural frequencies is incomplete FE model of the car body-in-white.

5.3.2 Mode shapes

Natural frequencies obtained from FEA and tests corresponding to major structural modes given in FEA results are given in Table 5.3.

Table 5.3 Mode shapes and corresponding natural frequencies from FEA and experiments

| Description of mode | FEA (Hz) | Test (Hz) | Difference % |
|----------------------------|-----------------|------------------|---------------------|
| 1 st torsional | 24.2 | 21.7 | +10.3 |
| 2 nd torsional | 30.1 | 27.7 | +7.9 |
| 3 rd torsional | 36.0 | 35.9 | +0.3 |
| 1 st bending | 42.2 | 41.1 | +2.6 |
| 2 nd bending | 49.2 | 47.3 | +3.8 |

An average of 4.9% difference is present between the natural frequencies corresponding to major structural modes described as pure bending or torsional. Test results are lower than the FEA results for major structural modes. However it can be seen if Table 5.2 is examined that there is no such a trend in the first 10 natural frequencies.

To see the compliance between the mode shape results of FEA and tests, the mode shapes are given in Figures 5.3-5.12. Displacement distribution patterns of the first five major structural modes of the body are given in Figures 5.3, 5.5, 5.7, 5.9, 5.11, gray-scale images are used in which light regions indicate z-displacement in positive direction and dark regions indicate z-displacement in negative direction. In test results, the deformed and the original bodies are given as wire frames with full lines and dashed lines, respectively.

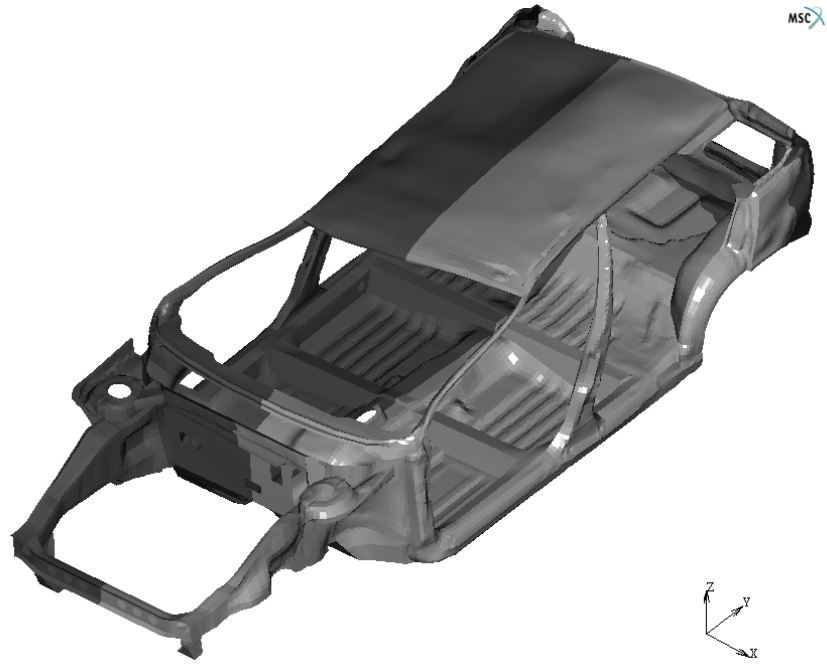


Figure 5.3 1st torsional mode @24.2 Hz, FEA

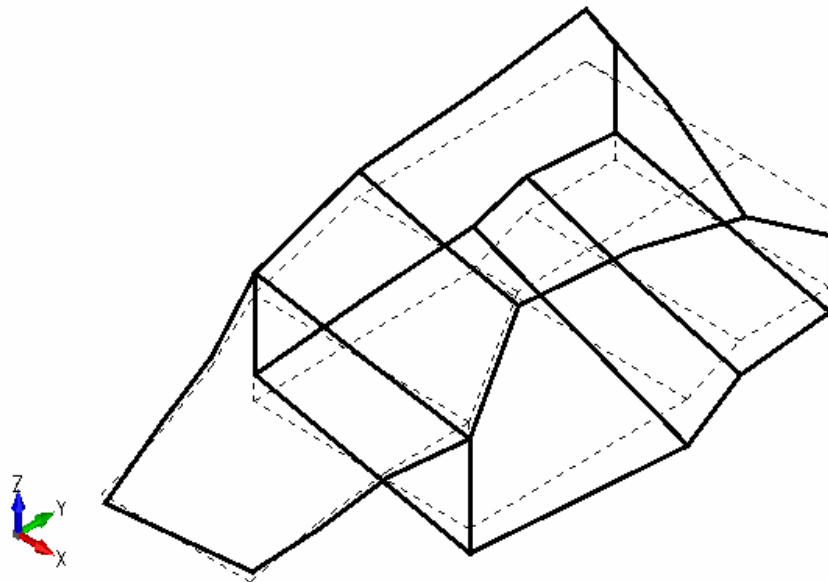


Figure 5.4 1st torsional mode @21.7 Hz, Test

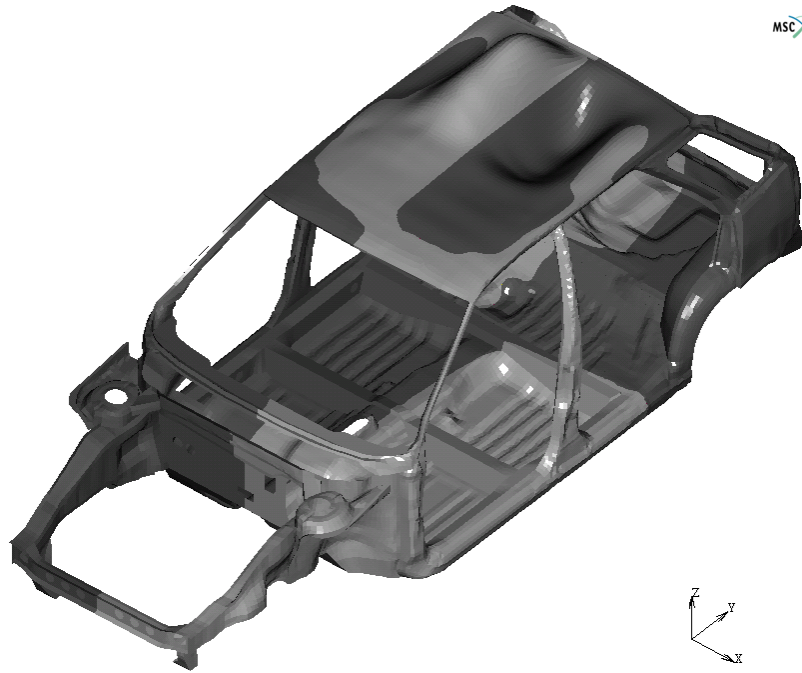


Figure 5.5 2nd torsional mode @30.1 Hz, FEA

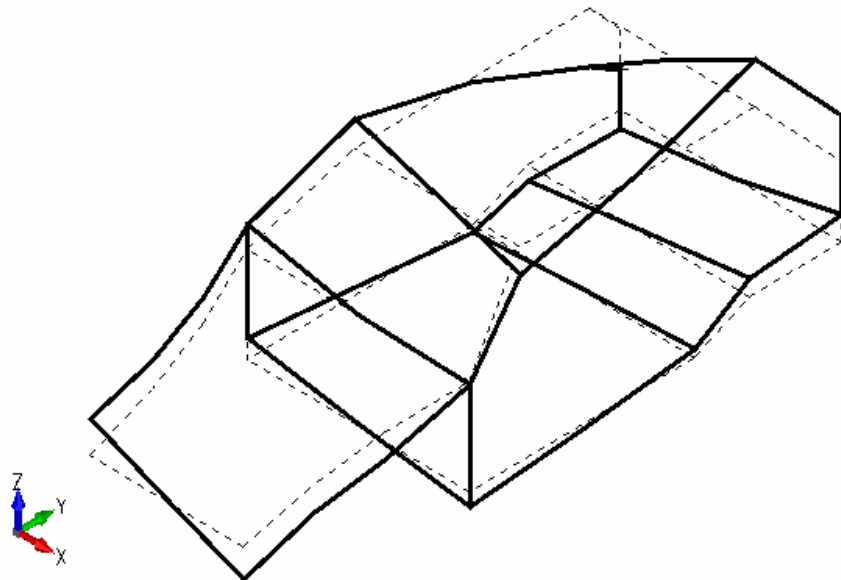


Figure 5.6 2nd torsional mode @27.7 Hz, Test

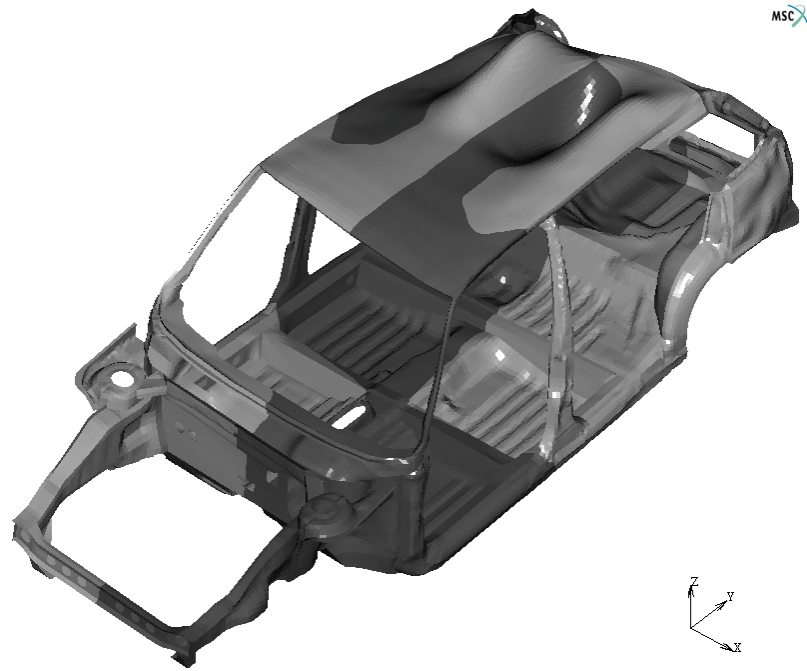


Figure 5.7 3rd torsional mode @36.0 Hz, FEA

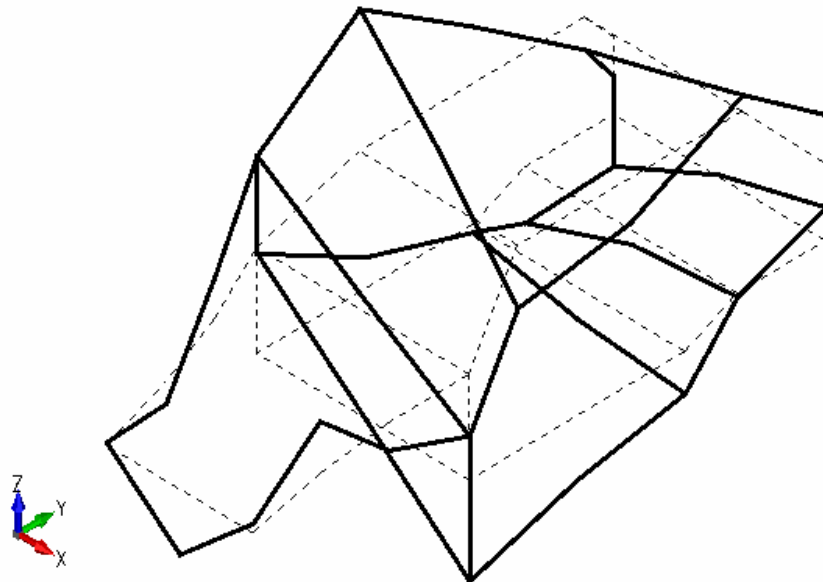


Figure 5.8 3rd torsional mode @35.9 Hz, Test



Figure 5.9 1st bending mode @42.2 Hz, FEA

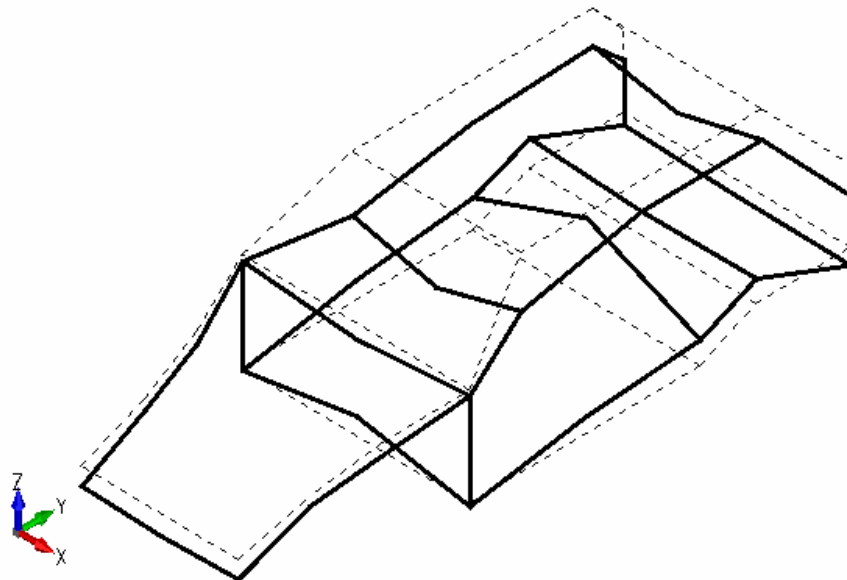


Figure 5.10 1st bending mode @41.1 Hz, Test

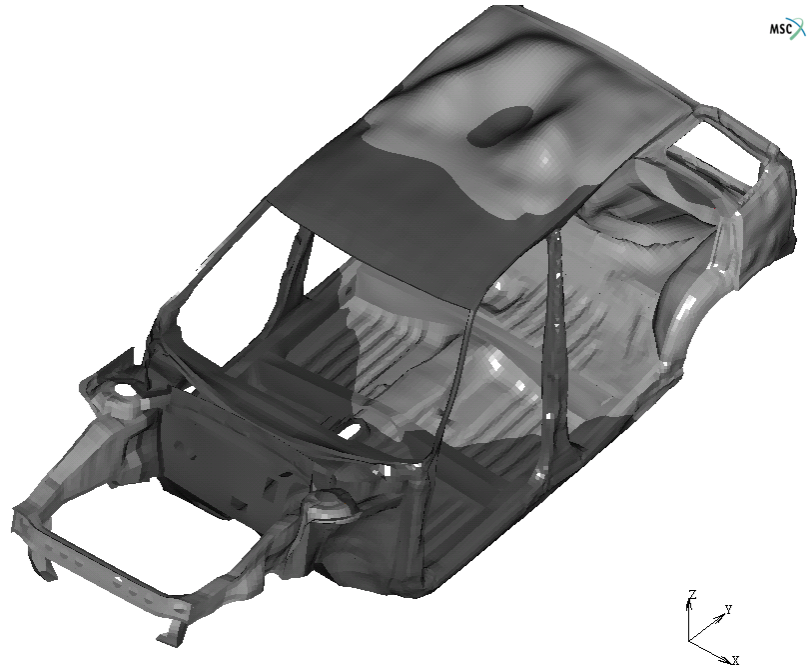


Figure 5.11 2nd bending mode @49.2 Hz, FEA

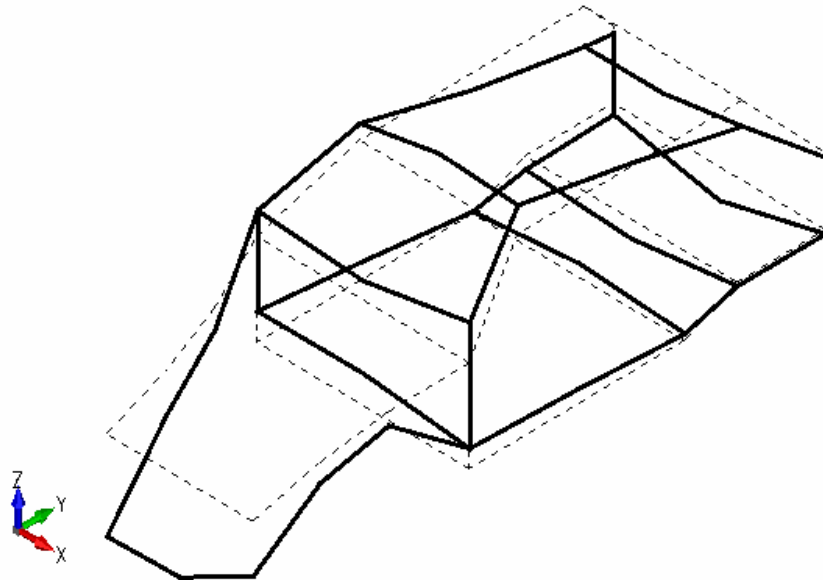


Figure 5.12 2nd bending mode @47.3 Hz, Test

The similarity between the resultant mode shapes is obvious from the figures. Examining the FEA results, it is observed that the roof has its own shapes at these natural frequencies. To justify the conformity between the FEA and experimental results, measurements are taken at 49 points on the roof using the same experimental procedure done for the body-in-white. The solid and wire frame models of the roof is given in Figure 5.13.

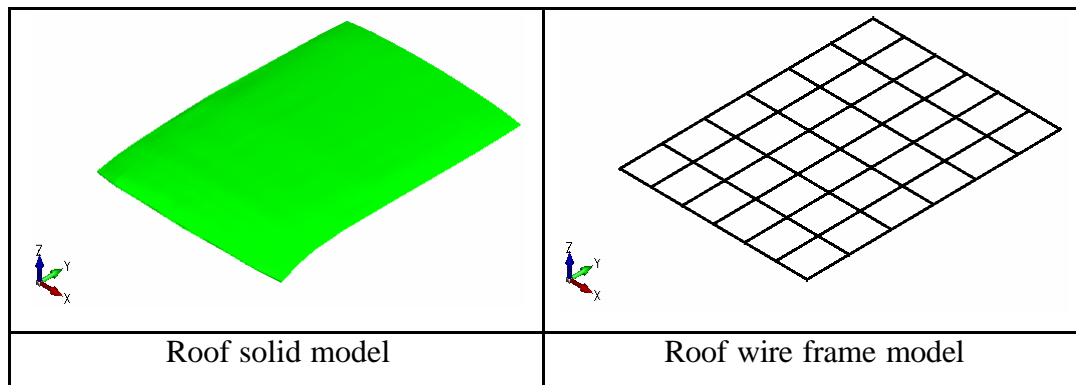


Figure 5.13 Roof models

Using the results of FRF measurements, the shapes of the roof at these natural frequencies given in 5.3.2 are shown using the wire frame model. The resultant shapes are shown in Figure 5.14-5.18. Original shape is given in dashed lines where the deformed shape is given in full lines.

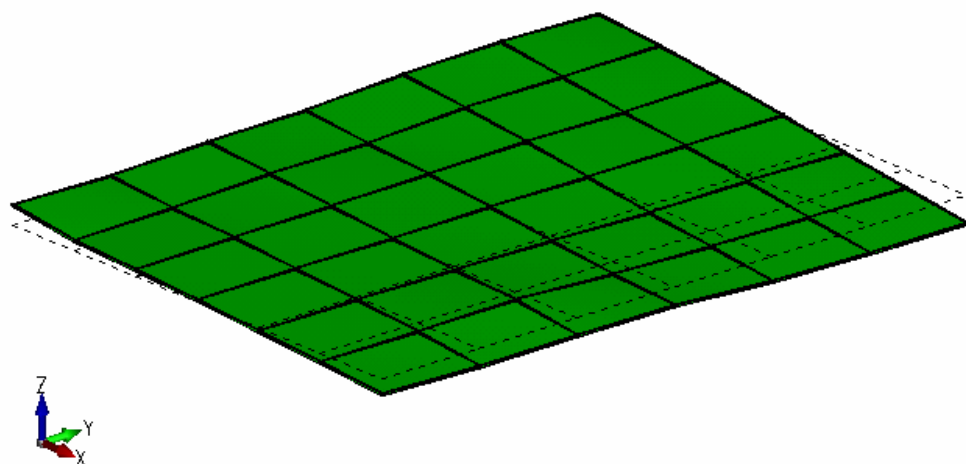


Figure 5.14 Roof shape @21.7 Hz, Test

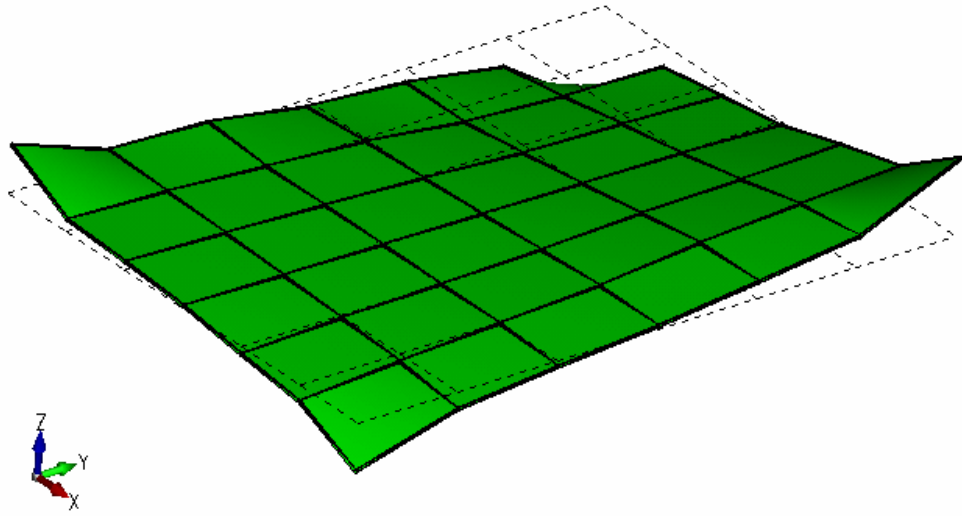


Figure 5.15 Roof shape @27.7 Hz, Test

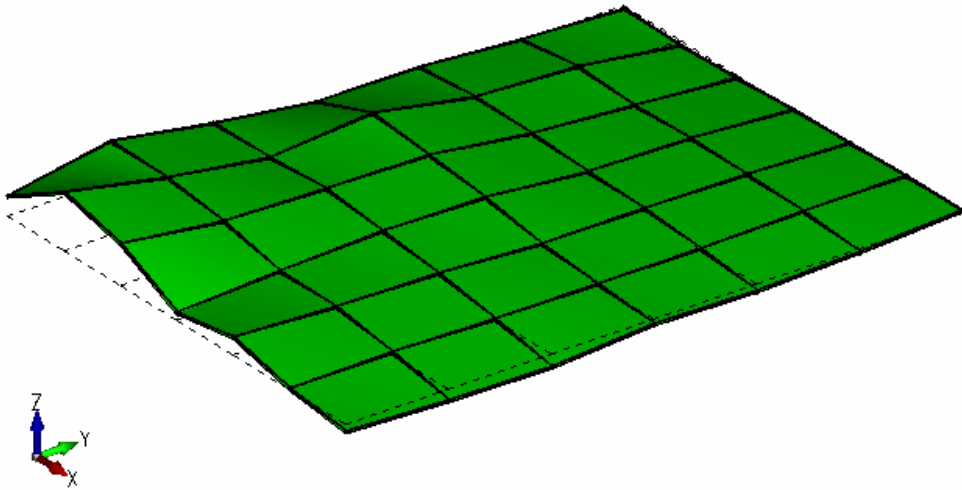


Figure 5.16 Roof shape @35.9 Hz, Test

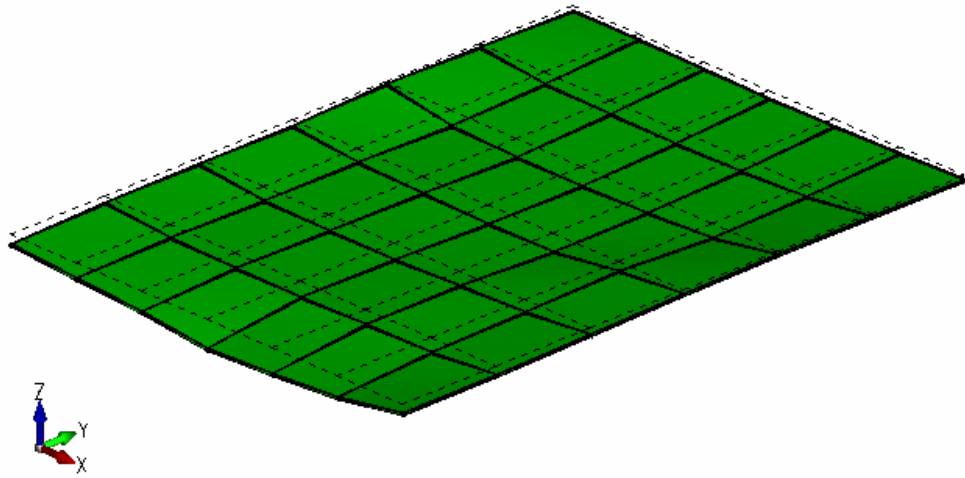


Figure 5.17 Roof shape @41.1 Hz, Test

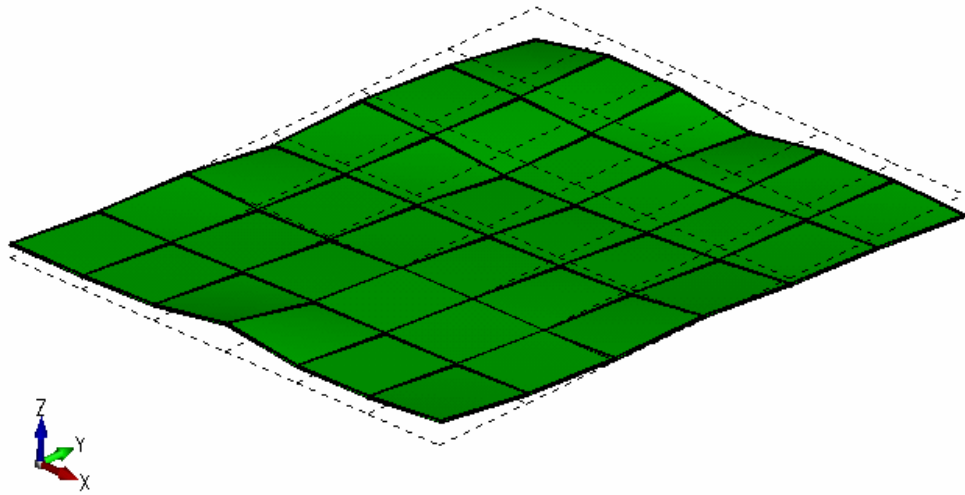


Figure 5.18 Roof shape @47.3 Hz, Test

To make the shapes more visible, surfaces are given in rendered mode for wire frame model. Except the shape at 35.9 Hz, the experimental shapes of the roof correlate with the shapes given in FEA solutions.

5.3.3 Frequency response functions

Nine points from 34 measurement locations are selected to compare the frequency responses obtained by FEA and experiments. The nodes corresponding to these locations are found in FEM. Displacement data for each of these 9 nodes are taken from the finite element harmonic analysis job results. These points are shown in body-in-white wire frame model in Figure 5.19. These points are selected randomly; there is no any specific reason to pick these locations. The only idea behind the selection is to have distant positions.

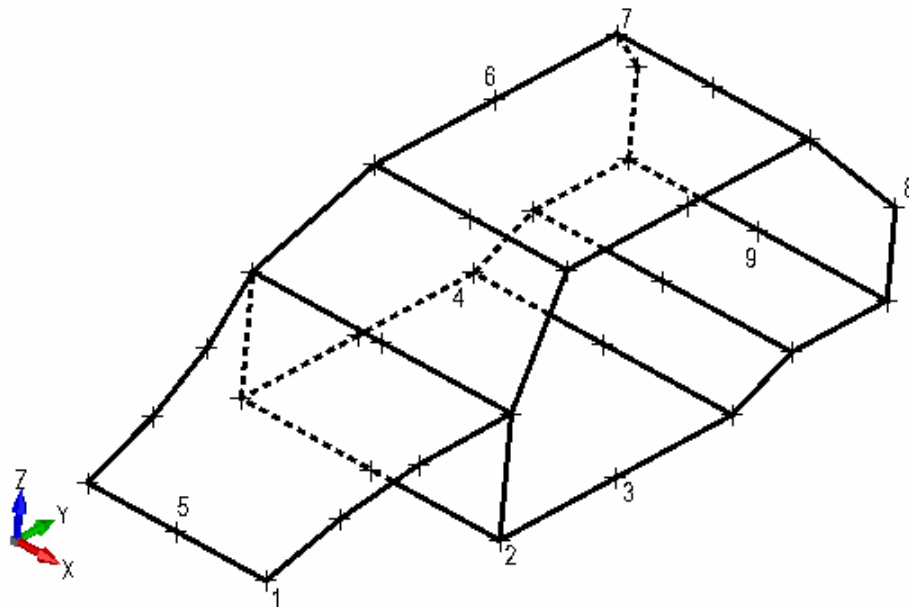


Figure 5.19 FEA vs. Test FRF plot locations

From the harmonic analysis FE result file, the node numbers corresponding to the locations shown in the figure from 1 to 9 are found as 639, 13455, 16008, 33843, 112, 27859, 43046, 14135 and 51841, respectively. Since the harmonic analysis has been performed using a unit force, i.e. 1 N, and displacements at these nodes have been obtained from the harmonic analysis, the resultant transfer functions are obtained as receptances. Receptances for both analytical and experimental are given in the same FRF plots in Figure 5.20-5.28.

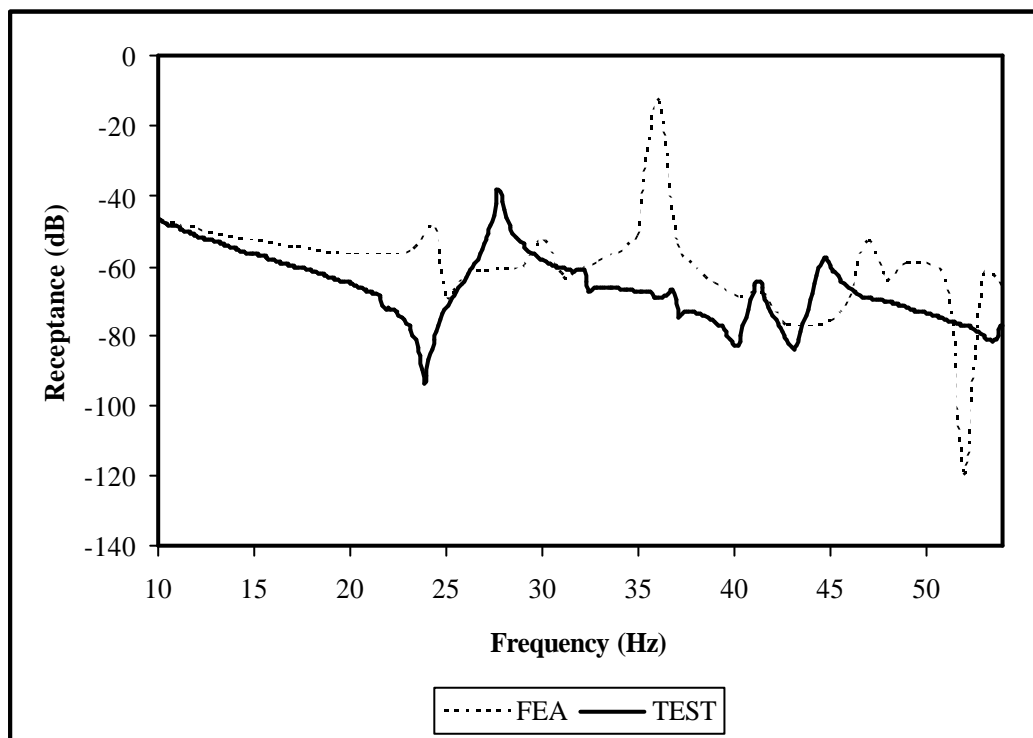


Figure 5.20 FEA vs. Test FRF plot @location 1, node 639

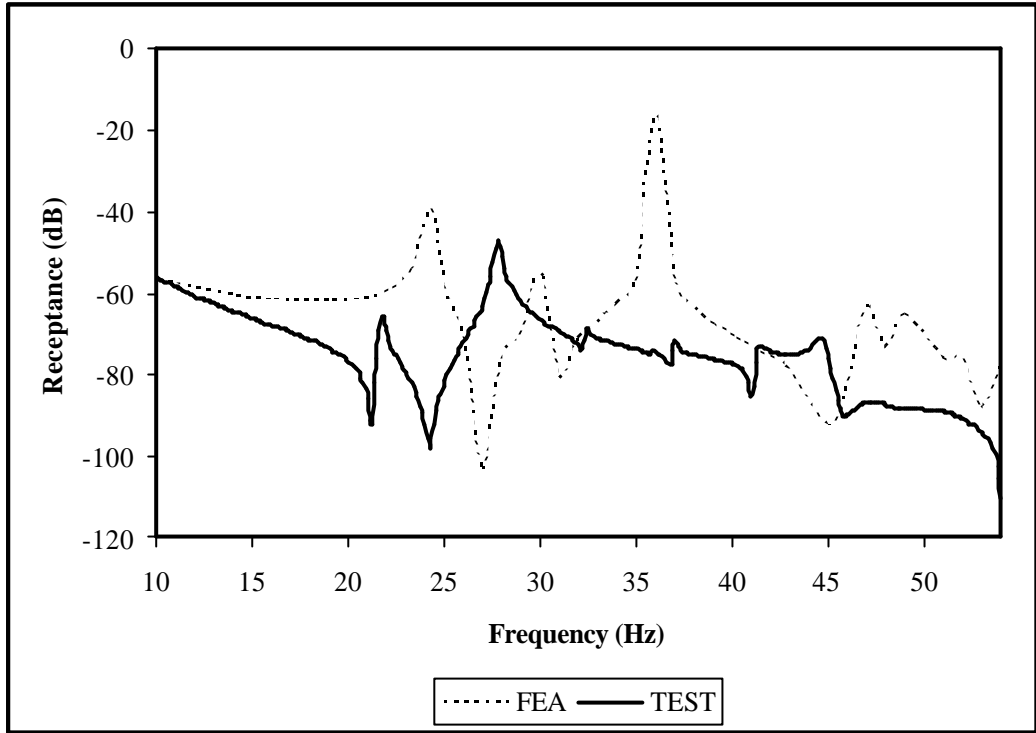


Figure 5.21 FEA vs. Test FRF plot @location 2, node 13455

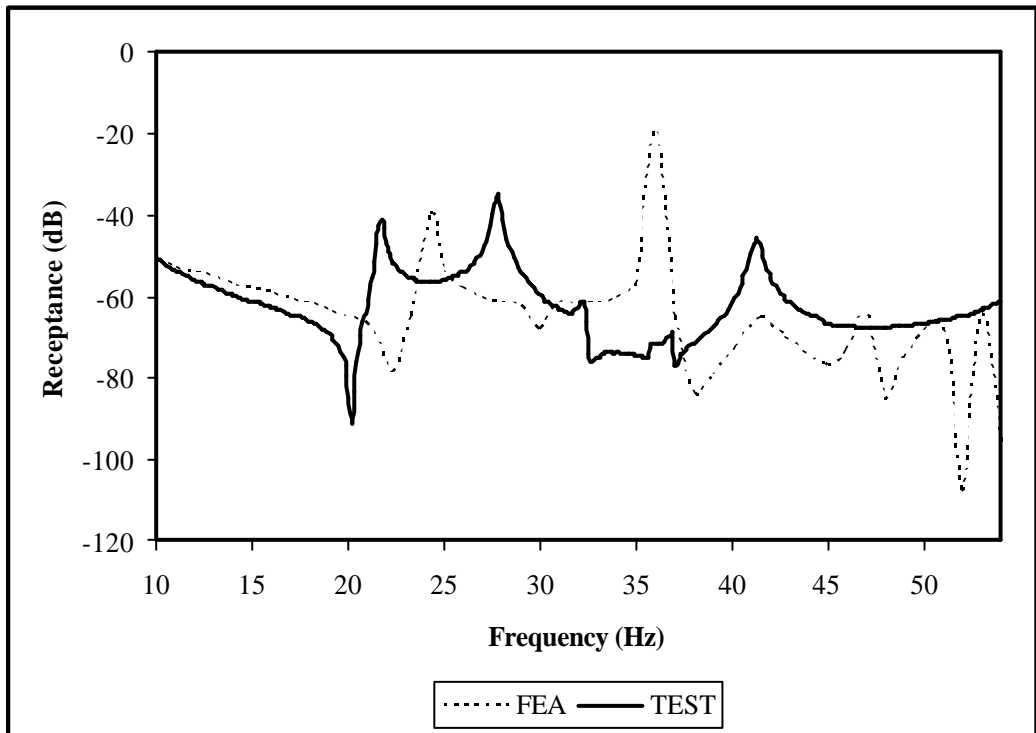


Figure 5.22 FEA vs. Test FRF plot @location 3, node 16008

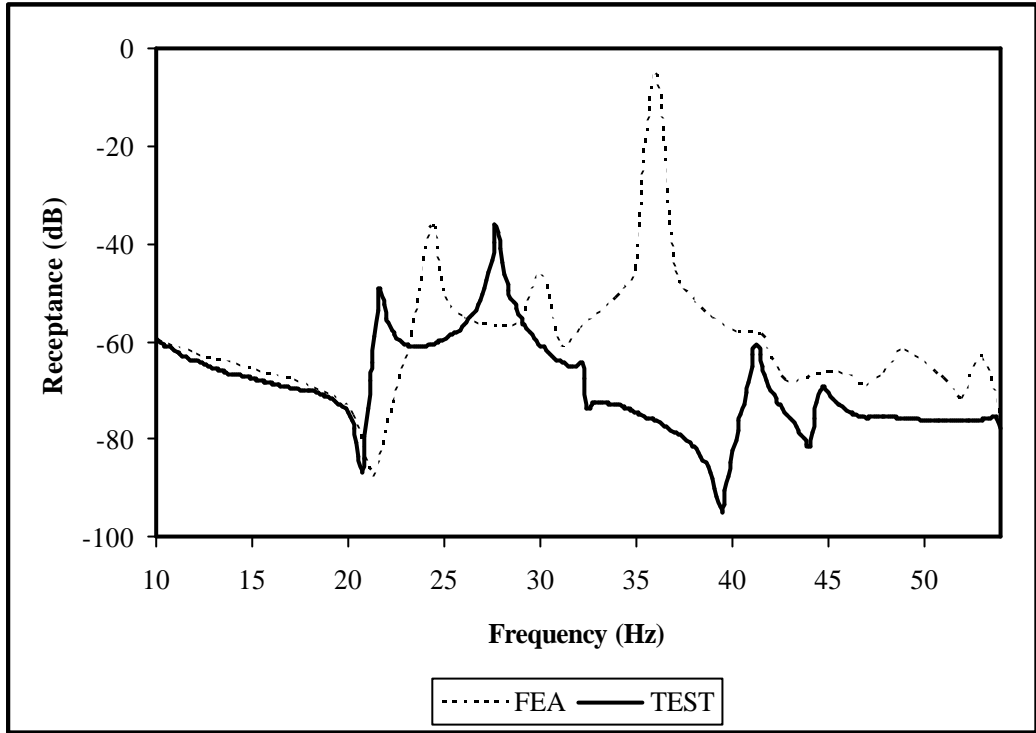


Figure 5.23 FEA vs. Test FRF plot @location 4, node 33843

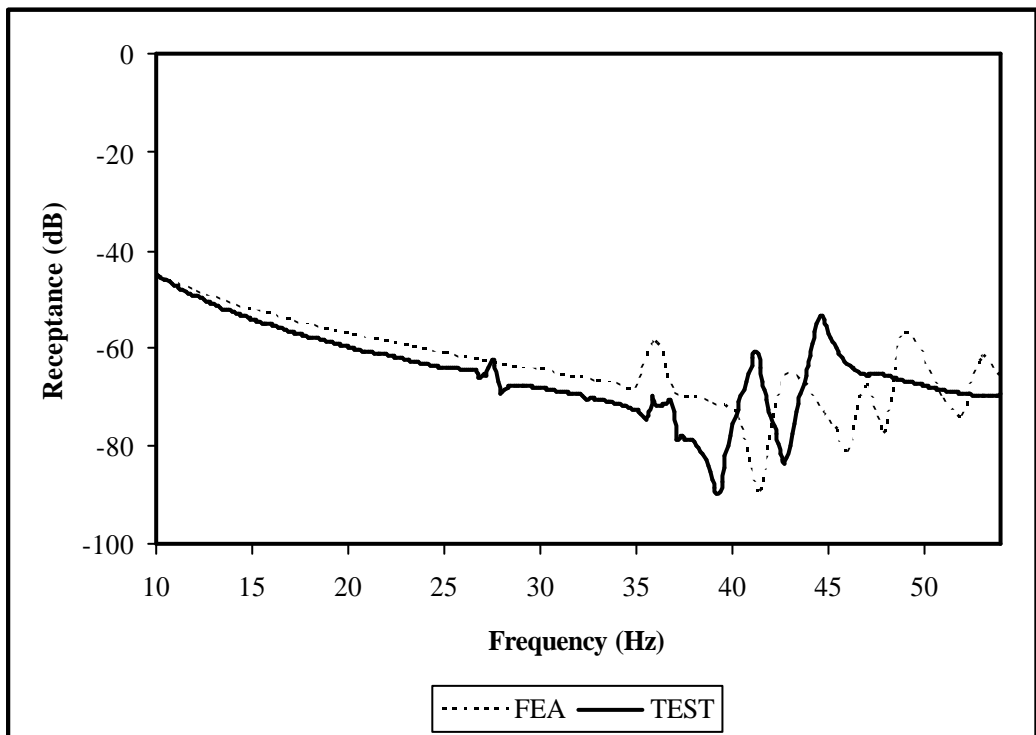


Figure 5.24 FEA vs. Test FRF plot @location 5, node 112

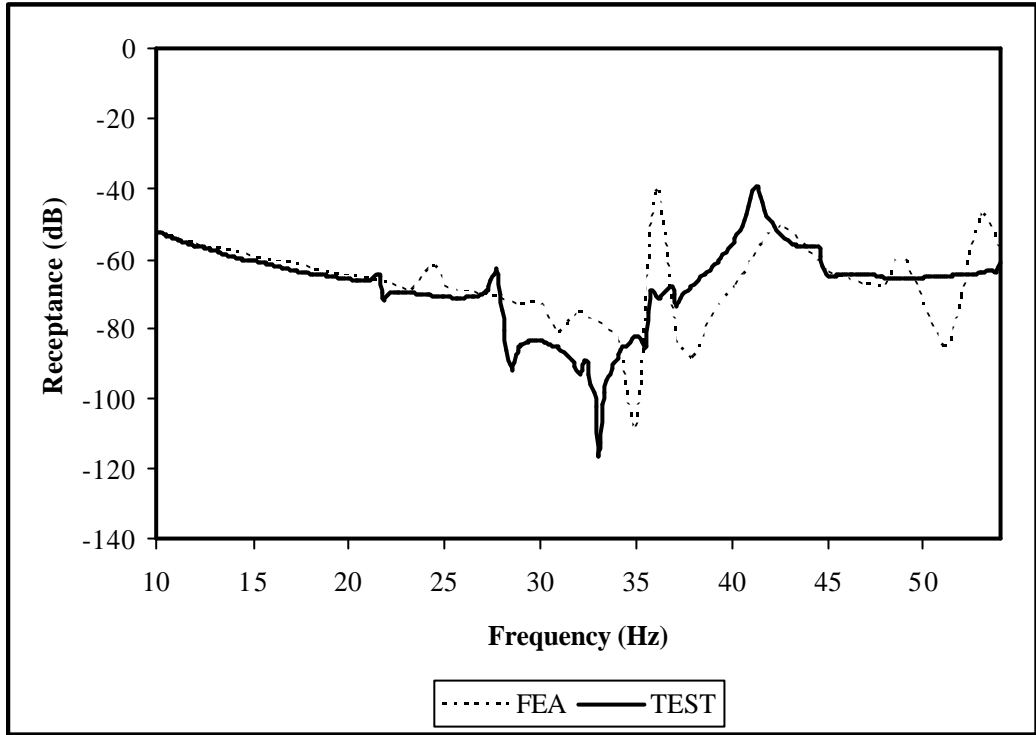


Figure 5.25 FEA vs. Test FRF plot @location 6, node 27859

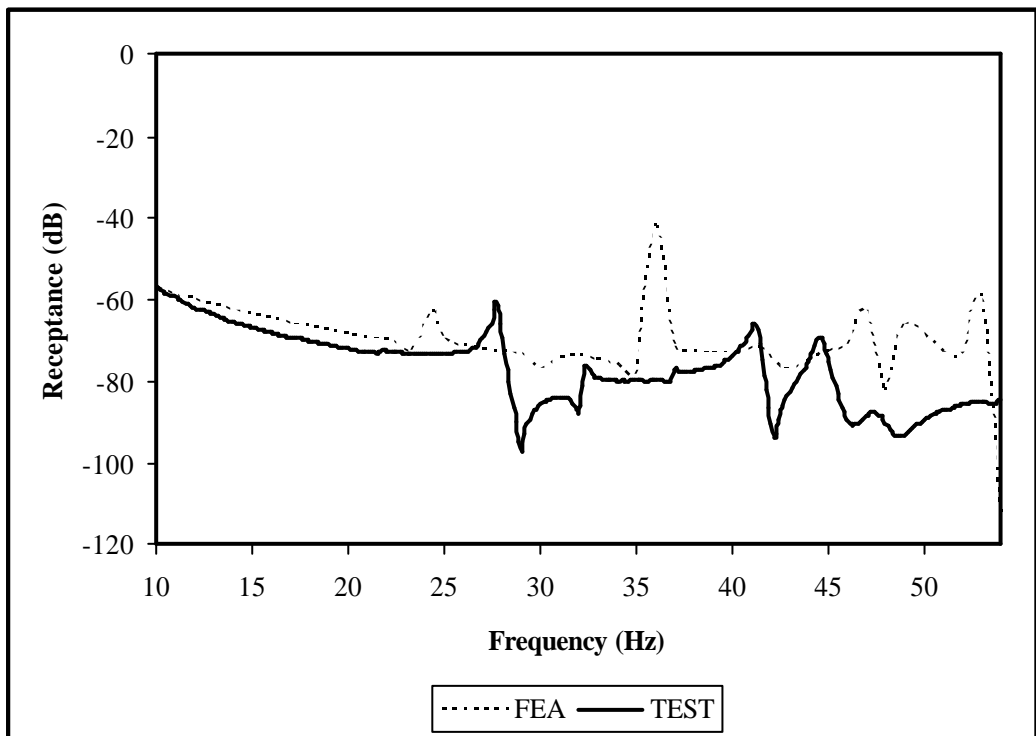


Figure 5.26 FEA vs. Test FRF plot @location 7, node 43046

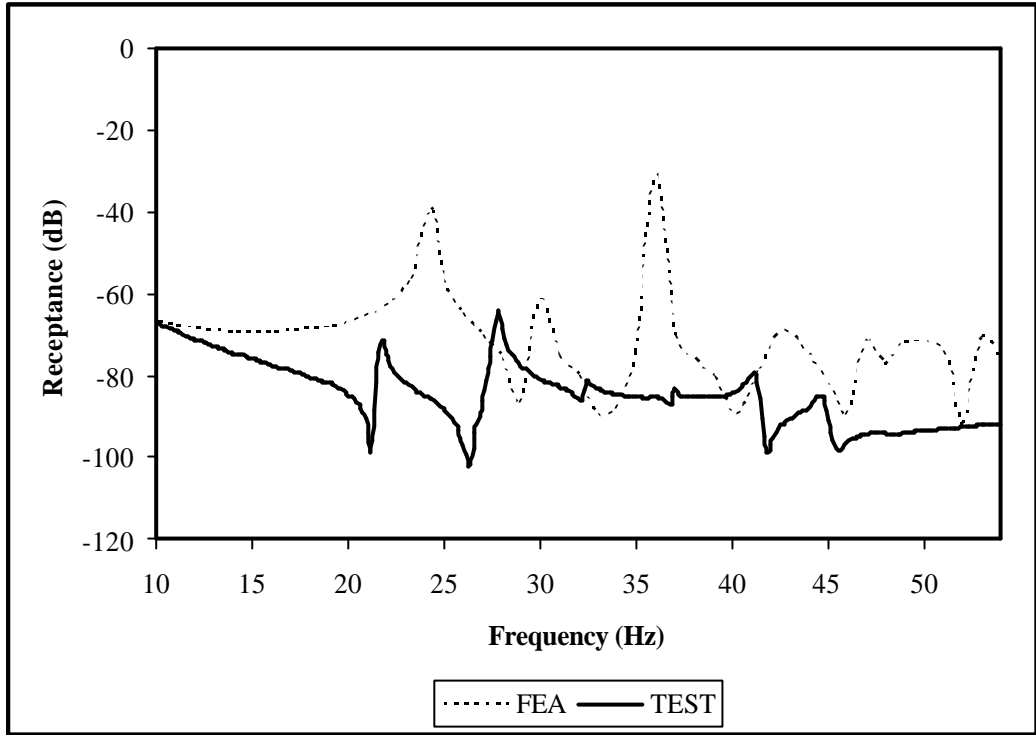


Figure 5.27 FEA vs. Test FRF plot @location 8, node 14135

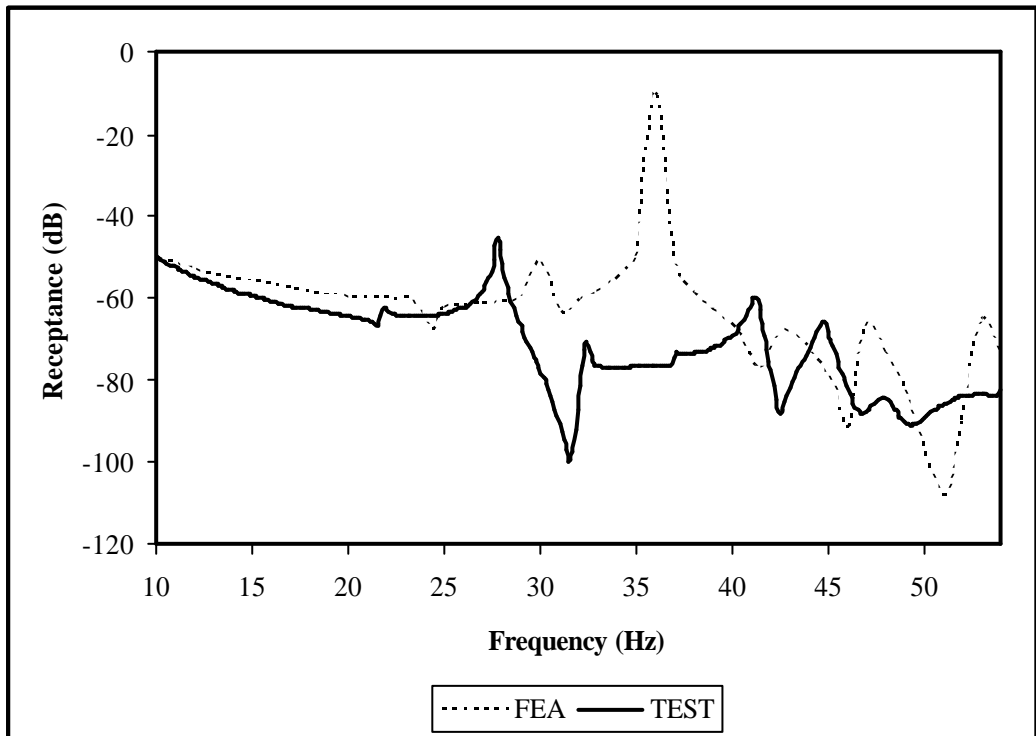


Figure 5.28 FEA vs. Test FRF plot @location 9, node 51841

There are some shifts in the resonance frequencies for FEA and experimental frequency response functions. The FEA uses fully free-free boundary conditions for the body-in-white model. In the experiments the body is suspended to approach truly free boundary conditions. Also it should be remembered that the FEM does not contain any damping where the actual system is damped considerably. These are the main effects on the differences in frequency response functions. In addition to these, it is difficult to make every detail in FE model as they are in actual system. For such a big structure, FEA analysis results are acceptable with respect to the experimental results. In addition to these, it is not practically possible to take measurements exactly from the same location indicated in FEM due to the surface roughness or additional parts on body-in-white. Test results are more reliable since the measurements are taken from the body-in-white providing free-free boundary conditions.

CHAPTER 6

DISCUSSION AND CONCLUSION

6.1 TEST SETUP

The most important and difficult part in vibration testing is to support the test structure. It is even more difficult when the supporting conditions are selected to be free-free. For small structures, some very soft elastic ropes are used to hang the structure. When the test structure is large such as the car body-in-white used in this study, then it is not so easy to hang the structure using elastic ropes. First of all, it is hard to keep the body and instruments safe with this kind of supporting. In addition, it is difficult to find such elastic ropes to suspend the car body-in-white and provide low stiffness. In this study, air springs are used to support the body-in-white from bottom. They are connected to suspension connection points of body-in-white. It is obvious that using this suspension, the body will have rigid body frequencies. Setting the pressures inside the air springs to 1 bar, one of the rigid body frequencies is estimated as 4.7 Hz. The results of FRF measurements show that the highest rigid body frequency is at 6.9 Hz. This value is acceptable for vibration testing since it falls into range 4.1-8.2 Hz. This range is 10-20% of the lowest bending mode frequency (41.1 Hz). From natural frequencies and mode shapes points of view, it is unnecessary to examine below 10 Hz. So the frequency range is selected as 10-100 Hz for 34 measurement locations which will be used in mode identification.

6.2 EXPERIMENTAL PROCEDURE AND TEST RESULTS

The main objective of this thesis study is to obtain transfer functions, frequency response functions in frequency domain, for the car body-in-white. It is not aimed to measure the acceleration (m/s^2) and force levels (N). Simply the FRFs as accelerances (acceleration/force) are measured. Then dividing this FRF by $(j\omega)$ twice, the receptances (displacement/force) are calculated. The peaks in FRF plots are enough to determine the natural frequencies, and imaginary parts of FRFs are enough to estimate the mode shapes of the body-in-white. Natural frequencies and corresponding mode shapes are given in Chapter 4. The same results are obtained from two different B&K Type 4384 accelerometers. These accelerometers are controlled using B&K Calibration Exciter Type 4294 (Appendix 9). Also the same FRFs are obtained from both accelerometers at the same location. In SPL measurements, Castle GA 601 Microphone Calibrator (Appendix 10) is used to calibrate the microphone.

As mentioned in Chapter 4, force applied should be constant in the test frequency range, i.e. 10-100 Hz. Force is almost constant in this range; its spectrum is shown in Figure 4.3. Using this same force as input, necessary measurements are made moving the accelerometer to 34 measurement locations.

Among the shaker excitation techniques, swept sine measurements provide extremely good signal-to-noise ratios and can characterize nonlinear systems. Therefore, linear swept sine is used in the experiments to excite the body-in-white in the selected frequency range. Resolution is very important in this kind of excitation. The resolution is adjusted as 801 points/sweep (maximum available in analyzer). In the linear sweep mode, the frequency step size is constant throughout the sweep. So the tests are performed with frequency increments of 0.118 Hz. This resolution is quite enough for the experiments. In sine sweep testing, it is necessary to have enough time to settle the structure after each frequency and to measure the response at this frequency. Settling time, the delay between changing the source frequency and starting the measurement at each point, is arranged as 1 s. Integration time, the amount of time that each point

is measured, is adjusted as 0.5 s. These values are automatically adjusted by the analyzer once the frequency range and the resolution are selected. In addition to these arrangements, in sine sweep, analyzer rejects the overloaded data and repeats the measurement at that overloaded frequency during the measurements. This prevents any overloaded data to be stored and processed.

As a rule of thumb, the mass of the accelerometers used in vibration testing should be $1/10^{\text{th}}$ of the mass of the test structure. The mass of the accelerometers used is 17 grams. This value is much smaller than the $1/10^{\text{th}}$ of the weight of the body-in-white.

Accelerometer mounting is another important subject in vibration testing. The most common way is to use bees-wax whenever it is not possible mounting the accelerometer using studs. In all measurements, beeswax is used to mount the accelerometers to body-in-white. The measurement results are satisfactory using this mounting method. The noise level is very low in measured data.

Two FRF measurements taken at the same location using two different accelerometers are shown in Figure 6.1. One of them is taken using B&K

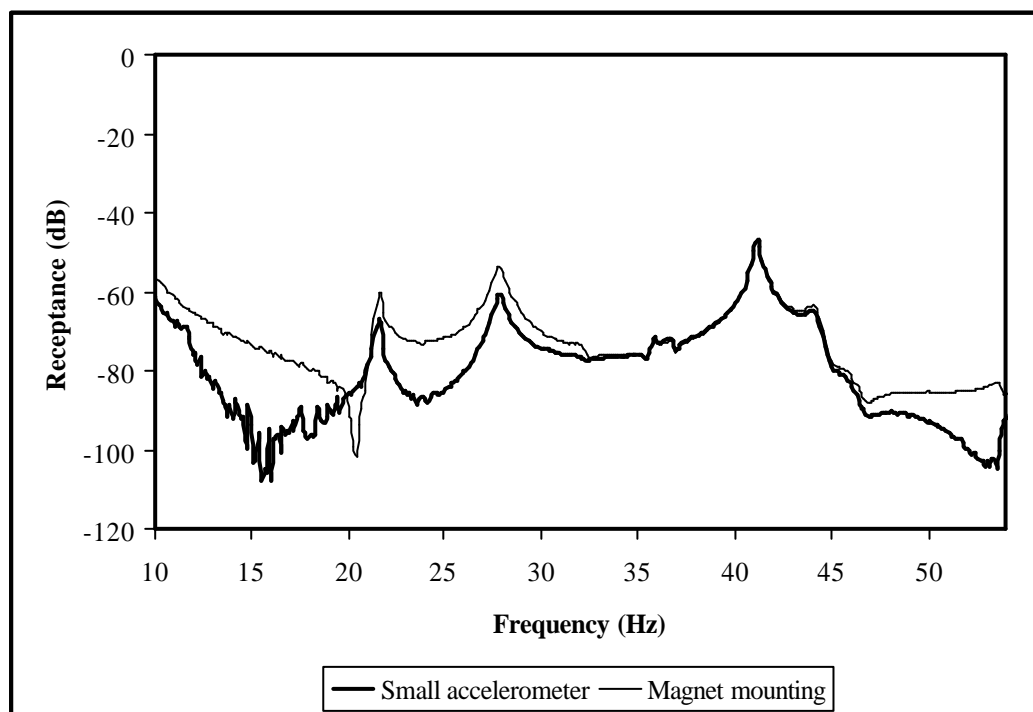


Figure 6.1 Accelerometer selection and mounting effects on FRF

Miniature Accelerometer Type 4375 which has a weight of 2.4 grams only (Appendix 11). Since this accelerometer is very light, the data contains noise throughout all frequency range. The other measurement is taken using the same accelerometer used in the experiments with a different mounting method. A magnet base is used to attach the accelerometer to body-in-white. In this case, again the noise can be observed in FRF measurement especially in lower frequencies. Thus, it may be concluded that accelerometer used (B&K Type 4384) with bees-wax mounting gives satisfactory results.

21 flexible modes exist in the frequency range of interest. These modes and natural frequencies are separated enough from each other particularly for major structural modes. Typically, frequencies of torsional modes are lower than that of bending modes for car bodies. The same result is observed from the experiments for car body-in-white under test. Resonances occur almost at the same frequencies for vibration and SPL measurements in the frequency range 10-100 Hz. There are small differences about 0.3 Hz between these resonance frequencies of vibration and SPL measurements. This small variation is due to the resolution difference present between the vibration and SPL measurements.

Pick picking method is used to display the mode shapes of body-in-white. Modes are identified easily by examination of deformed and original shapes of body-in-white wire frame model at resonances. 13 out of 21 flexible modes are identified as pure torsional or bending modes. The rest of the modes are defined as combination of torsional and bending.

6.3 FEA AND EXPERIMENTAL RESULTS

5-10% differences exist between the natural frequencies obtained from experiments and FEA. This difference can also be observed from the FRF plots in the previous chapter. The body-in-white model created in FEA program consists of sheet metals with different thicknesses throughout the body. However, the body contains a lot of sheet metal parts welded together forming more complex shapes which are not so easy to model. These welded parts are not modeled as

they are. Thus, at these locations the stiffness and damping values are different in the finite element model and in body-in-white. Actually in the model, damping is not included at all. For example, the roof of the body-in-white contains several supporting metals which are not included in the model. As a result of this, the shapes of the roof at major structural resonances given for experimental and FEA results are not the same. Nevertheless, they are similar and the results of the FEA are acceptable. The boundary condition, like suspension used in the experiments, also affects the results. Including these conditions and damping in the FEM would give better results.

6.4 CONCLUSION

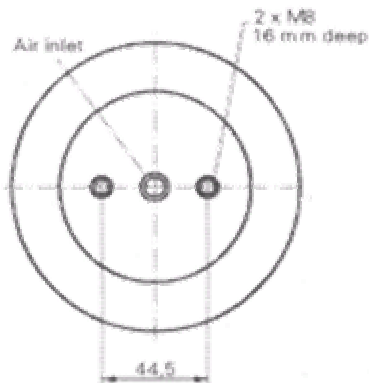
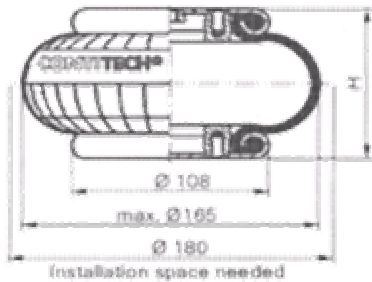
In this study, natural frequencies and mode shapes of the car body-in-white have been obtained experimentally. Since the necessary test conditions are satisfied, the results are reliable. According to the test results, the FE model can be used for further analysis and sufficient results can be obtained. However, in order to rely more on the results of finite element analysis, it is better to make necessary updates to FE model using the experimental results. FEA and experimental results may be used for model updating studies.

6.5 RECOMMENDATION FOR FUTURE STUDIES

The shaker is attached to left front suspension attachment point and the body-in-white is excited from this single point. It would be better if any additional measurements are made exciting the structure from other locations. Also to excite torsional and bending modes separately, the body may be excited using two shakers from two corners with 90 degree phase difference. The results can be used to compare the results presented in this thesis study. Finally, using these experimental results the FEM can be updated in future studies.

APPENDIX 1

CONTITECH FS 70-7 AIR SPRING TECHNICAL DETAILS



Technical data:

| | |
|------------------------------------|---------|
| Minimum pressure | 0 bar |
| Return force to min. height | < 200 N |
| Overall weight with clamped plates | 1.2 kg |
| Installation space needed | 180 mm |

Vibration isolation:

| Pressure [bar] | 3 | 4 | 5 | 6 | 7 | 8 | Volume [l] |
|------------------------|------|------|------|------|------|------|------------|
| Force [kN] | 2.5 | 3.3 | 4.1 | 5.0 | 5.9 | 6.6 | 7.0 |
| Spring rate [N/cm] | 1180 | 1480 | 1820 | 2080 | 2370 | 2660 | |
| Natural frequency [Hz] | 3.5 | 3.4 | 3.3 | 3.3 | 3.2 | 3.2 | |

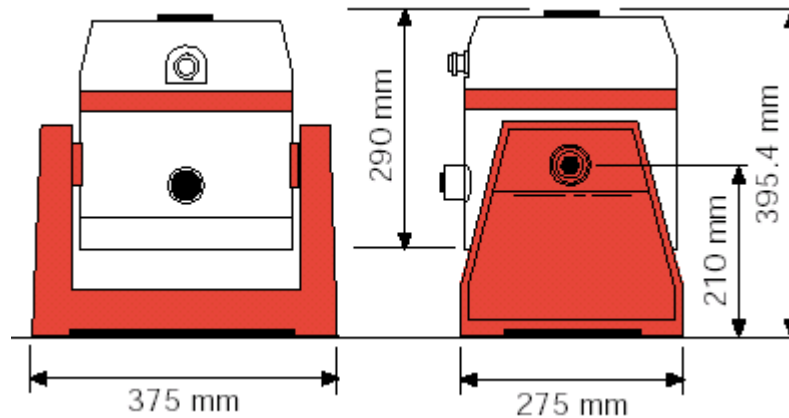
Pneumatic applications – static characteristic values

| Pressure [bar] | 3 | 4 | 5 | 6 | 7 | 8 | Volume [l] | |
|----------------|-----|-----|-----|-----|-----|-----|------------|-----|
| Height [mm] | 100 | 1.9 | 2.5 | 3.2 | 3.9 | 4.5 | 5.2 | 1.0 |
| | 90 | 2.5 | 3.3 | 4.1 | 5.0 | 5.9 | 6.6 | 0.9 |
| | 80 | 3.0 | 4.0 | 5.0 | 6.0 | 7.1 | 8.0 | 0.8 |
| | 70 | 3.4 | 4.6 | 5.7 | 6.9 | 8.0 | 9.2 | 0.7 |
| | 60 | 3.8 | 5.1 | 6.3 | 7.6 | 8.8 | 9.9 | 0.6 |

APPENDIX 2

LDS V450 SHAKER TECHNICAL DETAILS

Dimensions



Technical Features

- Rated force, sine vector, with air forced-cooling 311 N (70 lbf)
- Rated force, random, with air forced-cooling 218 N (49 lbf)
- Natural cooling 177 N (40 lbf)
- Useful frequency range DC to 7.5 kHz
- Maximum displacement 19 mm (0.75 in) peak to peak
- Overtravel protection 20 mm (0.79 in) peak to peak
- Maximum velocity 2.5 m/s (98.4 in/s)
- Maximum acceleration, bare table 74 g
- Fundamental resonance frequency (bare table) 6000 Hz $\pm 3\%$
- Mass/Spring resonance (bare table) 32 Hz
- Effective mass of moving system 0.426 kg (0.94 lb)
- Armature guidance(upper and lower) Laminated spider
- Suspension axial stiffness 1.79 kgf/mm (100 lbf/in) $\pm 10\%$
- Maximum armature current (forced cooling) 11 A
- Maximum armature current (natural cooling) 6.3 A
- Armature coil resistance at 20°C $\pm 10\%$ 0.9 Ω

APPENDIX 3

AGILENT 35665A 2-CHANNEL DYNAMIC SIGNAL ANALYZER TECHNICAL SPECIFICATIONS



- 1-channel at 102.4 kHz, 2 channels at 51.2 kHz
- 100, 200, 400, 800 lines of resolution
- Built in 3.5" floppy disk
- Tachometer input
- Source: Random, burst random, pink noise, sine, swept-sine, arbitrary, periodic chirp, burst chirp
- 3.2 M Sample time-capture buffer (optional)
- Measurements: linear spectrum, cross-spectrum, power spectral density, frequency response, time waveform, auto-correlation, cross-correlation, histogram, PDF, CDF
- Optional real-time octave, computed order tracking, swept-sine, curve fit, synthesis, and arbitrary source.

APPENDIX 4

BRUEL & KJAER IMPEDANCE HEAD TYPE 8001 TECHNICAL SPECIFICATIONS

| | |
|---|---|
| Reference sensitivity | At 50 Hz 23 °C |
| Cable capacitance | 110 pF |
| Accelerometer charge sensitivity | 3.31 pC/ms ⁻² or 31.3 pC/g |
| Accelerometer capacitance (including cable) | 1038 pF |
| Maximum transverse sensitivity at 30 Hz | 1.5 % |
| Force gauge charge sensitivity | 306 pC/N |
| Force gauge voltage sensitivity | 396 mV/N |
| Force gauge capacitance (including cable) | 773 pF |
| Base strain sensitivity of force gauge | 3x10 ⁻³ N/μStrain |
| Stiffness below accelerometer | 25x10 ⁷ N/m |
| Mass below force gauge | 2.2 gram |
| Max. Screw-down torque | 0.5 Nm |
| Weight | 31 gram |
| Material | Titanium & stainless steel |
| Mounting thread | 10-32 UNF-2B |
| Electrical connector | Miniature coaxial 10-32 UNF-2A thread |
| Humidity | Sealed |
| Max. Temperature | 260 °C or 500 °F |
| Magnetic sensitivity (50 Hz) | < 20 mV/T |
| Acoustic sensitivity | < 0.003 ms ⁻² or 0.03g at 154 dB SPL |

APPENDIX 5

BRUEL & KJAER ACCELEROMETER TYPE 4384 TECHNICAL SPECIFICATIONS

| | |
|---|--|
| Reference sensitivity | At 159.2 Hz, 100ms ⁻² and 23 °C |
| Charge sensitivity | 1.011 pC/ms ⁻² or 9.92 pC/g |
| Voltage sensitivity | 0.797 mV/ms ⁻² or 7.81 mV/g |
| Typical capacitance | 110 pF |
| Maximum transverse sensitivity at 30 Hz | 1.1 % |
| Typical undamped natural frequency | 62 kHz |
| Humidity | Welded, sealed |
| Max. Temperature | -74 to +250 °C or -100 to 482 °F |
| Magnetic sensitivity (50 Hz) | < 20 mV/T |
| Acoustic sensitivity | < 0.01 ms ⁻² at 154 dB SPL |
| Construction | Delta shear |
| Mounting torque | 1.8 Nm, min 0.5 Nm, 3.5 Nm |
| Weight | 11 gram |
| Material | Titanium, ASTM Grade 2 |
| Piezoelectric material | PZ23 |
| Mounting thread | 10-32 UNF-2B |
| Seismic mass | 2.6 gram |
| Max. shock acceleration | 200 kms ⁻² peak |

APPENDIX 6

BRUEL & KJAER CHARGE AMPLIFIER TYPE 2635 TECHNICAL SPECIFICATIONS



| | |
|---|---|
| Charge input | Via 10-32 NF and BNC coaxial socket Max. input: $\sim 10^5$ pC |
| Sensitivity conditioning | 3 digit dial-in of transducer sensitivity from 0.1 to 10.99 pC/ms ⁻² |
| Amplifier sensitivity | 0.01 mV to 10 V/pC corresponding to -40 to +80 dB with transducer capacitance of 1 nF |
| Calibrated output ratings (selectable in 10 dB steps) | Acceleration: 0.1 mV to 1 V/ms ⁻² Velocity: 10 mV to 100 V/ms ⁻¹ Displacement: 0.1 mV to 10 V/mm |
| Signal output | Via 10-32 NF and BNC coaxial socket Max.output: 8V (8 mA) peak |
| Frequency range | Acceleration: Switchable 0.2 or 2 Hz to 100 kHz Velocity: Switchable 1 or 10 Hz to 1 kHz Displacement: Switchable 1 or 10 Hz to 1 kHz |
| Test oscillator | 159 Hz ($\omega=1000$ rad/s) sinusoid, factory preset for test level of 1 V |
| Overload indicator | Overload led lights when input or output of amplifier is overloaded |
| Dimensions | Height: 132.6 mm (5.22 in) Width: 69.5 mm (2.74 in) Depth: 200 mm (7.87 in) |
| Weight | 1.45 kg (3.2 lb) including batteries |

APPENDIX 7

BRUEL & KJAER MICROPHONE TYPE 4165 TECHNICAL SPECIFICATIONS



| | |
|------------------------------------|---|
| Frequency response characteristics | Free-field, 0° incidence |
| Lower limiting frequency (-3 dB) | 1 Hz to 2 Hz |
| Cartridge thermal noise | 14.5 dB(A) |
| Diaphragm resonance frequency | 14 kHz (90° phase-shift) |
| Mean temperature coefficient | -0.0007 dB/°C (-10°C < t < +50°C) |
| Equivalent air volume | 40 mm ³ (250 Hz) |
| Expected long-term stability | >600 years/dB at 20 °C |
| Influence of static pressure | -0.01 dB/kPa, typical |
| Influence of vibration | 60 dB re.20 μPa and 1 ms ⁻² axial vibration |
| Influence of magnetic field | 30 dB re.20 μPa in 50 Hz, 80 A/m field |
| Influence of humidity | 0.004 dB/%RH |
| Diameter | 13.2 mm (0.51 in) (with grid) 12.7 mm (0.49 in) (without grid) |
| Height | 16.3 mm (0.63 in) (with grid) 15.2 mm (0.59 in) (without grid) |
| Suitable preamplifiers | Type 2639, 2645, 2660, 2669B, 266L |
| Thread for preamplifier mounting | 11.7 mm – 60 UNS |

* Picture is representative (type 4190).

APPENDIX 8

BRUEL & KJAER MICROPHONE PREAMPLIFIER TYPE 2660 TECHNICAL SPECIFICATIONS



| | |
|--|--|
| Frequency response | 14 Hz to 4 kHz ± 1 dB 10 Hz to 10 kHz ± 2 dB 7 Hz to 12.5 kHz +2, -3 dB |
| Cartridge lower limiting frequency (-3 dB) | 5 to 7 Hz |
| Preamplifier gain | 20 dB ± 0.1 dB |
| Upper limit of dynamic range | Safety limit: 154 dB peak Upper limit of system: 102 dB re.20 μ Pa |
| Resonance frequency | 7 kHz |
| Equivalent volume | 40 mm ³ (250 Hz) |
| Expected long-term stability | >250 years/dB at 20 °C |
| Cartridge dimensions | \varnothing 23.77 x 25 mm with protection grid \varnothing 23.77 x 23 mm without grid |
| Preamplifier input stage dimensions | \varnothing 12.7 x 83 mm |
| Preamplifier output stage dimensions | \varnothing 25 x 175 mm |
| Cartridge vibration sensitivity | 20 mPa/ms ⁻² or 60 dB equivalent SPL at 1 ms ⁻² (f<1 kHz) |
| Preamplifier vibration sensitivity | 400 μ V or 46dB equivalent SPL at 1 ms ⁻² |
| Ambient pressure range | 925 to 1025 mbar |
| Coaxial input adaptor | JJ 2617 |
| Grid and preamplifier mounting threads | 23.11 mm – 60 UNS |

APPENDIX 9

BRUEL & KJAER CALIBRATION EXCITER TYPE 4294 TECHNICAL SPECIFICATIONS



| | |
|----------------------|---|
| Vibration system | Electromagnetic exciter with internal built-in accelerometer for servo regulation of vibration amplitude |
| Frequency | 159.15 Hz \pm 0.02% (1000rad/s) |
| Acceleration | 10 ms ⁻² (RMS) \pm 3% |
| Velocity | 10 mms ⁻¹ (RMS) \pm 3% |
| Displacement | 10 μ m (RMS) \pm 3% |
| Transverse amplitude | Less than 5% of main axis amplitude |
| Distortion | Less than 2% for 10 to 70 gram load; less than 7% for 0 to 10 gram. |
| Warm-up time | Less than 5 seconds |
| Signal duration | 103 \pm 1 s with automatic stop |
| Maximum load | 70 grams |
| Maximum load | 70 gram |
| Mounting torque | Max. 0.5 Nm |
| Mounting thread | 10-32 UNF |
| Dimensions | Length: 155 mm (6.1 in) Diameter: 52 mm (2.05 in) Weight: 500 grams (17.6 oz.) including battery and leather case |

APPENDIX 10

CASTLE MICROPHONE CALIBRATOR TYPE GA 601 TECHNICAL SPECIFICATIONS



| | |
|---|--|
| Nominal sound pressure level at 101.3 kPa (760 mm Hg), 20 °C, 65% | 94 dB relative to 20 μ Pa |
| Tolerance (dB) | ± 0.5 dB Class 2; ± 0.3 dB Class 1 |
| Stability (dB) | ± 0.2 dB Class 2; ± 0.1 dB Class 1 |
| Nominal frequency at 101.3 kPa (760 mm Hg), 20 °C, 65% | 1 kHz |
| Tolerance (%) | 4% dB Class 2; 2% dB Class 1 |
| Harmonis distortion | < 3% |
| Temperature range | -10 °C to +60 °C |
| Cavity diameter | 12.7 mm (0.5 in) |
| Life | 70 hours |
| Standards | Meets IEC942: 1988 Sound calibrators |
| Dimensions | Length: 140 mm Diameter: 51 mm |
| Weight | 230 gram |

APPENDIX 11

BRUEL & KJAER ACCELEROMETER TYPE 4375 TECHNICAL SPECIFICATIONS

| | |
|---|---|
| Reference sensitivity | At 50 Hz, 100ms ⁻² and 24 °C |
| Charge sensitivity | 0.312 pC/ms ⁻² or 3.06 pC/g |
| Voltage sensitivity | 0.489 mV/ms ⁻² or 4.79 mV/g |
| Typical capacitance | 639 pF |
| Maximum transverse sensitivity at 30 Hz | 1.8 % |
| Typical undamped natural frequency | 55 kHz |
| Humidity | Welded, sealed |
| Magnetic sensitivity (50 Hz – 0.03 T) | 30 ms ⁻² /T |
| Acoustic sensitivity | 0.04 ms ⁻² at 154 dB SPL |
| Weight | 2.4 gram |
| Material | Titanium, ASTM Grade 2 |
| Piezoelectric material | PZ23 |
| Mounting thread | 10-32 UNF-2B |
| Seismic mass | 0.67 gram |
| Max. Shock acceleration | 250 kms ⁻² peak |

REFERENCES

- [1] KARDON, J.B., “*Standard of care*”, WestCon (Western Construction Consultants Association) Tribune, June Review, July 1999
- [2] KENNEDY, C.C.; PANCU, C.D.P., “*Use of vectors in vibration measurement and analysis*”, Journal of Aerospace Sciences, Vol 14., No.1 1, 1947, pp.603-625
- [3] FRAEIJIS, de Veubeke, B.M., “*A variational approach to pure mode excitation based on characteristic phase lag theory*”, AGARD Report 39, 1956
- [4] BISHOP, R.E.D.; GLADWELL, G.M.L., “*An investigation into the theory of resonance testing*”, Phil. Trans. Roy. Soc., Vol 225, Ser.A.No.1055, 1963, pp.241-280
- [5] LEWIS, R.D.; WRISLEY, D.L., “*A system for the excitation of pure nature modes of complex structures*”, Journal of Aeronautical Sciences, Vol. 17, No. 11, 1950, pp.705-722
- [6] TRASILL-NASH, R.W., “*On the excitation of pure natural modes in aircraft resonance testing*”, Journal of Aerospace Sciences, Vol 25, Dec. 1958, pp.775-778
- [7] ASHER, G.W., “*A method of normal mode excitation utilizing admittance measurements*”, Proc. of IAS National Spec. Meet. On Dyns. and Aeroelasticity, Nov. 1958, pp.69-76
- [8] EWINS, D.J., “*Modal testing: Theory and practice*”, London: Research Studies Press Ltd., January 1995
- [9] MASAASI, S.; SCHUUICHIRO, I.; KUNIHIRO, Y.; KIMITAKA, A., “*Development of aluminum body for the most fuel efficient vehicle*”, JSAE Review 21 (2000) 511-516, March 2000

- [10] KAMAL, M.M.; WOLF, JR., J.A., “*Finite element applications in vibration problems*”, The Design Engineering Technical Conference, Chicago, Illinois, September 1977, pp. 67-87
- [11] OSAWA, T.; SCHILLER, T.; ABRISHAMAN, M.; CAMPBELL, B.; STOKES, W., “*Incorporation of analytical simulations into the NVH design and development process of the Nissan Quest*”, Nissan R&D, Inc., SAE 922121, 1992, pp. 1560-1570
- [12] LIM, T.C.; STEYER, G.C., “*Hybrid experimental-analytical simulation of structure-borne noise and vibration problems in automotive systems*”, SAE International Congress and Exposition, 1992
- [13] VENEZIA, Jr., James J, “*Vibration modeling and experimental analysis of a locomotive cab*”, M.S. Thesis, Virginia Polytechnic Institute and State University, May 1997, pp.10-11
- [14] DEITERS, T.A.; HUNT, D.L.; OSBORNE, E., “*A comparison of excitation methods to the Taurus vehicle modal test*”, 1993
- [15] MALY, J.R.; PENDLETON, S.; SALMANOFF, J.; BLOUNT, G.J.; MATHEWS, K., “*Hubble space telescope solar array damper*”, Smart Structures and Materials: Passive Damping and Isolation, Newport Beach, CA, March 1999
- [16] HUTIN, C., “*Modal analysis using appropriated excitation techniques*”, Structural Analysis, Sound & Vibration, October 2000
- [17] KAYA, Hüseyin, “*Application of experimental modal analysis and system identification on skewed steel grid frame and 3D finite element model update*”, M.S. Thesis, Civil Engineering Department, Middle East Technical University, January 2004
- [18] RUST, K.J., “*Introduction to accelerometers and calibration techniques*”, MTS System Corporation, October 29, 1997
- [19] DØSSING, O., “*Structural testing part 1: Mechanical mobility measurements*”, Bruel&Kjaer, April 1987
- [20] AVITABLE, P., “*Modal space-in our little world*”, *Modal Testing with Questions Notes*, 1999-2001

- [21] DUNN, J.W., "*The mechanical analysis of vehicle structures and vehicle systems*", Proceedings of Naula I Motorna Vozila Symposium, s.E1/1-23, Bled, Yugoslavia, 1979
- [22] ASHORY, M.R., "*High quality modal testing methods*", pp.18-26, PhD. Thesis, Imperial College of Science, Technology and Medicine, University of London, March 1999
- [23] Bruel&Kjaer, "*Modal exciter configuration guide*", www.bksv.com
- [24] CRAGGS, A., "*The low frequency response of car bodies*", August 1965
- [25] ÖZGEN, G.O., "*Finite element modeling and analysis of a passenger car body structure*", M.S. Thesis, Mechanical Engineering Department, Middle East Technical University, August 2001